Journal of Volcanology and Geothermal Research 390 (2020) 106684

Contents lists available at ScienceDirect

Journal of Volcanology and Geothermal Research

journal homepage: www.elsevier.com/locate/jvolgeores

Invited Review Article

Towards more realistic values of elastic moduli for volcano modelling

Michael J. Heap[a,*], Marlène Villeneuve[b], Fabien Albino[c], Jamie I. Farquharson[d], Elodie Brothelande[e], Falk Amelung[d], Jean-Luc Got[f], Patrick Baud[a]

[a] Institut de Physique de Globe de Strasbourg (UMR 7516 CNRS, Université de Strasbourg/EOST), 5 rue René Descartes, 67084, Strasbourg cedex, France
[b] Department of Geological Sciences, University of Canterbury, Private Bag 4800, Christchurch, New Zealand
[c] School of Earth Sciences, University of Bristol, Bristol, UK
[d] Rosenstiel School of Marine and Atmospheric Science, University of Miami, Miami, USA
[e] Carnegie Institute for Science, Washington, USA
[f] IS Terre, Université de Savoie, Chambéry, France

ARTICLE INFO

Article history:
Received 19 July 2019
Received in revised form
24 September 2019
Accepted 5 October 2019
Available online 2 November 2019

Keywords:
Young's modulus
Elastic moduli
Mogi
Elastic half-space
Volcanic rock
Upscaling

ABSTRACT

The accuracy of elastic analytical solutions and numerical models, widely used in volcanology to interpret surface ground deformation, depends heavily on the Young's modulus chosen to represent the medium. The paucity of laboratory studies that provide Young's moduli for volcanic rocks, and studies that tackle the topic of upscaling these values to the relevant lengthscale, has left volcano modellers ill-equipped to select appropriate Young's moduli for their models. Here we present a wealth of laboratory data and suggest tools, widely used in geotechnics but adapted here to better suit volcanic rocks, to upscale these values to the scale of a volcanic rock mass. We provide the means to estimate upscaled values of Young's modulus, Poisson's ratio, shear modulus, and bulk modulus for a volcanic rock mass that can be improved with laboratory measurements and/or structural assessments of the studied area, but do not rely on them. In the absence of information, we estimate upscaled values of Young's modulus, Poisson's ratio, shear modulus, and bulk modulus for volcanic rock with an average porosity and an average fracture density/quality to be 5.4 GPa, 0.3, 2.1 GPa, and 4.5 GPa, respectively. The proposed Young's modulus for a typical volcanic rock mass of 5.4 GPa is much lower than the values typically used in volcano modelling. We also offer two methods to estimate depth-dependent rock mass Young's moduli, and provide two examples, using published data from boreholes within Kīlauea volcano (USA) and Mt. Unzen (Japan), to demonstrate how to apply our approach to real datasets. It is our hope that the data and analysis presented herein will assist in the selection of elastic moduli for volcano modelling. To this end, we provide a Microsoft Excel© spreadsheet containing the data and necessary equations to calculate rock mass elastic moduli that can be updated when new data become available. The selection of the most appropriate elastic moduli will provide the most accurate model predictions and therefore the most reliable information regarding the unrest of a particular volcano or volcanic terrain.

1. Introduction

The ascent of magma from depth towards the Earth's surface is inevitably associated with crustal deformation, often detectable by various geodetic techniques such as the global positioning system (GPS) or interferometric synthetic aperture radar (InSAR). Understanding and modelling the surface deformation signals accompanying magma migration is a key component of modern volcanology, as it provides one of the principal tools by which we can interpret deformation patterns and evaluate the potential for future volcanic activity. Elastic analytical solutions and numerical models are widely used in volcanology to interpret ground deformation signals detected at the surface (e.g., Amelung et al., 2000; Bazargan and Gudmundsson, 2019). Fundamentally, these models are underpinned by the elastic moduli of the volcanic medium. For example, the inflation and/or deflation of a magma body is often modelled as a pressurised spherical cavity within a homogeneous elastic half-space. With the assumption that the chamber is subject to uniform internal pressure, an approximate solution to this problem is given by McTigue (1987), equivalent to the point-source approximation popularised by Mogi (1958). The so-called "Mogi model" (see Fig. 1) describes vertical displacement above a spheri-

* Corresponding author.
E-mail address: heap@unistra.fr (M.J. Heap).

https://doi.org/10.1016/j.jvolgeores.2019.106684
0377-0273/

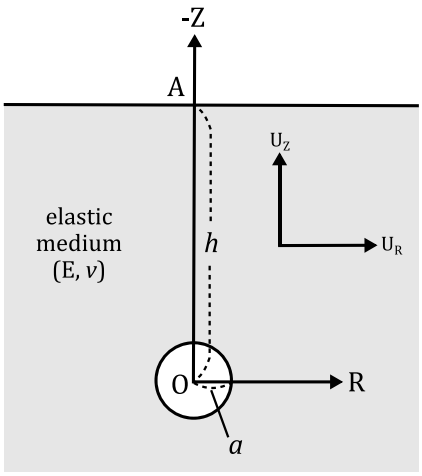

Fig. 1. Schematic diagram (redrawn from Mogi, 1958) showing a pressurised sphere (white circle) within a semi-infinite elastic body (in grey). U_Z and U_R are the displacements in the direction vertical and radial to the surface, respectively. a is the source radius, h is the source depth (from the surface, A, to the centre of the sphere, O), and E and ν are the Young's modulus and Poisson's ratio of the elastic medium, respectively.

cal source in an elastic half-space, and may be cast in terms of either a pressure change (Eq. (1a)) or a volumetric change (Eq. (1b)):

$$Uz_{max} = \Delta P \frac{a^3}{h^2} \frac{2(1-\nu^2)}{E} \quad (1a)$$

$$Uz_{max} = \frac{\Delta V}{\pi} \frac{(1-\nu)}{h^2} \quad (1b)$$

where ΔP is the source overpressure (overpressure is defined as the pressure above lithostatic pressure), a is the source radius, h is the source depth, and E and ν are the Young's modulus (the ratio of stress to strain) and Poisson's ratio (the ratio of transverse strain to axial strain) of the elastic medium, respectively. The source volume change of an incompressible magma source in an elastic medium is related to pressure change as a function of both E and ν such that $\Delta V = \pi \Delta P a^3 \left[(1-\nu)/E\right]$, making Eqs. (1a) and (1b) equivalent. Eq. (1a) shows that the pressure change inferred from the inversion of geodetic data depends on the Young's modulus and Poisson's ratio of the elastic medium. Eq. (1b) shows that the volume changes of a pressure source or magma body, ΔV, can be inferred without constraints on the Young's modulus of the half-space. However, the sought-after parameter is often the source or magma body overpressure, ΔP, which depends heavily on the chosen Young's modulus, but less so on the chosen Poisson's ratio (Eq. (1a); Fig. 2a). Overpressure, ΔP, is of importance because failure of the host-rock followed by intrusion/eruption is considered to occur when the overpressure reaches a threshold value (e.g., Gudmundsson, 1988; Tait et al., 1989; Pinel and Jaupart, 2000; Grosfils, 2007; Albino et al., 2010; Gudmundsson, 2012; Albino et al., 2018). We also highlight that Mogi source modelling that assumes a viscoelastic half-space (e.g., Bonafede and Ferrari, 2009) often necessitates the bulk modulus, K, which represents the ratio of volumetric stresses and strains (i.e. the inverse of material compressibility). The Mogi model described above, which uses the concept of a "nucleus of strain", represents one type of analytical model and is primarily used to interpret surface deformation obtained from geodetic data. Another, the "cavity" or "two-dimensional hole" model, calculates the stresses at and away from the boundary of a finite-size magma body within an elastic half-space (see Gudmundsson, 2006). The tensile stresses calculated using cavity or two-dimensional hole models also depend heavily on the elastic moduli used to describe the half-space (e.g., Gudmundsson and Brenner, 2004; Gudmundsson, 2006).

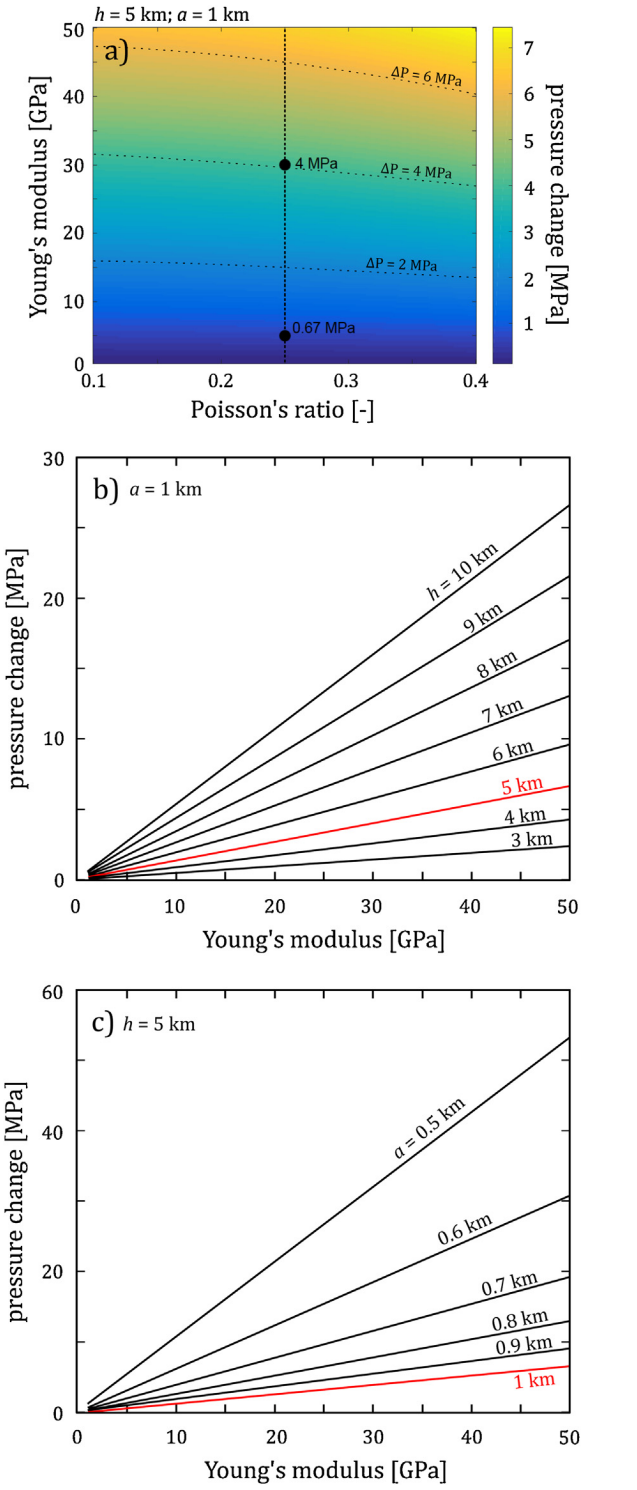

Fig. 2. Effect of the elastic parameters on the pressure change inferred inside a spherical magmatic source assuming a unit vertical displacement of 1 cm. (a) Pressure change as a function of elastic parameters, Young's modulus and Poisson's ratio. The source has a fixed depth, h =5 km, and a fixed radius, a = 1 km. The two black dots mark the pressure change for a Poisson's ratio of 0.25 and Young's moduli of 5 (leading to a pressure change of 0.67 MPa) and 30 GPa (leading to a pressure change of 4 MPa). (b) Pressure change as a function of Young's modulus for a fixed source radius (a = 1 km) and source depths ranging from 3 to 10 km. Red line (h =5 km) corresponds to the data plotted in panel (a). (c) Pressure change as a function of Young's modulus for a fixed source depth (h =5 km) and source radii ranging from 0.5 to 1 km. Red line (a = 1 km) corresponds to the data plotted in panel (a). (For interpretation of the references to colour in this figure legend, the reader is referred to the web version of this article).

A second commonly modelled scenario is the intrusion of a dyke. The importance of the elastic properties of the host rock for dyke propagation has been highlighted in experimental studies (e.g., Kavanagh et al., 2006; Taisne et al., 2011; Kavanagh et al., 2013, 2018), and they are required in numerical models designed to study, for example, dyke overpressure and the propensity for dyke propagation or stalling (e.g., Taisne and Jaupart, 2009; Maccaferri et al., 2010; Gudmundsson, 2011; Rivalta et al., 2015). Numerical modelling has shown that dyke-induced surface stresses, the depth of the dyke tip, and the displacement measured on the surface depend very much on the chosen Young's moduli for the edifice-forming layers (Bazargan and Gudmundsson, 2019). Recently, numerical models that require values of Young's modulus have also been used to better understand the origin of tilt signals at Tungurahua volcano, Ecuador (Neuberg et al., 2018; Marsden et al., 2019).

Even in the simplest case (the Mogi model), poorly selected values of the relevant Young's modulus can result in drastic differences in the estimated source parameters. We illustrate this in Fig. 2. First, we show in Fig. 2a, for a pressure source with a radius of 1 km and a depth of 5 km, that the calculated pressure change would be 0.67 and 4 MPa if the Young's modulus of the medium were set at 5 and 30 GPa, respectively (for a Poisson's ratio of 0.25). Fig. 2b and c show how the Young's modulus can influence the calculated pressure change in more detail. Fig. 2b shows the pressure change as a function of the Young's modulus of an elastic medium containing a spherical magmatic source (with a fixed radius of 1 km) for different source depths, ranging from 3 to 10 km, and Fig. 2c shows the pressure change as a function of the Young's modulus at a fixed depth of 5 km for different source radii, ranging from 0.5 to 1 km. Fig. 2 highlights the first-order control of the Young's modulus on the pressure source characteristics, and therefore the accuracy of the model predictions (e.g., eruption forecasting) very much rests on the accuracy of the Young's modulus (or Young's moduli if a layered medium is considered) used to describe the elastic medium.

In reviewing the methods typically used to ascertain the elastic properties of a given elastic half-space (using a sample of 50 papers that focus on ground deformation modelling; Table 1), we note a very wide range of Young's modulus was used in the sampled studies, spanning about three orders of magnitude (from 0.1 to 90), while a Poisson's ratio of 0.25 was used in the majority of the studies. Of these 50 papers, ten did not provide the Young's modulus used in their modelling (Table 1), although we note that Young's modulus is not required for studies interested in calculating volume changes only. Half of the papers either did not state the elastic properties they used or stated that "standard values" were used without any further justification or reference (Table 1). The remaining studies used one of three methods to help guide their choice of elastic properties. The most common method (used in eight of the sampled studies; Table 1) is to derive the Young's modulus from seismic wave velocities using local tomography surveys (e.g., Ellis et al., 2007; Grandin et al., 2010; Masterlark et al., 2012; Wauthier et al., 2015; Albino et al., 2018):

$$E_d = {V_p}^2 \rho_r \frac{(1-2\nu)(1+\nu)}{(1-\nu)} \quad (2)$$

where E_d is referred to as the "seismic Young's modulus" (also referred to as the "dynamic Young's modulus"), V_p is the measured P-wave velocity, and ρ_r the density of the host rock. Although tomography surveys are increasingly available for active volcanoes, a major limitation of this method is that moduli calculated using elastic wave velocities are associated with a sampling frequency much higher (on the order of seconds) than the duration of the modelled volcanic processes (days to years). The elastic moduli determined using laboratory deformation data (stress and strain; often called the "static Young's modulus") are considered more appropriate when modelling crustal scale processes that are characterised by a propagation or displacement rate slower than several kilometres per second (e.g., Gudmundsson (2011) and references therein). Manconi et al. (2010), for example, highlighted the absence of available elastic moduli determined using laboratory deformation data for tuff from Campi Flegrei (Italy) as one of the potential limitations of their study. Elastic moduli determined from elastic wave velocities (high sampling frequency) are typically higher than those determined from laboratory stress-strain data (low sampling frequency) (e.g., Cheng and Johnston, 1981; Eissa and Kazi, 1988; Ciccotti and Mulargia, 2004; Gudmundsson, 2011; Martínez-Martínez et al., 2012), even at effective pressures (assuming a simple effective pressure law where the effective pressure is simply the confining pressure minus the pore fluid pressure) as high as 130 MPa (Blake et al., 2019). Therefore, because moduli measured using laboratory stress-strain data are considered more relevant for modelling volcanic processes (e.g., Manconi et al., 2010), a correction factor or a frequency dependence relationship is necessary to convert the moduli inferred from seismic waves to the moduli required for modelling. Unfortunately, there is no universal correction factor. Laboratory experiments indicate that this correction factor could vary between 0.25 and 1, depending on the confining pressure, pore fluid pressure, and microcrack density (e.g., Cheng and Johnston, 1981; Gudmundsson, 1990; Adelinet et al., 2010). A second strategy, used in a limited number of papers (four of the studies sampled; Table 1), consists of deriving elastic parameters from the modelling of long-term ground deformation (crust loading/unloading) related to ice-cap retreat or aquifer recharge. In such cases, the model used—a surface point load—has fewer variables than the models of magmatic sources and permits the estimation of the elastic parameters. This method has been mainly used for volcanoes in Iceland, where surface ground displacements caused by the variations of ice-cap thickness during the year can be modelled to derive the crustal Young's modulus (e.g., Grapenthin et al., 2006; Pinel et al., 2007; de Zeeuw-van Dalfsen et al., 2012). However, the extent of this approach is limited as it requires a crustal deformation signal independent from volcanic processes and very accurate geodetic data (in both time and space). A third and final approach uses elastic properties taken from experimental studies on rock samples and is used in seven of the studies sampled (Table 1). However, this method suffers from scaling issues: the mechanical properties of a laboratory rock sample (typically cylinders that have a diameter between 10 and 50 mm; i.e. sample volumes between ~1.5 and ~200 cm^3) are measured on a lengthscale shorter than the macroscopic fracture spacing (i.e. laboratory measurements are made on nominally intact materials). Laboratory-derived elastic moduli will therefore, in most circumstances, grossly overestimate the Young's modulus of a rock mass. Only one paper in our sample, by Holohan et al. (2011), clearly refers to a study that considers the elastic properties of a rock mass (the work of Schultz, 1996). We additionally note that elastic analytical solutions and numerical models often assume a uniform and constant Young's modulus for the entire medium. Although such models necessitate a degree of simplification, and models that assume a constant Young's modulus have provided valuable insight, the mechanical properties of a volcanic edifice vary in space and time. Manconi et al. (2007) found, for example, that using layers characterised by different elastic moduli can significantly affect the pattern of vertical and radial displacements (see also, for example, Crescentini and Amoruso, 2007; Geyer and Gottsmann, 2010; Hautmann et al., 2010; Bazargan and Gudmundsson, 2019) and studies by Carrier et al. (2015) and Got et al. (2017) adopted a model in which the elastic parameters of the medium varied as a function of the observed seismicity rate to help explain the observed surface displacements at Piton de la Fournaise (La Réunion, France) and Grimsvötn volcano (Iceland), respectively.

Table 1
Summary of the elastic parameters, and their justification, used in 50 volcano modelling papers.

Reference	Context	Volcano	Young's modulus (GPa)	Poisson's ratio (-)	Shear modulus (GPa)	Constraints
Yun et al. (2006)	reservoir	Sierra Negra (Galapagos)	75	0.25	30	No justification
Jónsson et al. (2005)	reservoir	Sierra Negra (Galapagos)	25-37.5	0.25	10-15	No justification
Jónsson (2009)	reservoir	Sierra Negra (Galapagos)	25	0.25	10	Laboratory values (Rubin and Pollard, 1987)
Bagnardi et al. (2013)	reservoir	Fernandina (Galapagos)	25	0.25	10	Laboratory values (Jónsson, 2009; Rubin and Pollard, 1987)
Baker and Amelung (2012)	reservoir	Kīlauea (Hawai'i)	75	0.25	30	No justification (volume calculation)
Amelung et al. (2007)	reservoir	Mauna Loa (Hawai'i)	Not mentioned	Not mentioned	Not mentioned	No justification (volume calculation)
Davis (1986)	reservoir	Kīlauea (Hawai'i)	0.75	0.25	0.3	"Substantially less than the seismic modulus"
Pagli et al. (2006)	reservoir	Askja (Iceland)	75	0.25	30	No justification (volume calculation)
De Zeeuw van Dalfsen et al. (2012)	reservoir	Askja (Iceland)	30	0.25	12	Ice load variation (Pinel et al., 2007; Grapenthin et al., 2006)
Grapenthin et al. (2010)	reservoir	Hekla (Iceland)	40	0.25	16	Ice load variation (Grapenthin et al., 2006)
Pinel et al. (2007)	reservoir	Katla (Iceland)	24-34	0.25	9.6-13.6	Ice load variation
Cayol and Cornet (1998a)	reservoir	Mt. Etna (Italy)	Not mentioned	0.21	Not mentioned	No justification (volume calculation)
Lundgren et al. (2003)	reservoir	Mt. Etna (Italy)	75	0.25	30	No justification (volume calculation)
Obrizzo et al. (2004)	reservoir	Mt. Etna (Italy)	25	0.25	10	No justification
Palano et al. (2008)	reservoir	Mt. Etna (Italy)	75	0.25	30	"Typical value of crustal rigidity which is found to be an average rigidity value for Etna"
Todesco et al. (2004)	reservoir	Campi Flegrei (Italy)	12.5	Not mentioned	5	No justification
Elsworth et al. (2008)	reservoir	Soufriere Hills (Montserrat)	7.5	0.25	3	No justification (volume calculation)
Masterlark et al. (2012)	reservoir	Okmok (Aleutian Islands)	3D distribution	0.29 (crust) and 0.15 (caldera)	20	Seismic velocities (Christensen and Mooney, 1995; Christensen, 1996; Wang, 2000; Masterlark et al., 2010)
Delgado et al. (2014)	reservoir	Hudson (Chile)	25	0.25	10	Fractured crust (Segall, 2010)
Galgana et al. (2014)	reservoir	Taal (Philippines)	75 (crust) and 12.5 (reservoir)	0.25	30 (crust) and 5 (caldera fill)	Previous work (Bonafede, 1986; Masters and Shearer, 1995)
Grosfils (2007)	reservoir	Model	60	0.25	24	"average value" (Newman et al., 2001; Gudmundsson, 2002)
Ellis et al. (2007)	reservoir	Taupō (New Zealand)	75 (crust) and 12.5 (caldera fill)	0.25	30 (crust) and 5 (caldera fill)	Seismic data (Newman et al., 2006)
Newman et al. (2006)	reservoir	Long Valley (USA)	12.5	0.25	5	Previous work (Bonafede et al., 1986)
Bonafede et al. (1986)	reservoir	Campi Flegrei (Italy)	25	0.25	10	No justification
Holohan et al. (2011)	reservoir	Model (elastic and frictional)	0.7-12.9	0.15-0.25	0.3-5.2	Scaled laboratory experiments (Schulz, 1996)
Folch and Martí (2004)	reservoir	Thermoelastic caldera model	60	0.25	24	No justification
Nakao et al. (2013)	reservoir	Shinmoedake (Japan)	Not mentioned	Not mentioned	Not mentioned	No justification (volume calculation)
Lu et al. (2000)	reservoir	Westdahl (Aleutian Islands)	Not mentioned	Not mentioned	Not mentioned	No justification (volume calculation)
Peltier et al. (2009)	reservoir	Whakaari (New Zealand)	30	0.25	12	No justification (Cayol and Cornet, 1997)
Newman et al. (2012)	reservoir	Santorini (Greece)	Not mentioned	Not mentioned	Not mentioned	No justification (volume calculation)
Bagnardi and Amelung (2012)	reservoir and intrusion	Fernandina (Galapagos)	Not mentioned	0.25	Not mentioned	No justification (volume calculation)
Bagnardi et al. (2014)	reservoir and dyke	Kīlauea (Hawai'i)	Not mentioned	0.25	Not mentioned	No justification (volume calculation)
Puglisi and Bonforte (2004)	reservoir and dyke and sill	Mt. Etna (Italy)	Not mentioned	Not mentioned	Not mentioned	No justification
Hautmann et al. (2013)	reservoir and dyke	Soufriere Hills (Monserrat)	25	0.25	10	Seismic velocities and dynamic/static correction (Paulatto et al., 2010; Wang, 2000)
Ukawa et al. (2006)	reservoir and sill	Iwo-jima (Japan)	Not mentioned	Not mentioned	Not mentioned	No justification
Nishimura et al. (2001)	reservoir and faults	Miyakejima (Japan)	Not mentioned	Not mentioned	Not mentioned	No justification (volume calculation)

Table 1 (*Continued*)

Reference	Context	Volcano	Young's modulus (GPa)	Poisson's ratio (-)	Shear modulus (GPa)	Constraints
Wauthier et al. (2013)	shallow dyke	Nyamulagira (DR of Congo)	5	0.25	2	Seismic velocities and dynamic/static correction (Cheng and Johnson, 1981; Mavonga, 2010)
Wauthier et al. (2012)	shallow dyke	Nyiragongo (DR of Congo)	5	0.25	2	Seismic velocities and dynamic/static correction (Cheng and Johnson, 1981; Mavonga, 2010)
Wauthier et al. (2015)	deep dyke	Nyamulagira (DR of Congo)	90	0.25	36	Seismic velocities and dynamic/static correction (Cheng and Johnson, 1981; Mavonga, 2010)
Fukushima et al. (2005)	dyke	Piton de la Fournaise (La Reunion, France)	5	0.25	2	Laboratory values (Cayol and Cornet, 1998)
Cayol and Cornet (1998b)	dyke	Piton de la Fournaise (La Reunion, France)	5	0.25	2	Laboratory values (van Herdeen, 1987; Cheng and Johnston, 1981)
Jousset et al. (2003)	dyke	Usu volcano (Japan)	75	0.25	30	No justification (volume calculation)
Bonaccorso and Davis (1999)	conduit	Mt. Etna (Italy) and Mt. St. Helens (USA)	0.1 (fill material)	0.25	0.04 (fill material)	Previous work (Davis et al., 1974; Rubin and Pollard, 1988; Bonaccorso, 1996; Chadwick et al., 1988)
Chadwick et al. (1988)	conduit	Mt. St. Helens (USA)	1 (crust) and 0.1 (crater fill)	0.25	0.4 (crust) and 0.04 (crater fill)	Rock/soil properties (Vyalov, 1986; Birch, 1966; Oddsson, 1981)
Anderson et al. (2010)	conduit	Mt. St. Helens (USA)	1	0.25	0.4	Previous work (Chadwick et al., 1988)
Grandin et al. (2010)	rift	Mando-Hararo (Ethiopia)	30	0.25	12	Seismic velocities (Berckhemer et al., 1975; Stein et al., 1991; Touloukian, 1981)
Hamling et al. (2009)	rift	Dabbahu (Ethiopia)	80	0.25	32	No justification
Keir et al. (2011)	rift	Afar (Ethiopia)	75	0.25	30	No justification
Cayol and Cornet (1997)	circular horizontal fracture	model (mixed BEM)	50	0.21	20	Laboratory values (Touloukian, 1981)
Beauducel et al. (2000)	volcano model	Merapi (Indonesia)	30	0.25	12	No justification

We consider that our review of the modelling literature does not reflect a lack of will or understanding on the part of the authors of these studies, but rather highlights the paucity of studies that (1) provide laboratory-derived Young's moduli for volcanic rocks (from stress-strain data) and (2) tackle the topic of upscaling these values to the relevant lengthscale: the "volcano scale". It is clear that there is a need for a study that not only provides a large dataset of Young's moduli derived from laboratory experiments performed on different types of volcanic rocks (compiled datasets for the elastic properties of rocks (e.g., Gudmundsson, 2011; Schön, 2015) highlight that rock physical property measurements are typically biased towards sedimentary rocks and that few data exist for volcanic rocks), but also a user-friendly method (i.e. a method that can be improved with detailed prior information, such as the porosity or the structure of the volcanic rock mass in question, but does not demand it) with which these data can be upscaled to the volcano lengthscale. The selection of the most appropriate elastic moduli will, in turn, provide the most accurate model predictions and therefore the most reliable information regarding the unrest of a particular volcano or volcanic terrain.

We will focus here on providing values of Young's modulus for volcano modelling, due to its aforementioned importance (Eq. (1a); Fig. 2). This review paper is structured to first discuss the influence of various parameters (porosity, rock type, microcrack density, pore shape, alteration, temperature, confining pressure, water-saturation, and strain rate) on the Young's modulus determined using laboratory stress-strain data (on the lengthscale of a laboratory sample). In the interests of self-consistency and comparability, this contribution will largely focus on measurements made in the laboratory at the University of Strasbourg (France). We will then present a method, which takes into account the structural state of a rock mass, to upscale the Young's moduli measured in the laboratory: the Hoek-Diederichs equation (Hoek and Diederichs, 2006), a tool borrowed from the geotechnical toolbox. We then outline how this method, and our dataset, can be used to derive values of elastic moduli (Young's modulus, Poisson's ratio, shear modulus, and bulk modulus) for the modelling of volcanic systems, even when the *a priori* knowledge of the rock characteristics or rock mass structure is zero or almost zero. We then present two methods to estimate depth-dependent elastic moduli. We also provide two examples, using published data from boreholes within Kīlauea volcano (Hawai'i, USA) and Mt. Unzen (Japan), to demonstrate how to apply our approach to real datasets. Finally, we outline the limitations of our approach and possible directions for further improvements. A Microsoft Excel© spreadsheet containing the data and necessary equations to calculate rock mass elastic moduli accompanies this contribution as Supplementary Material. This spreadsheet, and the aforementioned equations, can therefore be easily updated when new data become available.

2. Factors influencing Young's modulus on the sample lengthscale

The experimental data that form the basis of this study are unpublished values of Young's modulus calculated from 276 uniaxial compression experiments performed on volcanic rocks in the laboratory at the University of Strasbourg. To ensure self-consistency and maximise comparability, we chose here to restrict our analysis to measurements performed using the same deformation apparatus and, importantly, to measurements of Young's

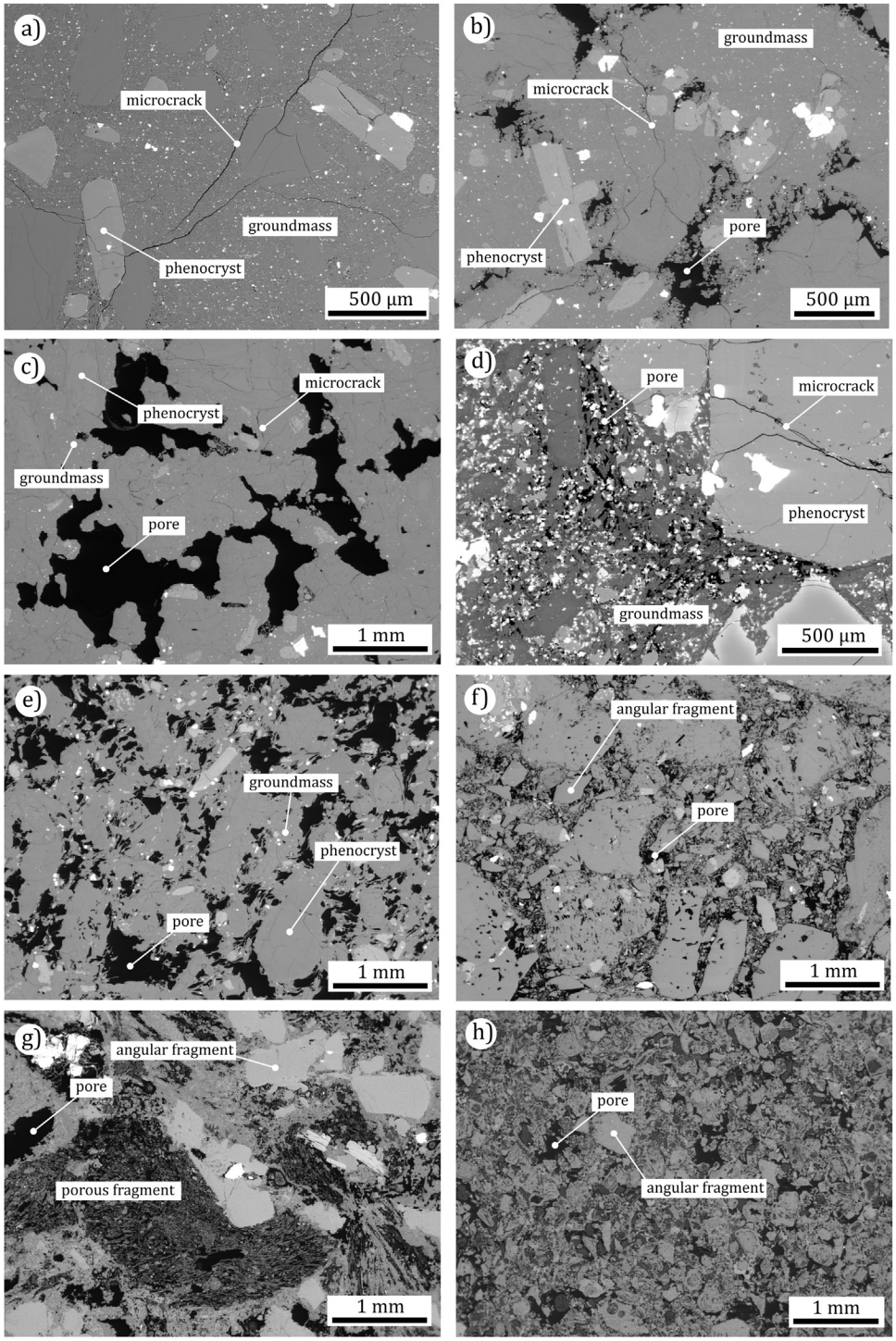

Fig. 3. Backscattered scanning electron images of selected rock types from this study, highlighting the variability in the microstructure of volcanic rocks. Black in the images represents void space (pores and microcracks) (a) Low-porosity andesite from Volcán de Colima (Mexico). (b) Medium-porosity andesite from Volcán de Colima. (c) High-porosity andesite from Volcán de Colima. (d) Low-porosity basalt from Mt. Etna (Italy). (e) High-porosity dacite from Mt. St. Helens (USA). (f) High-porosity welded block-and-ash flow (BAF) from Mt. Meager (Canada). (g) High-porosity tuff from Mt. Epomeo (Italy). (h) High-porosity tuff from Whakaari volcano (New Zealand).

modulus determined using the same method. The dataset includes dacites, andesites, basalts, tuffs, and welded pyroclastic rocks. Although the Young's modulus from these experiments is, for the most part, unreported, the mechanical data typically originate from published works. The samples originate from the following volcanoes/volcanic areas: Mt. St. Helens (USA; Heap et al., 2016), Chaos Crags (Lassen National Park, USA), Volcán de Colima (Mexico; Heap et al., 2014a, 2015a, 2018a), Gunung Merapi (Indonesia; Kushnir et al., 2016), Whakaari/White Island volcano (New Zealand; Heap et al., 2015b), Mt. Ruapehu (New Zealand; Farquharson et al., 2019), the Kumamoto prefecture (Japan), Kick 'em Jenny volcano (Grenada, Lesser Antilles; Dondin et al., 2017), Mt. Etna (Italy; Zhu et al., 2016), Stromboli (Italy), Krafla (Iceland, from the 1975-84 fissure eruption), Volvic (Chaîne des Puys, France), Campi Flegrei (Italy; Heap et al., 2018b), Mt. Epomeo (Italy; Marmoni et al., 2017; Heap et al., 2018c), and Mt. Meager (Canada; Heap et al., 2015c).

Backscattered scanning electron microscope (SEM) images of select samples, showing the range of microstructures and microtextures, are provided in Fig. 3.

The connected porosities, ϕ, of the samples (cylinders with a diameter of 20 or 25 mm and a nominal length of 40 or 60 mm, respectively) were first measured using either the triple weight water saturation technique or helium pycnometry. The triple weight method requires the dry and wet mass of the sample (m_{dry} and m_{sat}, respectively), and the wet mass of the sample while submerged in water, m_{sub} (see Guéguen and Palciauskas, 1994), such that:

$$\phi = \frac{m_{sat} - m_{dry}}{m_{sat} - m_{sub}} \quad (3)$$

The samples were dried in a vacuum oven at 40 °C for at least 48 h prior to the measurement of dry mass. To saturate the samples, vacuumed-dried samples were placed inside a belljar that was vacuumed for at least 12 h before degassed deionised water (using a Venturi siphon with municipal water as the motive fluid) was introduced into the belljar whilst under vacuum. For the helium pycnometry method, connected porosities were calculated using the skeletal (connected) volume of the sample measured by the helium pycnometer, V_{pyc}, and the bulk volume of the sample determined from the sample dimensions, V_b:

$$\phi = 1 - \frac{V_{pyc}}{V_b} \quad (4)$$

The samples were dried in a vacuum oven at 40 °C for at least 48 h prior to their measurement in the pycnometer.

The samples were then deformed in a uniaxial loadframe (Fig. 4a; $\sigma_1 > 0$ MPa; σ_2 and $\sigma_3 = 0$ MPa; where σ_1, σ_2, and σ_3 are the maximum, intermediate, and minimum principal compressive stresses, respectively) at a constant strain rate of 1.0×10^{-5} s^{-1} until macroscopic failure. We consider compressive stresses and strains as positive. Samples were either deformed dry (i.e. oven-dried for at least 48 h in a vacuum at 40 °C) or wet (i.e. vacuum-saturated in deionised water). Wet samples were deformed inside a deionised water bath (Fig. 4a). A lubricating wax was applied to the end-faces of the dry samples to avoid problems associated with friction between the sample and the pistons during loading. We consider that the permeabilities of the saturated (wet) samples were high enough to avoid problems of desaturation during deformation at the imposed strain rate (i.e. the samples were "drained"; see Heap and Wadsworth, 2016). All experiments were conducted at ambient laboratory temperatures. During deformation, axial load and axial displacement were measured using a load cell and a linear variable differential transducer (LVDT), respectively (Fig. 4a). These measurements were converted to axial stress and axial strain using the sample dimensions. The axial displacement associated with the deformation of the load chain was removed from the measured values. The Young's modulus was taken as the slope of the uniaxial stress-strain curve within the linear elastic portion of the curve (Fig. 4b). This method provides the Young's modulus of volcanic rock on the sample lengthscale, referred to in this paper as the "intact" Young's modulus, E_i. "Intact" refers here to the absence of macrofractures within the laboratory sample, rather than the absence of natural microscale defects (e.g., microcracks).

However, there are many parameters that can influence the E_i of volcanic rock, including porosity, rock type, microcrack density, pore geometry, alteration, temperature, confining pressure, water-saturation, and strain rate. The influence of each of these parameters will now be reviewed in turn (using a combination of data unique to this study and, where needed, previously published data from the literature).

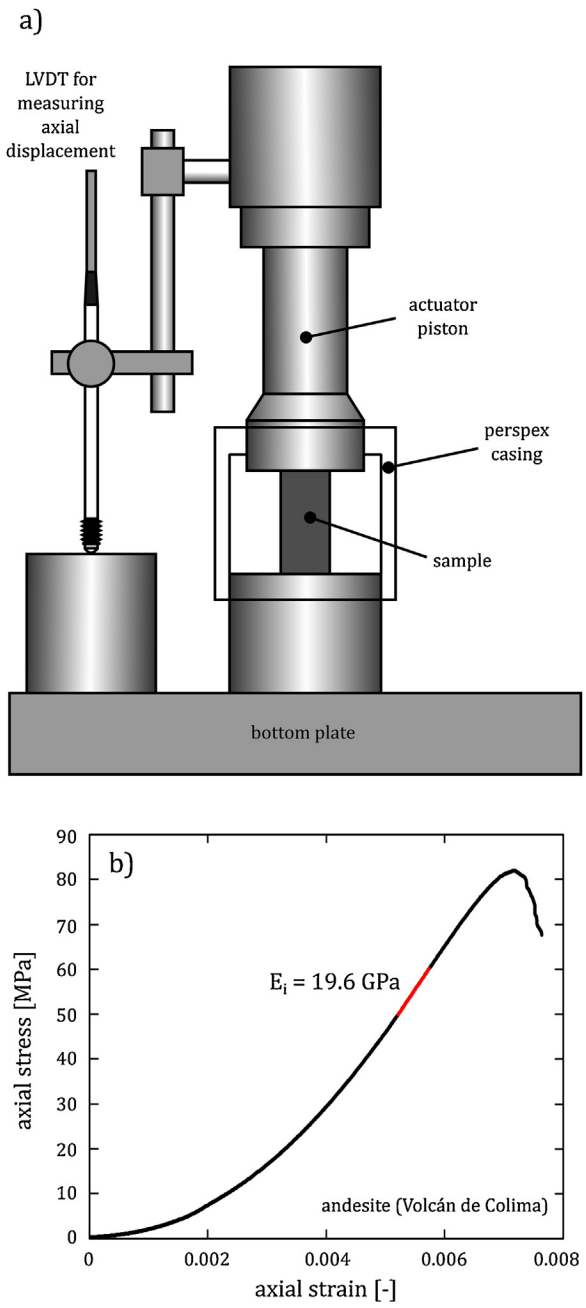

Fig. 4. (a) A schematic diagram of the uniaxial compressive loading apparatus at the University of Strasbourg. LVDT—linear variable differential transducer. (b) A uniaxial stress-strain curve for a sample of andesite from Volcán de Colima (Mexico). The intact Young's modulus was determined from the elastic portion of the curve (shown in red). (For interpretation of the references to colour in this figure legend, the reader is referred to the web version of this article).

2.1. The influence of porosity on intact Young's modulus

The intact Young's modulus as a function of connected porosity for volcanic rocks is shown in Fig. 5 (data in Table 2). These data show that intact Young's modulus increases nonlinearly as porosity decreases, in agreement, for example, with data for sedimentary rocks (e.g., Wong et al., 1997; Chang et al., 2006; Heap et al., 2019a), dacites from Mt. Unzen (Coats et al., 2018), andesites from Soufrière Hills volcano (Montserrat) (Harnett et al., 2019), and basalts from Pacaya volcano (Guatemala) (Schaefer et al., 2015). Low-porosity volcanic rocks (porosity of 0.01–0.02) can have an intact Young's modulus as high as almost 50 GPa, while high-porosity (porosity of

Table 2
Summary of the experimental data (porosity and intact Young's modulus) used for this study.

Rock type	Volcano	Experimental condition	Porosity (-)	Intact Young's modulus (GPa)
andesite	Volcán de Colima (Mexico)	wet	0.07	17.2
andesite	Volcán de Colima (Mexico)	wet	0.07	17.6
andesite	Volcán de Colima (Mexico)	wet	0.07	19.4
andesite	Volcán de Colima (Mexico)	wet	0.07	17.1
andesite	Volcán de Colima (Mexico)	wet	0.07	17.4
andesite	Volcán de Colima (Mexico)	dry	0.07	19.2
andesite	Volcán de Colima (Mexico)	dry	0.07	20.2
andesite	Volcán de Colima (Mexico)	dry	0.07	20.5
andesite	Volcán de Colima (Mexico)	dry	0.07	19.6
andesite	Volcán de Colima (Mexico)	dry	0.07	20.0
andesite	Volcán de Colima (Mexico)	dry	0.21	7.8
andesite	Volcán de Colima (Mexico)	dry	0.21	7.9
andesite	Volcán de Colima (Mexico)	dry	0.22	7.1
andesite	Volcán de Colima (Mexico)	dry	0.22	6.8
andesite	Volcán de Colima (Mexico)	dry	0.22	6.8
andesite	Volcán de Colima (Mexico)	wet	0.22	8.3
andesite	Volcán de Colima (Mexico)	wet	0.21	8.9
andesite	Volcán de Colima (Mexico)	wet	0.22	6.8
andesite	Volcán de Colima (Mexico)	wet	0.23	7.1
andesite	Volcán de Colima (Mexico)	wet	0.22	7.1
andesite	Volcán de Colima (Mexico)	dry	0.10	21.8
andesite	Volcán de Colima (Mexico)	dry	0.11	20.3
andesite	Volcán de Colima (Mexico)	dry	0.12	18.5
andesite	Volcán de Colima (Mexico)	dry	0.09	23.9
andesite	Volcán de Colima (Mexico)	dry	0.08	19.9
andesite	Volcán de Colima (Mexico)	dry	0.08	19.7
andesite	Volcán de Colima (Mexico)	dry	0.08	21.1
andesite	Volcán de Colima (Mexico)	dry	0.08	20.4
andesite	Volcán de Colima (Mexico)	dry	0.09	26.7
andesite	Volcán de Colima (Mexico)	dry	0.08	28.7
andesite	Volcán de Colima (Mexico)	dry	0.09	30.2
andesite	Volcán de Colima (Mexico)	dry	0.10	33.1
andesite	Volcán de Colima (Mexico)	dry	0.18	5.6
andesite	Volcán de Colima (Mexico)	dry	0.18	9.7
andesite	Volcán de Colima (Mexico)	dry	0.18	10.9
andesite	Volcán de Colima (Mexico)	dry	0.18	7.2
andesite	Volcán de Colima (Mexico)	dry	0.25	9.0
andesite	Volcán de Colima (Mexico)	dry	0.25	9.3
andesite	Volcán de Colima (Mexico)	dry	0.25	10.8
andesite	Volcán de Colima (Mexico)	dry	0.25	10.9
andesite	Volcán de Colima (Mexico)	wet	0.18	7.4
andesite	Volcán de Colima (Mexico)	wet	0.08	19.7
andesite	Volcán de Colima (Mexico)	wet	0.12	16.9
andesite	Volcán de Colima (Mexico)	dry	0.08	18.5
andesite	Volcán de Colima (Mexico)	dry	0.08	19.3
andesite	Volcán de Colima (Mexico)	dry	0.08	16.9
andesite	Volcán de Colima (Mexico)	dry	0.08	17.2
andesite	Volcán de Colima (Mexico)	dry	0.08	17.7
andesite	Volcán de Colima (Mexico)	dry	0.07	19.7
andesite	Volcán de Colima (Mexico)	dry	0.09	18.7
andesite	Volcán de Colima (Mexico)	dry	0.08	19.7
andesite	Volcán de Colima (Mexico)	dry	0.08	19.8
andesite	Volcán de Colima (Mexico)	dry	0.07	17.0
andesite	Volcán de Colima (Mexico)	dry	0.08	20.0
andesite	Volcán de Colima (Mexico)	dry	0.08	19.4
andesite	Volcán de Colima (Mexico)	dry	0.08	20.4
andesite	Volcán de Colima (Mexico)	dry	0.09	19.5
andesite	Volcán de Colima (Mexico)	dry	0.07	18.0
andesite	Volcán de Colima (Mexico)	dry	0.08	19.6
andesite	Volcán de Colima (Mexico)	dry	0.08	20.2
andesite	Volcán de Colima (Mexico)	dry	0.07	20.5
andesite	Volcán de Colima (Mexico)	dry	0.07	19.8
andesite	Volcán de Colima (Mexico)	dry	0.08	17.2
andesite	Whakaari (New Zealand)	dry	0.07	35.4
andesite	Whakaari (New Zealand)	dry	0.08	30.9
andesite	Whakaari (New Zealand)	dry	0.08	28.0
andesite	Whakaari (New Zealand)	dry	0.08	25.7
andesite	Whakaari (New Zealand)	dry	0.02	38.2
andesite	Whakaari (New Zealand)	wet	0.05	21.3
andesite	Kick 'em Jenny (Lesser Antilles)	wet	0.14	23.2
andesite	Kick 'em Jenny (Lesser Antilles)	wet	0.14	18.0
andesite	Kick 'em Jenny (Lesser Antilles)	wet	0.12	10.2
andesite	Ruapehu (New Zealand)	wet	0.17	18.3
andesite	Ruapehu (New Zealand)	wet	0.19	19.4
andesite	Ruapehu (New Zealand)	wet	0.21	17.6
andesite	Ruapehu (New Zealand)	wet	0.14	20.7

Table 2 (*Continued*)

Rock type	Volcano	Experimental condition	Porosity (-)	Intact Young's modulus (GPa)
andesite	Ruapehu (New Zealand)	wet	0.13	19.5
andesite	Ruapehu (New Zealand)	wet	0.20	18.1
andesite	Ruapehu (New Zealand)	wet	0.16	23.0
andesite	Ruapehu (New Zealand)	wet	0.19	18.6
andesite	Ruapehu (New Zealand)	wet	0.19	16.3
andesite	Kumamoto (Japan)	dry	0.13	16.9
andesite	Kumamoto (Japan)	dry	0.13	16.6
andesite	Kumamoto (Japan)	dry	0.13	16.2
andesite	Kumamoto (Japan)	dry	0.14	19.0
andesite	Kumamoto (Japan)	dry	0.14	16.8
andesite	Kumamoto (Japan)	wet	0.13	12.6
andesite	Kumamoto (Japan)	wet	0.13	9.2
andesite	Kumamoto (Japan)	wet	0.13	9.4
andesite	Kumamoto (Japan)	wet	0.14	8.6
andesite	Kumamoto (Japan)	wet	0.14	9.5
basaltic-andesite	Merapi (Indonesia)	dry	0.24	8.9
basaltic-andesite	Merapi (Indonesia)	dry	0.23	9.0
basaltic-andesite	Merapi (Indonesia)	dry	0.25	6.3
basaltic-andesite	Merapi (Indonesia)	dry	0.09	28.1
basaltic-andesite	Merapi (Indonesia)	dry	0.08	29.2
basaltic-andesite	Merapi (Indonesia)	dry	0.09	27.0
basaltic-andesite	Merapi (Indonesia)	dry	0.19	18.3
basaltic-andesite	Merapi (Indonesia)	dry	0.18	20.0
basaltic-andesite	Merapi (Indonesia)	dry	0.19	14.3
basaltic-andesite	Merapi (Indonesia)	dry	0.16	15.0
basaltic-andesite	Merapi (Indonesia)	dry	0.15	17.5
basaltic-andesite	Merapi (Indonesia)	dry	0.18	14.6
basaltic-andesite	Merapi (Indonesia)	dry	0.08	27.8
basaltic-andesite	Merapi (Indonesia)	dry	0.09	24.8
basaltic-andesite	Merapi (Indonesia)	dry	0.08	27.8
basalt	Mt. Etna (Italy)	wet	0.05	26.1
basalt	Mt. Etna (Italy)	wet	0.05	25.1
basalt	Mt. Etna (Italy)	wet	0.05	26.0
basalt	Mt. Etna (Italy)	wet	0.05	26.0
basalt	Mt. Etna (Italy)	dry	0.05	31.4
basalt	Mt. Etna (Italy)	dry	0.05	30.8
basalt	Mt. Etna (Italy)	dry	0.05	29.0
basalt	Mt. Etna (Italy)	dry	0.05	29.2
basalt	Mt. Etna (Italy)	dry	0.05	31.5
basalt	Mt. Etna (Italy)	wet	0.10	18.7
basalt	Mt. Etna (Italy)	wet	0.07	18.3
basalt	Mt. Etna (Italy)	wet	0.14	16.1
basalt	Mt. Etna (Italy)	dry	0.10	19.7
basalt	Mt. Etna (Italy)	dry	0.14	16.2
basalt	Mt. Etna (Italy)	dry	0.14	17.0
basalt	Mt. Etna (Italy)	dry	0.15	16.6
basalt	Mt. Etna (Italy)	dry	0.12	15.1
basalt	Mt. Etna (Italy)	dry	0.14	14.0
basalt	Mt. Etna (Italy)	dry	0.15	15.0
basalt	Mt. Etna (Italy)	dry	0.12	14.9
basalt	Mt. Etna (Italy)	dry	0.13	13.9
basalt	Mt. Etna (Italy)	dry	0.12	14.9
basalt	Mt. Etna (Italy)	dry	0.12	16.0
basalt	Mt. Etna (Italy)	dry	0.04	36.9
basalt	Stromboli (Italy)	dry	0.13	27.3
basalt	Volvic (France)	wet	0.20	15.0
basalt	Volvic (France)	dry	0.20	17.1
basalt	Volvic (France)	wet	0.21	13.9
basalt	Volvic (France)	wet	0.20	14.4
basalt	Volvic (France)	wet	0.21	15.0
basalt	Volvic (France)	dry	0.21	15.4
basalt	Volvic (France)	wet	0.21	14.7
basalt	Volvic (France)	dry	0.20	16.8
basalt	Volvic (France)	dry	0.21	15.2
basalt	Volvic (France)	dry	0.21	16.1
basalt	Volvic (France)	wet	0.21	15.1
basalt	Volvic (France)	dry	0.21	16.1
basalt	Krafla (Iceland)	dry	0.39	10.0
basalt	Krafla (Iceland)	dry	0.40	9.8
basalt	Krafla (Iceland)	dry	0.40	10.3
basalt	Krafla (Iceland)	dry	0.40	10.4
basalt	Krafla (Iceland)	dry	0.40	9.4
basalt	Krafla (Iceland)	dry	0.42	9.1
basalt	Krafla (Iceland)	dry	0.43	9.8
basalt	Krafla (Iceland)	dry	0.39	9.9
dacite	Mt. St. Helens (USA)	wet	0.31	5.3
dacite	Mt. St. Helens (USA)	wet	0.37	2.3

Table 2 (*Continued*)

Rock type	Volcano	Experimental condition	Porosity (-)	Intact Young's modulus (GPa)
dacite	Mt. St. Helens (USA)	wet	0.22	9.3
dacite	Mt. St. Helens (USA)	wet	0.18	13.5
dacite	Chaos Crags (dome C) (USA)	dry	0.15	9.0
dacite	Chaos Crags (dome C) (USA)	dry	0.15	9.9
dacite	Chaos Crags (dome C) (USA)	dry	0.15	9.4
dacite	Chaos Crags (dome C) (USA)	dry	0.15	9.0
dacite	Chaos Crags (dome C) (USA)	dry	0.15	10.0
dacite	Chaos Crags (dome C) (USA)	dry	0.15	9.3
dacite	Chaos Crags (dome C) (USA)	dry	0.16	10.2
dacite	Chaos Crags (dome C) (USA)	dry	0.16	9.5
welded BAF	Mt. Meager (Canada)	dry	0.11	12.9
welded BAF	Mt. Meager (Canada)	dry	0.13	12.7
welded BAF	Mt. Meager (Canada)	dry	0.10	17.4
welded BAF	Mt. Meager (Canada)	dry	0.11	15.1
welded BAF	Mt. Meager (Canada)	dry	0.13	13.6
welded BAF	Mt. Meager (Canada)	dry	0.13	12.2
welded BAF	Mt. Meager (Canada)	dry	0.12	15.4
welded BAF	Mt. Meager (Canada)	dry	0.15	15.3
welded BAF	Mt. Meager (Canada)	dry	0.12	13.6
welded BAF	Mt. Meager (Canada)	dry	0.11	15.6
welded BAF	Mt. Meager (Canada)	dry	0.23	4.8
welded BAF	Mt. Meager (Canada)	dry	0.19	5.8
welded BAF	Mt. Meager (Canada)	dry	0.22	5.2
welded BAF	Mt. Meager (Canada)	dry	0.24	4.1
welded BAF	Mt. Meager (Canada)	dry	0.17	7.2
welded BAF	Mt. Meager (Canada)	dry	0.16	6.9
welded BAF	Mt. Meager (Canada)	dry	0.10	6.6
welded BAF	Mt. Meager (Canada)	dry	0.16	5.1
welded BAF	Mt. Meager (Canada)	dry	0.18	6.1
welded BAF	Mt. Meager (Canada)	dry	0.07	20.2
welded BAF	Mt. Meager (Canada)	dry	0.09	17.3
welded BAF	Mt. Meager (Canada)	dry	0.08	18.8
welded BAF	Mt. Meager (Canada)	dry	0.07	14.5
welded BAF	Mt. Meager (Canada)	dry	0.04	21.5
welded BAF	Mt. Meager (Canada)	dry	0.03	12.5
welded BAF	Mt. Meager (Canada)	dry	0.03	17.4
welded BAF	Mt. Meager (Canada)	wet	0.13	14.8
welded BAF	Mt. Meager (Canada)	wet	0.14	10.8
welded BAF	Mt. Meager (Canada)	wet	0.14	13.7
welded BAF	Mt. Meager (Canada)	wet	0.13	14.8
welded BAF	Mt. Meager (Canada)	wet	0.11	14.6
welded BAF	Mt. Meager (Canada)	wet	0.12	13.8
welded BAF	Mt. Meager (Canada)	wet	0.10	13.6
welded BAF	Mt. Meager (Canada)	wet	0.13	14.1
welded BAF	Mt. Meager (Canada)	dry	0.15	12.6
welded BAF	Mt. Meager (Canada)	dry	0.13	13.0
welded BAF	Mt. Meager (Canada)	wet	0.14	12.0
welded BAF	Mt. Meager (Canada)	wet	0.10	16.0
tuff	Campi Flegrei (Italy)	wet	0.46	1.3
tuff	Campi Flegrei (Italy)	dry	0.46	1.6
tuff	Campi Flegrei (Italy)	wet	0.44	1.5
tuff	Campi Flegrei (Italy)	dry	0.47	1.3
tuff	Campi Flegrei (Italy)	wet	0.47	1.1
tuff	Campi Flegrei (Italy)	dry	0.45	1.3
tuff	Campi Flegrei (Italy)	dry	0.46	1.6
tuff	Campi Flegrei (Italy)	wet	0.45	1.1
tuff	Campi Flegrei (Italy)	dry	0.45	1.8
tuff	Campi Flegrei (Italy)	wet	0.50	4.1
tuff	Campi Flegrei (Italy)	wet	0.50	4.1
tuff	Campi Flegrei (Italy)	wet	0.50	3.8
tuff	Campi Flegrei (Italy)	wet	0.50	4.1
tuff	Campi Flegrei (Italy)	dry	0.50	4.0
tuff	Campi Flegrei (Italy)	dry	0.50	4.0
tuff	Campi Flegrei (Italy)	dry	0.50	4.0
tuff	Campi Flegrei (Italy)	dry	0.50	3.2
tuff	Campi Flegrei (Italy)	dry	0.50	4.2
tuff	Campi Flegrei (Italy)	wet	0.47	1.1
tuff	Campi Flegrei (Italy)	wet	0.47	0.6
tuff	Campi Flegrei (Italy)	wet	0.46	1.2
tuff	Campi Flegrei (Italy)	wet	0.47	1.4
tuff	Campi Flegrei (Italy)	wet	0.46	1.2
tuff	Campi Flegrei (Italy)	wet	0.46	1.3
tuff	Campi Flegrei (Italy)	wet	0.45	0.5
tuff	Campi Flegrei (Italy)	wet	0.45	1.0
tuff	Campi Flegrei (Italy)	wet	0.46	0.6
tuff	Campi Flegrei (Italy)	dry	0.47	1.0
tuff	Campi Flegrei (Italy)	dry	0.45	1.4

Table 2 (*Continued*)

Rock type	Volcano	Experimental condition	Porosity (-)	Intact Young's modulus (GPa)
tuff	Campi Flegrei (Italy)	dry	0.46	1.3
tuff	Campi Flegrei (Italy)	dry	0.46	1.1
tuff	Campi Flegrei (Italy)	dry	0.45	1.1
tuff	Campi Flegrei (Italy)	dry	0.45	1.3
tuff	Campi Flegrei (Italy)	dry	0.45	1.5
tuff	Campi Flegrei (Italy)	dry	0.46	1.7
tuff	Campi Flegrei (Italy)	dry	0.50	1.3
tuff	Campi Flegrei (Italy)	dry	0.46	1.2
tuff	Mt. Epomeo (Italy)	dry	0.48	2.6
tuff	Mt. Epomeo (Italy)	wet	0.44	2.1
tuff	Mt. Epomeo (Italy)	wet	0.49	1.0
tuff	Mt. Epomeo (Italy)	dry	0.45	1.2
tuff	Mt. Epomeo (Italy)	dry	0.21	14.7
tuff	Mt. Epomeo (Italy)	dry	0.21	11.4
tuff	Mt. Epomeo (Italy)	wet	0.21	11.0
tuff	Mt. Epomeo (Italy)	dry	0.20	9.5
tuff	Mt. Epomeo (Italy)	dry	0.44	0.8
tuff	Mt. Epomeo (Italy)	dry	0.44	0.5
tuff	Whakaari (New Zealand)	wet	0.41	2.3
tuff	Whakaari (New Zealand)	dry	0.42	2.4
tuff	Whakaari (New Zealand)	wet	0.42	1.7
tuff	Whakaari (New Zealand)	dry	0.39	3.3
tuff	Whakaari (New Zealand)	wet	0.44	1.8
tuff	Whakaari (New Zealand)	dry	0.41	1.7
tuff	Whakaari (New Zealand)	dry	0.40	2.7
tuff	Whakaari (New Zealand)	dry	0.44	1.7
tuff	Whakaari (New Zealand)	dry	0.49	1.0
tuff	Whakaari (New Zealand)	dry	0.44	0.7
tuff	Whakaari (New Zealand)	dry	0.37	2.1
tuff	Whakaari (New Zealand)	dry	0.36	2.1
tuff	Whakaari (New Zealand)	dry	0.39	1.6
tuff	Whakaari (New Zealand)	wet	0.47	1.0
tuff	Whakaari (New Zealand)	dry	0.47	1.4
tuff	Whakaari (New Zealand)	wet	0.47	1.4
tuff	Whakaari (New Zealand)	dry	0.46	1.5
tuff	Whakaari (New Zealand)	wet	0.46	1.3
tuff	Whakaari (New Zealand)	dry	0.49	1.4
tuff	Whakaari (New Zealand)	dry	0.47	0.8
tuff	Whakaari (New Zealand)	dry	0.45	1.5
tuff	Whakaari (New Zealand)	wet	0.46	1.2
tuff	Whakaari (New Zealand)	wet	0.47	1.3
tuff	Whakaari (New Zealand)	wet	0.45	1.3
tuff	Whakaari (New Zealand)	wet	0.46	1.3
tuff	Whakaari (New Zealand)	dry	0.46	1.5
tuff	Whakaari (New Zealand)	dry	0.46	1.6
tuff	Whakaari (New Zealand)	wet	0.28	8.7

0.4–0.5) volcanic rocks are typically characterised by intact Young's moduli as low as only a couple of GPa (Fig. 5). We further highlight that there is a large degree of scatter within the overall trend of the data. For example, the intact Young's modulus for a volcanic rock with a porosity of 0.02 can vary from ~12 GPa up to ~40 GPa (Fig. 5). The scatter in these data for a given porosity is the result of microstructural differences (e.g., pore shape and size, porosity type (pores and microcracks), isolated porosity) (e.g., Fig. 3).

2.2. The influence of rock type on intact Young's modulus

The elastic properties of different rock-forming minerals are different (e.g., Anderson et al., 1968; Bass, 1995). Therefore, since different volcanic rock types can contain different minerals, and in different proportions, it is reasonable to assume that rock type will exert an influence on the elastic properties measured on the sample lengthscale. Fig. 6 also shows the intact Young's modulus as a function of connected porosity (i.e. the same graph as Fig. 5; data in Table 2), however, unlike Fig. 5, the data points are now grouped by rock type: dacite, andesite, basalt, tuff, and block-and-ash flow (a welded granular material of dacitic composition). It is

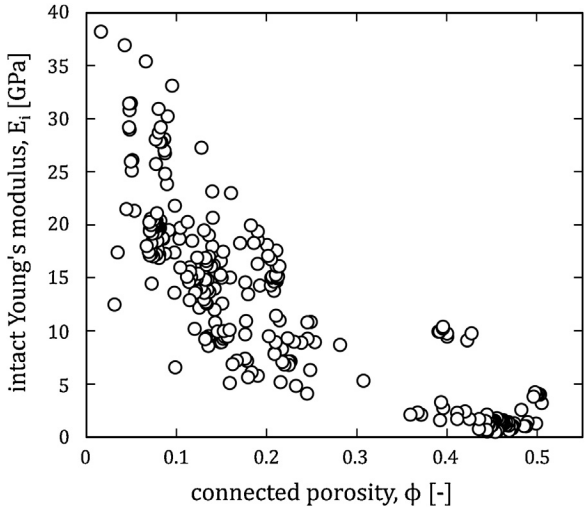

Fig. 5. The intact Young's modulus for various volcanic rocks (see Table 2) as a function of connected porosity.

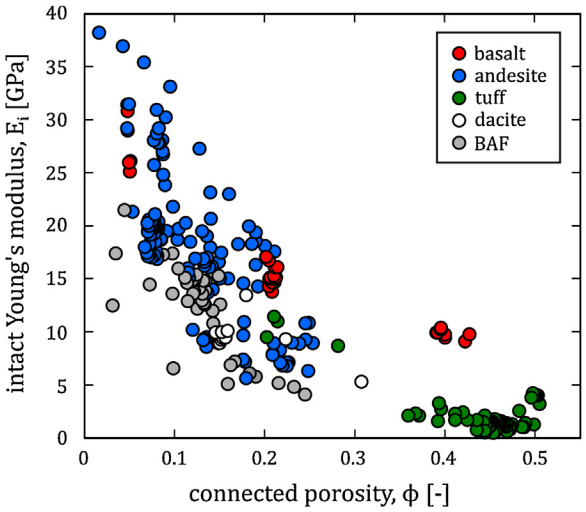

Fig. 6. The intact Young's modulus for various volcanic rocks (see Table 2) as a function of porosity. The data are separated by rock type: basalt (red symbols), andesite (blue symbols), tuff (green symbols), dacite (white symbols), and welded block-and-ash flow deposit (BAF; grey symbols). (For interpretation of the references to colour in this figure legend, the reader is referred to the web version of this article).

clear from the data in Fig. 6 that the Young's modulus of volcanic rock cannot be differentiated solely based on rock type (at least for the broad-stroke rock type classifications used herein). For example, the Young's modulus of andesite can vary from ~1 GPa up to almost 50 GPa (Fig. 6). This assertion agrees with data for sedimentary rocks: low- and high-porosity sandstones and limestones can be very stiff and very soft, respectively (e.g., Wong et al., 1997; Baud et al., 2000a; Vajdova et al., 2004; Chang et al., 2006; Baud et al., 2017; Heap et al., 2019a).

2.3. The influence of microcrack density on intact Young's modulus

It is well known that microcracks lower the Young's modulus of rock (e.g., Walsh, 1965a; Budiansky and OöConnell, 1976; Gudmundsson, 2011). The influence of microcrack density on the Young's modulus of volcanic rock has been investigated using cyclic stressing experiments (e.g., Heap et al., 2009, 2010; Kendrick et al., 2013; Schaefer et al., 2015; Cerfontaine and Collin, 2018). These experiments allow the Young's modulus of the same sample to be determined as a function of progressive damage (microcrack) accumulation. Mitchell and Faulkner (2012), for example, showed that the microcrack density increased from 3 to 15 mm^{-1} as granite was repeatedly cycled towards macroscopic failure. Fig. 7a shows the intact Young's modulus of a basalt from Mt. Etna as a function of increasing amplitude stress cycles (data from Heap et al., 2009). Heap et al. (2009) did not quantify the microcrack density as a function of cycle number and so Young's modulus is plotted as a function of cycle number in Fig. 7a (although it is assumed here that microcrack density increased with increasing cycle number). The sample (25 mm in diameter and 75 in length) was first loaded at a constant strain rate of 7×10^{-6} s^{-1} to a uniaxial stress of 20 MPa and then unloaded to 8 MPa at the same rate. The maximum stress was increased by 10 MPa in each subsequent cycle until the sample failed macroscopically. The results show that the Young's modulus of the basalt was reduced from ~32 GPa to ~23 GPa (a decrease of about 30%) with progressive pre-failure microcrack accumulation (Fig. 7a). Similar experiments performed on dacite from Mt. St. Helens also show that Young's modulus decreases with increasing microcrack accumulation (data from Kendrick et al., 2013; Fig. 7b), in accordance with other cyclic stressing experiments on volcanic rocks (e.g., Heap et al., 2010; Schaefer et al., 2015). A decrease in Young's modulus was also observed in dacites from Mt. St. Helens (Kendrick et al., 2013) and Mt. Unzen (Coats et al., 2018) and andesites from Volcán de Colima (Heap et al., 2014a) following thermal-stressing experiments (experiments designed to impart thermal microcrack damage into a rock sample).

2.4. The influence of pore geometry on intact Young's modulus

Volcanic rocks often contain pores that display a wide variety of geometric characteristics (e.g., Wright et al., 2009; Shea et al., 2010; Colombier et al., 2017). The stiffness of a volcanic rock containing elongated pores will depend on the orientation of the pore major axis relative to the loading direction (e.g., Bubeck et al., 2017; Griffiths et al., 2017). Bubeck et al. (2017), for example, showed that the intact Young's modulus of basalt samples (37 mm in diameter; deformed at a strain rate of 5×10^{-6} s^{-1}) from Kīlauea volcano was almost double when measured on cores prepared perpendicular to the flow direction (so that the pore major axis was subparallel to the loading direction). Griffiths et al. (2017) showed, using numerical modelling, that the Young's modulus of a sample with a porosity of 0.1 can vary between ~70 and ~28 GPa depending on the pore aspect ratio and the direction of the pore major axis relative to the loading direction. Despite the large effect documented in these studies (Bubeck et al., 2017; Griffiths et al., 2017), the anisotropy of Young's modulus in volcanic rocks remains largely unstudied in the laboratory and offers an inviting avenue for future research.

2.5. The influence of alteration on intact Young's modulus

The circulation of hydrothermal fluids can alter the rocks through which they pass (e.g., del Potro and Hürlimann, 2009; Pola et al., 2012; Wyering et al., 2014; Frolova et al., 2014; Mayer et al., 2016; Mordensky et al., 2019; Heap et al., 2019b). Depending on the style of alteration, alteration may increase or decrease the Young's modulus of volcanic rock (Frolova et al., 2014). Since porosity exerts a first-order influence on the Young's modulus of a volcanic rock (Fig. 5), pore- and microcrack-filling alteration (porosity decreasing alteration) increases the Young's modulus, while alteration leading to mineral dissolution (porosity increasing alteration) decreases the Young's modulus (Frolova et al., 2014). Values of Young's moduli for altered volcanic rocks are rare and, without an unaltered sample with which to compare, it is difficult to assess the influence of alteration in detail. Recently, Mordensky et al. (2018) measured the intact Young's modulus of variably altered andesites from Pinnacle Ridge on Mt. Ruapehu. The samples measured by Mordensky et al. (2018) were 20 mm in diameter and 40 mm in length, and were deformed in uniaxial compression at a strain rate of 1×10^{-5} s^{-1}. A subset of their data, showing the intact Young's modulus of unaltered and altered rocks from the same rock unit, is shown in Fig. 8a. These data show that the alteration reduced the connected porosity, as a result of hydrothermal precipitation (Mordensky et al., 2018), and increased the Young's modulus (Fig. 8a). Pore-filling alteration has also been observed to increase the elastic moduli of tuffs from Ngatamariki (New Zealand) (Durán et al., 2019). Heap et al. (2019c) showed that hydrothermal alteration (silicification) increased the stiffness of an essentially cohesionless ignimbrite deposit (the Ohakuri ignimbrite in New Zealand) to a rock with a Young's modulus of up to 20 GPa. Although these data (Fig. 8a; Durán et al., 2019; Heap et al., 2019c) show that Young's modulus increases with increasing alteration, we stress that these data represent only one type of alteration (pore- and microcrack-filling). Porosity-decreasing acid sulphate leaching, for example, reduced the Young's modulus of andesites and opalites from the Upper-Koshelevsky geothermal field (Kamchatka Peninsula; Frolova et al., 2014; Fig. 8b). More data now are required to fully understand the

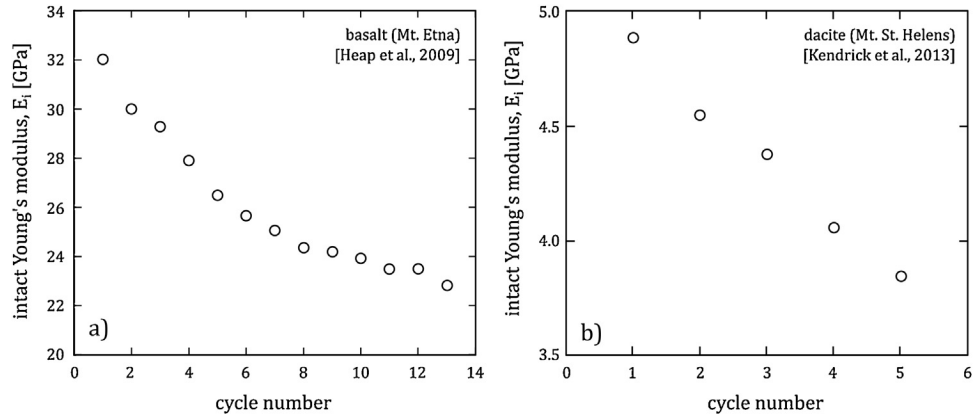

Fig. 7. (a) The intact Young's modulus of a basalt from Mt. Etna (Italy) as a function of increasing amplitude stress cycles (data from Heap et al., 2009). (b) The intact Young's modulus of a dacite from Mt. St. Helens (USA) as a function of increasing amplitude stress cycles (data from Kendrick et al., 2013).

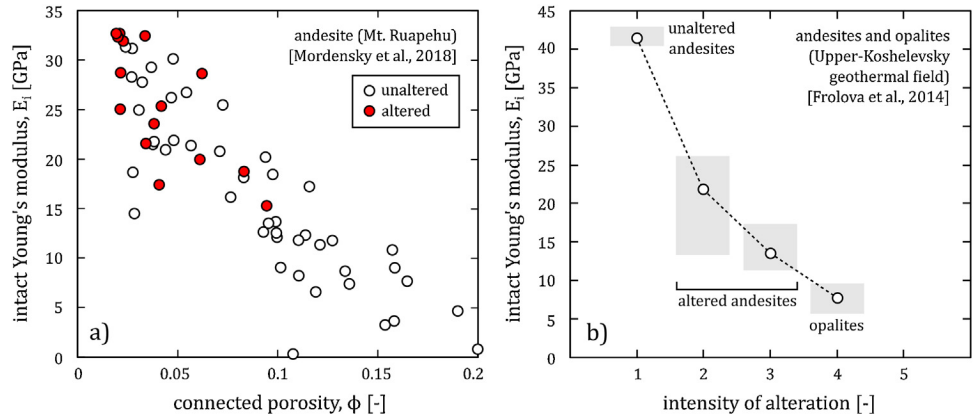

Fig. 8. (a) The intact Young's modulus of andesites from Mt. Ruapehu (New Zealand) as a function of connected porosity (data from Mordensky et al., 2018). Red symbols—altered andesite; white symbols—unaltered andesite. (b) The intact Young's modulus of andesites and opalites from the Upper-Koshelevsky geothermal field (Kamchatka Peninsula) as a function of alteration intensity (data from Frolova et al., 2014). White symbols—average values; grey boxes—maximum and minimum values. Alteration intensity was determined using detailed petrological and geochemical analyses (see Frolova et al. (2014) for details). (For interpretation of the references to colour in this figure legend, the reader is referred to the web version of this article).

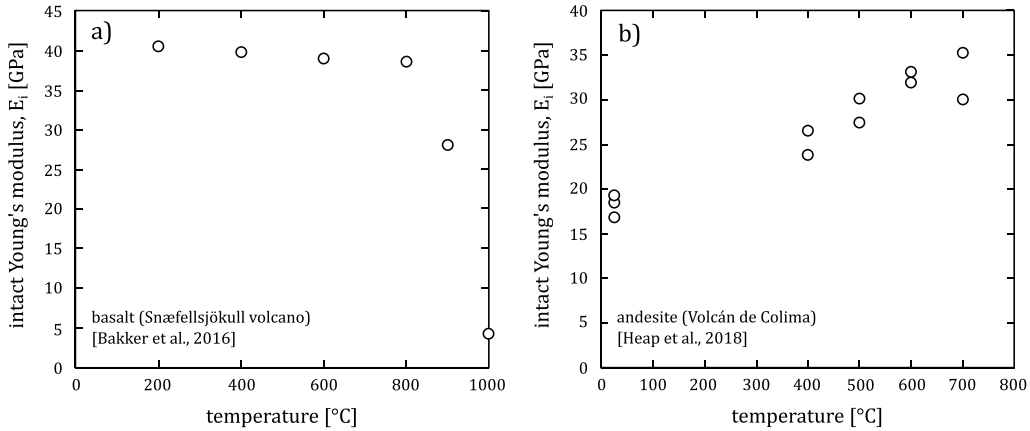

Fig. 9. (a) The intact Young's modulus of a basalt from Snæfellsjökull volcano (Iceland) as a function of temperature (data from Bakker et al., 2016). (b) The intact Young's modulus of an andesite from Volcán de Colima (Mexico) as a function of temperature (data from Heap et al., 2018a).

influence of alteration on the Young's modulus of volcanic rocks. When more data are available, the Young's modulus for altered volcanic rocks could be incorporated into numerical models using geophysical methods that can provide a detailed spatial distribution of hydrothermally altered zones, such as electrical tomography (e.g., Rosas-Carbajal et al., 2016; Byrdina et al., 2017; Ghorbani et al., 2018; Ahmed et al., 2018).

2.6. The influence of temperature on intact Young's modulus

High temperature can greatly influence the mechanical and physical properties of materials, including rocks (e.g., Evans et al., 1990). In the case of volcanic rocks, groundmass glass, if present, can behave as a liquid at high temperature as long as the deformation proceeds at a rate slower than the relaxation timescale of

the melt (e.g., Dingwell, 1996). Since we focus herein in the elastic deformation of a volcanic edifice, we do not consider deformation experiments performed above the threshold glass transition temperature of the amorphous glassy groundmass (e.g., Lavallée et al., 2013), experiments more relevant to study the deformation of magma rather than the edifice rock. The data in Fig. 9a, from Bakker et al. (2016), show the Young's modulus of an oven-dry sample of basalt from Snæfellsjökull volcano (Iceland) deformed in compression at a confining pressure of 50 MPa, temperatures from 200 to 1000 °C, and using a constant strain rate of 1×10^{-5} s^{-1}. The samples deformed in Bakker et al. (2016) were 12 mm in diameter and 30 mm in length. An important feature shown by these data is that the intact Young's modulus is largely unchanged until 900 °C (Fig. 9a). The Young's modulus is reduced from ~40 GPa (<900 °C) to ~28 and ~5 GPa at temperatures of 900 and 1000 °C, respectively (Fig. 9a). These authors explain the reduction in Young's modulus at high temperature as the result of the activation of deformation mechanisms associated with the switch from sample-scale brittle (localised microcracking and shear fracture formation) to sample-scale ductile (distributed microcracking or cataclastic pore collapse) behaviour (Bakker et al., 2016). Experiments performed on basalt from Pacaya volcano (Schaefer et al., 2015), basalt from Seljavellir (at the base of Eyjafjallajökull, Iceland) (Lamur et al., 2018), and dacite from Mt. Unzen (Coats et al., 2018) also showed that the intact Young's modulus was lower at high temperature (>800 °C) than at room temperature. Similarly, the Young's modulus of andesite from Mt. Shasta (USA) was reduced from ~21 GPa at a temperature of 20–300 °C to ~17 GPa at 600 °C and, finally, to ~7 GPa at 900 °C (Smith et al., 2009). Fig. 9b shows data from high-temperature uniaxial experiments on oven-dry andesite from Volcán de Colima (Heap et al., 2018a). These experiments were performed on samples 20 mm in diameter and 40 mm in length at a strain rate of 1×10^{-5} s^{-1} and temperatures between 20 and 700 °C. The data of Fig. 9b show that the Young's modulus increases with increasing temperature. Young's modulus increases from ~17 GPa at room temperature to ~35 GPa at a temperature of 700 °C (Fig. 9b). These authors attributed the increase in Young's modulus at high temperature as the result of the closure of microcracks due to the thermal expansion of the material at high temperature (Heap et al., 2018a). Whether the Young's modulus of volcanic rock increases or decreases as a function of temperature may therefore be related to the pre-existing microcrack density. However, we note that the magnitude of the increase in Young's modulus as a function of temperature for the andesites shown in Fig. 9b (Heap et al., 2018a) may be reduced if the experiments were performed at elevated pressure (which should serve to close some of the microcracks prior to heating). High temperatures may also induce chemical reactions in volcanic rocks that can influence the Young's modulus. For example, dehydroxylation reactions in zeolite-bearing tuff (from Campi Flegrei) reduced their Young's modulus following exposure to high temperature (Heap et al., 2012, 2014b). Further work is now required to better understand the influence of high temperature on the Young's modulus of volcanic rocks.

2.7. The influence of confining pressure (depth) on intact Young's modulus

Confining pressure is well known to close microcracks (e.g., Vinciguerra et al., 2005; Nara et al., 2011; Fortin et al., 2011), which can be abundant in volcanic rocks (e.g., Fig. 3; Heap et al., 2014a; Kushnir et al., 2016). Since microcracks can decrease the stiffness of rock (see above), an increase in confining pressure is therefore likely to increase the intact Young's modulus of volcanic rock. Fig. 10a and b show the intact Young's modulus of, respectively, a microcracked andesite from Volcán de Colima (porosity of ~0.08) and microcracked basalts from Mt. Etna (porosity of ~0.04 to ~0.08)

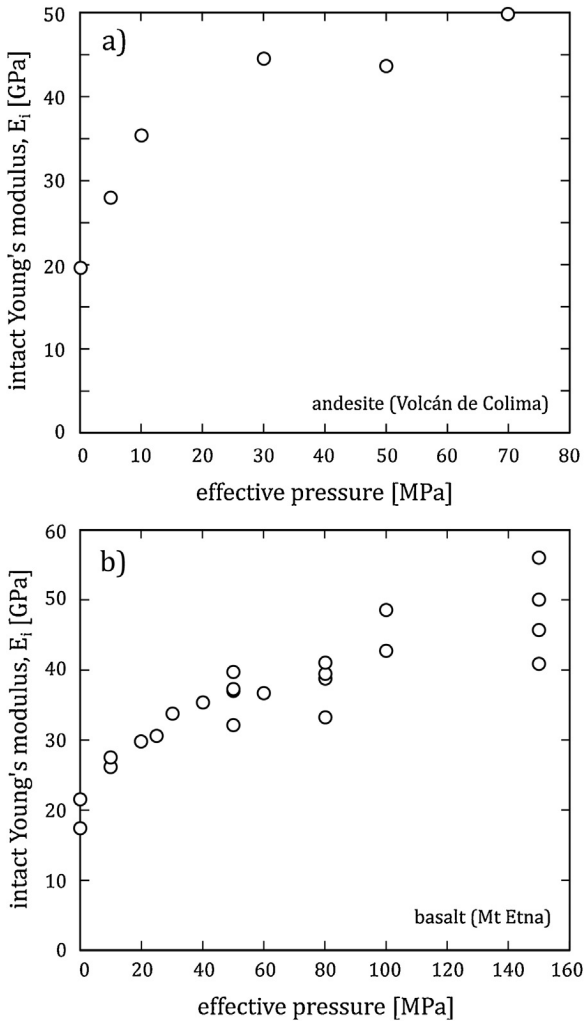

Fig. 10. (a) The intact Young's modulus of an andesite from Volcán de Colima (Mexico) as a function of effective pressure (confining pressure minus pore fluid pressure). (b) The intact Young's modulus of basalts from Mt. Etna (Italy) as a function of effective pressure.

as a function of effective pressure (up to 150 MPa; data available in Table 3). These constant strain rate (1×10^{-5} s^{-1}) experiments were performed in a triaxial deformation apparatus under a constant pore fluid pressure (deionised water) of 10 MPa and confining pressures up to 160 MPa (Heap et al., 2015a; Zhu et al., 2016). The results show that the Young's modulus of the andesite increased from ~20 GPa at room pressure to ~50 GPa at an effective pressure of 70 MPa (Fig. 10a), equivalent to a depth of about 2.5 km. The Young's modulus of the basalts from Mt. Etna increased from ~20 GPa at room pressure to ~40–55 GPa at an effective pressure of 150 MPa (Fig. 10b), equivalent to a depth of almost 6 km. Heap et al. (2011) also measured an increase in intact Young's modulus with increasing confining pressure for microcracked basalt from Mt. Etna. It is likely, however, that the intact Young's modulus of volcanic rocks that do not contain a pre-existing network of microcracks will not increase significantly as confining pressure (i.e. depth) is increased. Heap et al. (2014b) found that the Young's modulus (measured using elastic wave velocities) of porous tuff (from Campi Flegrei) increased with increasing confining pressure as a result of porosity reductions associated with inelastic pore collapse. More experiments are now needed to fully explore the influence of confining pressure on the Young's modulus of a range of volcanic rock types (with varying microcrack densities).

Table 3
Summary of the experimental data (porosity and intact Young's modulus) collected at elevated effective pressure used for this study (the data of Fig. 10).

Rock type	Volcano	Experimental condition	Effective pressure (MPa)	Porosity (-)	Intact Young's modulus (GPa)
andesite	Volcán de Colima (Mexico)	wet	5	0.07	28.0
andesite	Volcán de Colima (Mexico)	wet	10	0.07	35.4
andesite	Volcán de Colima (Mexico)	wet	30	0.08	44.6
andesite	Volcán de Colima (Mexico)	wet	50	0.08	43.6
andesite	Volcán de Colima (Mexico)	wet	70	0.08	49.9
basalt	Mt. Etna (Italy)	wet	0	0.05	21.6
basalt	Mt. Etna (Italy)	wet	0	0.08	17.5
basalt	Mt. Etna (Italy)	wet	10	0.05	27.6
basalt	Mt. Etna (Italy)	wet	10	0.05	26.2
basalt	Mt. Etna (Italy)	wet	20	0.05	29.8
basalt	Mt. Etna (Italy)	wet	25	0.05	30.7
basalt	Mt. Etna (Italy)	wet	30	0.05	33.8
basalt	Mt. Etna (Italy)	wet	40	0.05	35.4
basalt	Mt. Etna (Italy)	wet	50	0.05	37.2
basalt	Mt. Etna (Italy)	wet	50	0.05	37.0
basalt	Mt. Etna (Italy)	wet	50	0.05	39.7
basalt	Mt. Etna (Italy)	wet	50	0.08	32.1
basalt	Mt. Etna (Italy)	wet	60	0.05	36.7
basalt	Mt. Etna (Italy)	wet	80	0.05	39.5
basalt	Mt. Etna (Italy)	wet	80	0.05	38.8
basalt	Mt. Etna (Italy)	wet	80	0.05	41.1
basalt	Mt. Etna (Italy)	wet	80	0.08	33.3
basalt	Mt. Etna (Italy)	wet	100	0.04	42.8
basalt	Mt. Etna (Italy)	wet	100	0.05	48.6
basalt	Mt. Etna (Italy)	wet	150	0.05	45.7
basalt	Mt. Etna (Italy)	wet	150	0.05	56.1
basalt	Mt. Etna (Italy)	wet	150	0.05	50.1
basalt	Mt. Etna (Italy)	wet	150	0.08	40.9

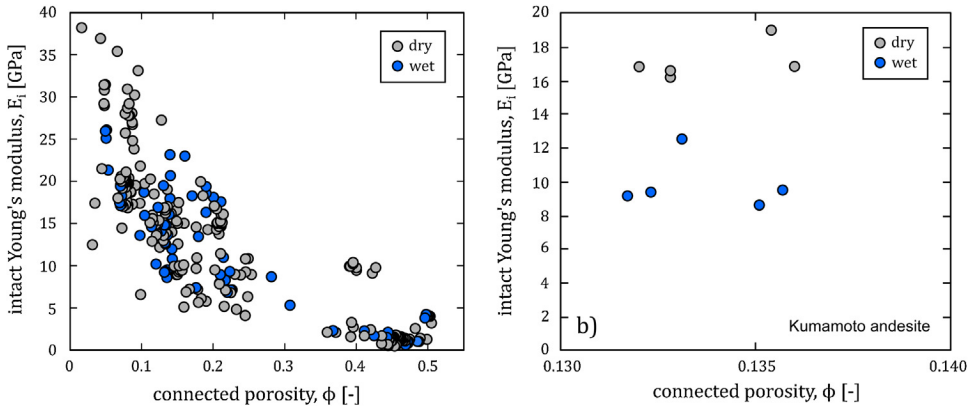

Fig. 11. (a) The intact Young's modulus for various volcanic rocks (see Table 2) as a function of porosity. Samples deformed dry—grey symbols; samples deformed wet—blue symbols. (b) The intact Young's modulus for Kumamoto andesite (see Table 2) as a function of porosity. Samples deformed dry—grey symbols; samples deformed wet—blue symbols. (For interpretation of the references to colour in this figure legend, the reader is referred to the web version of this article).

2.8. The influence of water saturation on intact Young's modulus

The presence of water in the void space of porous rock can influence its mechanical behaviour (e.g., Baud et al., 2000b; Zhu et al., 2011, 2016; Nicolas et al., 2016; Castagna et al., 2018). Since the rocks comprising a volcanic edifice are likely water saturated (e.g., Delcamp et al., 2016), the influence of water on the Young's moduli of volcanic rock is therefore an important consideration. Fig. 11a shows a graph of intact Young's modulus as a function of connected porosity (the same data presented in Figs. 5 and 6; Table 2) in which the data are separated into "wet" (blue symbols) and "dry" data (grey symbols). Although the presence of water has been shown to reduce the strength of tuff from Campi Flegrei (Heap et al., 2018b), for example, there appears to be no discernable influence on its Young's modulus (Table 2). However, samples of Kumamoto andesite (20 mm in diameter and 40 mm in length; deformed at a constant strain rate of 1×10^{-5} s^{-1}) show a systematic reduction in Young's modulus upon saturation with water, from ~17 to ~10 GPa (Fig. 11b). These data for Kumamoto andesite (Fig. 11b) are in accordance with the data of Zhu et al. (2011) and Zhu et al. (2016), which show a small, but systematic, decrease in Young's modulus for tuff (from Colli Albani, Italy) and basalt (from Mt. Etna) upon saturation with water, respectively. A small decrease in Young's modulus upon saturation has also been reported for porous sandstone (Heap et al., 2019a). It is unclear at present as to why the Young's modulus of some volcanic rocks decreases upon saturation (Fig. 11b), while others show no discernable change (Fig. 11a; Table 2). The absence of a measurable difference in some volcanic rocks may, in part, be related to the heterogeneity of volcanic rock samples prepared from the same block of material, suggesting that many more experiments would be required to understand how the presence of water influences the intact Young's modulus of volcanic rock. We note that, although we observe no measurable difference between the dry and wet Young's modulus measured using laboratory stress-strain data (Fig. 11a), it is well known that the P-wave velocity of microcracked rocks will increase upon saturation, especially if

the rock contains microcracks, resulting in a pronounced difference between dry and wet Young's modulus calculated from elastic wave velocities. For example, the P-wave velocity of andesites from Volcán de Colima increased from 2.34–3.11 to 3.91–4.98 km·s^{-1} upon saturation with water (Heap et al., 2014a). If moduli determined from stress-strain data are considered more relevant for modelling volcanic processes, a potentially large difference between the influence of water saturation on the Young's moduli measured using stress-strain data and elastic wave velocities poses a problem when deriving the Young's modulus from seismic wave velocities using local tomography surveys (see Eq. (2)).

2.9. The influence of strain rate on intact Young's modulus

Few experimental studies exist that have investigated the influence of strain rate on the intact Young's modulus of volcanic rock in the brittle regime. One such study, Lavallée et al. (2019), found that the intact Young's modulus of andesite samples from Volcán de Colima increased from 12.0 to 19.0 GPa as the uniaxial compressive strain rate was increased from 1×10^{-6} to 1×10^{-1} s^{-1} (Fig. 12a). These authors attributed the reduction in stiffness at lower strain rates as the result of the increased efficiency of time-dependent subcritical cracking. Coats et al. (2018) showed that the influence of strain rate on the Young's modulus of dacite samples from Mt. Unzen was unclear (Fig. 12b). Although the stiffest samples were those deformed at 1×10^{-1} s^{-1}, high-porosity samples deformed at 1×10^{-1} s^{-1} had a lower Young's modulus than similarly porous samples deformed at 1×10^{-3} s^{-1} (Coats et al., 2018; Fig. 12b). The scatter in these data (Fig. 12b) may reflect a high sample-to-sample heterogeneity, as discussed in Coats et al. (2018). However, although such fast strain rates (e.g., 10^{-1} s^{-1}) have high relevance for volcanic processes adjacent to the magma-filled conduit (where strain rates can be very high), we consider it unlikely that Young's moduli determined from these very fast strain rate experiments are suitable for elastic models that consider deformation on the scale of the volcanic edifice.

2.10. Summary of experimental observations

Based on the observations presented above, it is clear that porosity plays a key role in dictating the intact Young's modulus of a volcanic rock (Fig. 5). Rock type is a classification too coarse to provide useful insights on the Young's modulus of a volcanic rock (Fig. 6), but may exert some influence as to whether the rock is porous, microcracked, and/or altered. Microcracks will serve to reduce the Young's modulus (Fig. 7). If the pores within the rock are elongate (pore aspect ratios less than unity), then the Young's modulus will depend on their aspect ratio and the angle between the pore major axis and the direction of loading (Bubeck et al., 2017; Griffiths et al., 2017). The influence of alteration will depend on whether the alteration increases (Fig. 8a) or decreases (Fig. 8b) the porosity, resulting in increases or decreases to the Young's modulus, respectively. The influence of temperature (Fig. 9) and confining pressure (depth) (Fig. 10) likely depend on the pre-existing microcrack density of the rock. The Young's modulus of some volcanic rocks may be reduced upon saturation with water (Fig. 11), but there are not yet enough data to draw any firm conclusions. Strain rate increases the Young's modulus (Fig. 12); however we suggest that such fast strain rates (e.g., 10^{-1} s^{-1}) are largely irrelevant when considering edifice-scale deformation.

Although it is well known that volcanic rocks are very microstructurally and texturally complex (e.g., see Fig. 3), we propose here, based on the first order influence of porosity in controlling the intact Young's modulus of volcanic rock (Fig. 5), and, importantly, its relative ease of measure in the laboratory (and field), that porosity is the metric of greatest interest for our upscaling analysis.

3. Young's modulus on the rock mass lengthscale

We have shown that the intact Young's modulus, E_i, depends on rock physical attributes, such as porosity (Fig. 5), and environmental conditions, such as pressure (Fig. 10). However, since these values are measured on the sample lengthscale, they very much overestimate the Young's modulus of rock masses that, invariably, contain macroscopic fractures that serve to lower the Young's modulus. It is the Young's modulus of a rock mass, E_{rm} (or the "effective Young's modulus"), which is required for volcano modelling. A method to upscale laboratory measurements of Young's modulus was proposed by Priest (1993):

$$E_{rm} = \left(\frac{1}{E_i} + \frac{1}{\bar{s}k} \right)^{-1} \quad (5)$$

where $\bar{s}$ and k are the average fracture spacing and the fracture stiffness (in Pa m^{-1}), respectively (see also Gudmundsson, 2011; Liu et al., 2000). Although the average fracture spacing can be determined using fracture counts along line transects, or using more sophisticated techniques (e.g., Sanderson and Nixon, 2015; Healy et al., 2017), experiments designed to determine fracture stiffness are non-trivial and have shown that fracture stiffness depends on factors such as normal stress and surface roughness (e.g., Yoshioka and Scholz, 1989). It is also likely, for example, that fracture stiffness will vary from fracture to fracture within the same outcrop (due to differences in roughness and fracture filling). We opt here, therefore, to upscale our values of intact Young's modulus determined from laboratory experiments (Table 2) using the empirical Hoek-Diederichs equation (Hoek and Diederichs, 2006), a widely used tool in geotechnics. The advantages of this method, which is described in detail below, is that it requires a relatively quick assessment of the structure of a rock mass and does not necessitate additional experiments that require expensive laboratory equipment.

3.1. Presentation of the Hoek-Diederichs equation

The Hoek-Diederichs equation (Hoek and Diederichs, 2006) was formulated using measurements of the Young's modulus of a rock mass, E_{rm}, from *in situ* plate loading and jacking tests conducted in China and Taiwan. The rock masses for each *in situ* measurement were assigned a Geological Strength Index (GSI), a unitless value, described in detail below, that describes the rock mass structure (e.g., fracture density and quality) (Marinos et al., 2005). These E_{rm} data ($n = 494$) were plotted as a function of GSI and a sigmoid function was used to describe the data. The constants in the sigmoid function were then replaced by expressions that incorporate the GSI and the disturbance factor, D (a unitless parameter that describes the extent of blasting damage during large mining/tunnel excavations). Finally, E_i was incorporated into the equation using laboratory measured values, or by estimating E_i from the uniaxial compressive strength, σ_c, of the intact rock, using the following relation: $E_i = MR\sigma_c$ (see Deere, 1968; Palmström and Singh, 2001), were MR is the modulus ratio (i.e. E_{rm}/E_i). The final Hoek-Diederichs equation (Hoek and Diederichs, 2006) is as follows:

$$E_{rm} = E_i \left(0.02 + \frac{1 - \frac{D}{2}}{1 + e^{\left((60+15D-GSI)/11\right)}} \right) \quad (6)$$

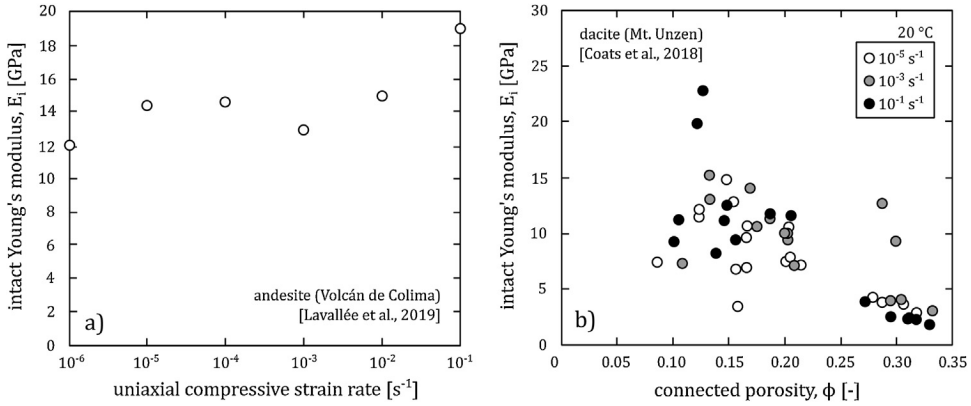

Fig. 12. (a) The intact Young's modulus for an andesite from Volcán de Colima (Mexico) as a function of uniaxial compressive strain rate (data from Lavallée et al., 2019). (b) The intact Young's modulus for dacites from Mt. Unzen (Japan) as a function of connected porosity (data from Coats et al., 2018). The data are organised by uniaxial compressive strain rate: 10^{-5} (white symbols), 10^{-3} (grey symbols), and 10^{-1} s^{-1} (black symbols).

Since anthropogenic damage using explosives is not relevant to our volcanic case study, we let $D = 0$ (we provide the full equation here for completeness). If $D = 0$, then Eq. (6) can be simplified to:

$$E_{rm} = E_i \left(0.02 + \frac{1}{1 + e^{((60 - GSI)/11)}} \right) \quad (7)$$

Our laboratory measurements (Table 2) provide the values for E_i; the other unknown in the Hoek-Diederichs equation (Eq. (7)) is the GSI (Marinos et al., 2005). The GSI is a unitless value that depends on the rock mass structure (i.e. fracture density) and the quality of these fractures (i.e. whether they are weathered and the presence/nature of fracture filling material) (Marinos et al., 2005) (Fig. 13). The GSI is a number from 0 to 100, where 0 represents an essentially cohesionless rock mass and 100 represents a pristine (fracture-free) rock mass (Fig. 13). Since volcanic rock masses are typically fractured and often disturbed, estimates of their GSI have been found within the range 8–80 (Moon et al., 2005; Apuani et al., 2005a, 2005b; del Potro and Hürlimann, 2008; Justo et al., 2010; Schaefer et al., 2013; Miranda et al., 2018) and are in agreement with values of Rock Mass Rating (RMR), another metric for describing the structure of a rock mass, found for volcanic rock masses (Watters et al., 2000; Okubo, 2004; Thomas et al., 2004). Schaefer et al. (2013), for example, found GSI values of 8–20 and 45–60 for, respectively, pyroclastic rocks and lavas and lava breccias from Pacaya volcano.

Since this method may be unfamiliar to a volcanological audience, we not only provide the GSI chart, but also examples of fractured volcanic rock masses for which we have assigned values of GSI (Fig. 13). Based on the GSI schemes of Marinos et al. (2005) and Hoek et al. (2013), and the more recent clarifications in Hoek and Brown (2019), we split volcanic rock masses into one of four categories: "blocky", "very blocky", "extremely blocky/disturbed", and "disintegrated" (Fig. 13). Hoek et al. (2013) proposed that the top and bottom row of the GSI scheme of Marinos et al. (2005) (termed "intact or massive" and "heavily fissured but unblocky" in our volcano GSI chart; Fig. 13) should not be included in the chart when GSI is to be used for strength or deformability assessments. As a result, these two categories are excluded in our GSI scheme for volcanic rock masses (Fig. 13). In any case, most volcanic rock outcrops typically range somewhere between blocky (GSI = 65–85) and disintegrated (GSI = 20–40) (Fig. 13; Moon et al., 2005; Apuani et al., 2005a, 2005b; del Potro and Hürlimann, 2008; Justo et al., 2010; Schaefer et al., 2013; Miranda et al., 2018).

The GSI estimate for the lengthscale of a laboratory sample (i.e. on the centimetric scale) would be, in general, 100. We highlight in Fig. 14 how GSI estimates can be influenced by the considered lengthscale. In this example, we show how increasing the lengthscale from about 20 m to about 150 m decreases the GSI estimate by about 20 (Fig. 14). In the example of Fig. 14, this is because the longer lengthscale includes a broader range of rock masses (and therefore incorporates more discontinuities between the different lava units, for example) that the shorter lengthscale does not. As a result, it is important to consider the appropriate lengthscale when making GSI assessments using the chart provided in Fig. 13. For modelling problems that require a single value of Young's modulus to characterise the modelled half-space, we recommend that the GSI estimate is made on the lengthscale of at least a couple of hundred metres, if possible. In engineering problems, however, rock masses are typically divided into domains of similar rock mass characteristics (see, for example, the Katse Arch Dam (Lesotho) case study in Schlotfeldt and Carter, 2018). Although this domain approach may not be straightforward for an active volcanic system (rock masses in engineering projects, unlike volcanic rock masses, are often easily accessible and observable), we encourage modellers to split their modelled half-space into GSI domains guided by either geological (e.g., site analysis) or geophysical (e.g., muon, electrical, and/or seismic tomography) methods. As outlined above, mechanical layering can greatly influence model output and interpretations (e.g., see Manconi et al., 2007; Bazargan and Gudmundsson, 2019).

Although there are several empirical equations for estimating rock mass deformability (see the reviews by, for example, Zhang (2017) and Kayabasi and Gokceoglu, 2018), one of the reasons we opted to use the Hoek-Diederichs equation (Hoek and Diederichs, 2006) is because it uses GSI to characterise the rock mass. Other approaches to estimate rock mass Young's modulus use other rock mass classification schemes (e.g., using RMR; Bieniawski, 1978; recently updated in Galera et al., 2007), a measure of joint spacing (e.g., using Rock Quality Designation, RQD; Deere and Deere, 1988; Zhang and Einstein, 2004), a mean spacing between discontinuities (e.g., Kulhawy and Goodman, 1980), or seismic characteristics (e.g., Bieniawski, 1984; Barton, 2006). We prefer to use GSI because its descriptive nature lends itself to rapid field or remote assessment. Galera et al. (2007) argue that RMR is more quantitative than GSI and is therefore preferable for engineering applications. However, all of the techniques that relate rock mass condition to deformability are empirical and, for application to volcano modelling, we consider that a simple descriptive method of rock mass classification is sufficient as along as a range of values is used that captures the inherent uncertainty. We further note that RQD has several weaknesses, such as requiring drill core (although it can be estimated in the field using the method developed by Schlotfeldt and Carter, 2018), as outlined in Pells et al. (2017) and in Schlotfeldt and Carter (2018), and that joint spacing methods do not take joint

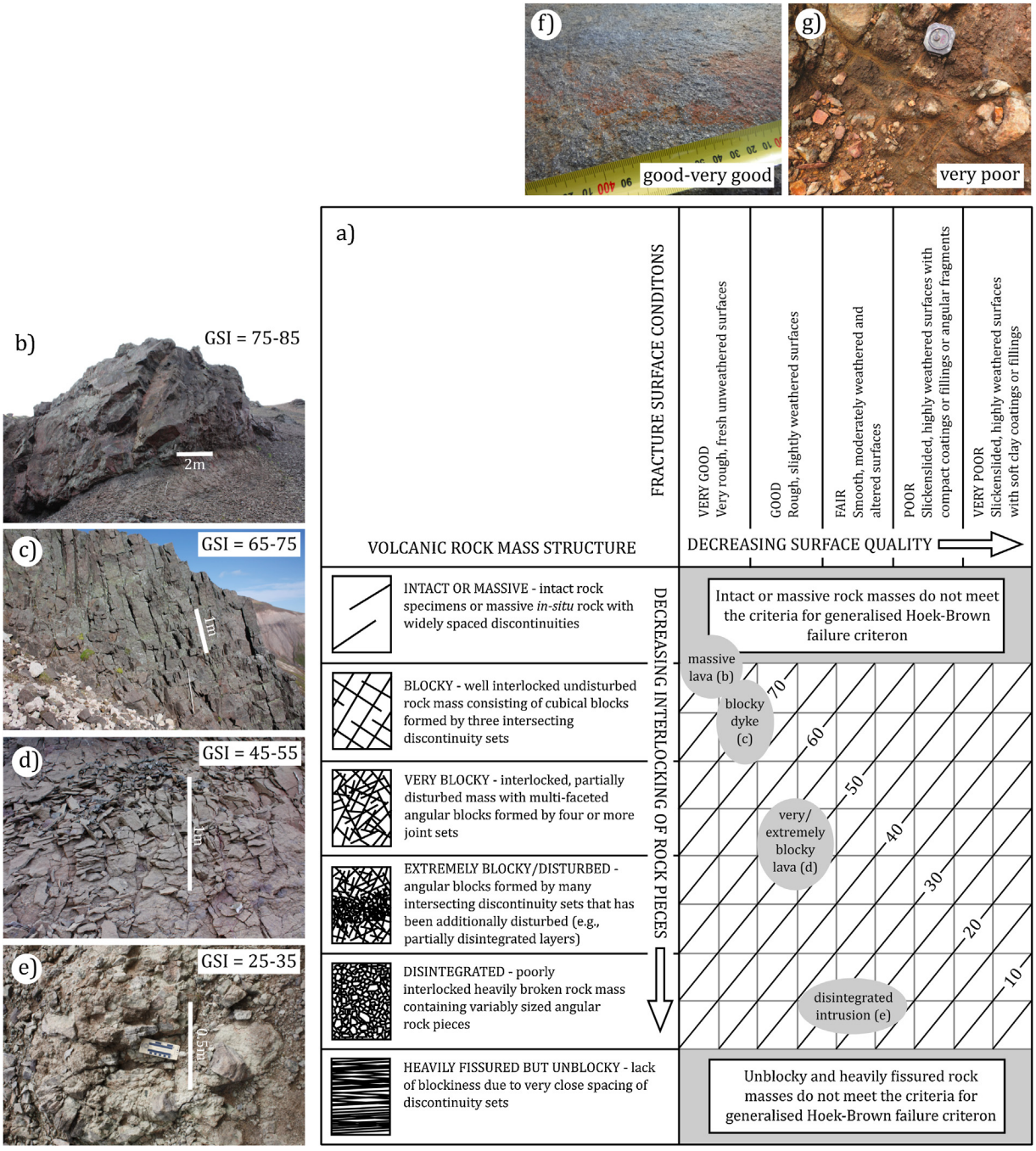

Fig. 13. Chart and photographs to be used to estimate the Geological Strength Index (GSI) of a volcanic rock mass (modified from Marinos et al., 2005). (a) The volcanic GSI chart. (b) Photograph of a massive lava outcrop (GSI = 75–85) (basalt flow near Húsafell, Iceland). (c) Photograph of a blocky dyke (GSI = 65–75) (dyke in Hvítserkur mountain, Borgarfjörður Eystri, Iceland). (d) Photograph of a very blocky/disturbed lava outcrop (GSI = 45–75) (ignimbrite near Húsafell, Iceland). (e) Photograph of a disintegrated intrusion (GSI = 25–35). (f) Photograph of a "good-very good" fracture surface. (g) Photograph of a "very poor" fracture surface (andesite lava from Mt. Ruapehu, New Zealand). We have straightened the lines defining the GSI values in accordance with the GSI scheme of Hoek et al. (2013).

condition into account. For applications where only RMR is available, GSI can be derived for RMR > 25 using: GSI = RMR_{89}' - 5, where RMR_{89}' is the version of RMR in Bieniawski (1989) with the groundwater rating set to 15 and the adjustment for joint orientation rating set to 0 (Hoek and Brown, 1997).

3.2. Estimating the Young's modulus of a fractured volcanic rock mass

To illustrate the influence of rock mass structure on the Young's modulus of a volcanic rock mass, we chose here a GSI value of 55 (a value that we consider represents a reasonable average for lavas and lava breccias; Moon et al., 2005; Apuani et al., 2005a, 2005b; del Potro and Hürlimann, 2008; Justo et al., 2010; Schaefer et al., 2013; Miranda et al., 2018). We consider that, without prior knowledge of the structure of a volcanic rock mass, a GSI of 55 represents a reasonable estimate. The values of Young's modulus in the graph of intact Young's modulus as a function of connected porosity (Fig. 5) can then be recalculated, assuming a GSI of 55, for a typically fractured volcanic rock mass (Fig. 15; using Eq. (7)). Fig. 15 shows that the Young's modulus of a typically fractured (GSI = 55) volcanic rock mass is much lower than the Young's modulus of a volcanic

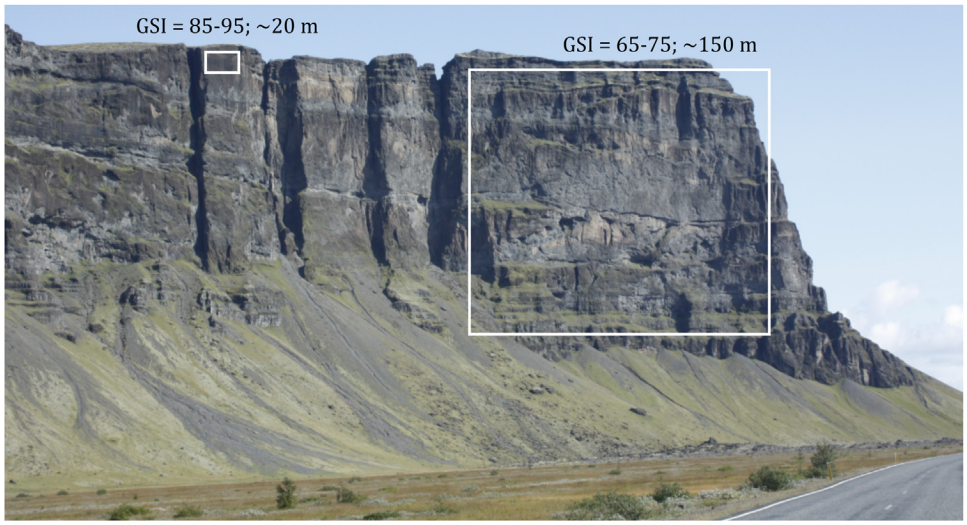

Fig. 14. Photograph of a rock outcrop (overthickened basalt lava flows near Núpsstaður, Iceland) showing how window-of-interest (i.e. lengthscale) can influence the estimation of the Geological Strength Index (GSI).

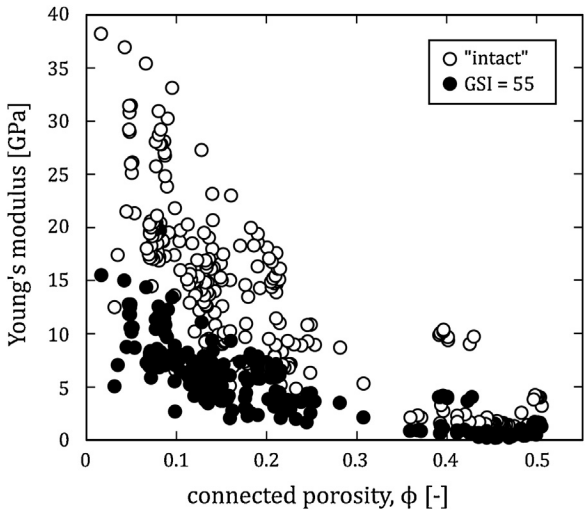

Fig. 15. The Young's modulus for rock masses with a Geological Strength Index (GSI) of 100 (i.e. intact rock; white symbols) and 55 (a typically fractured volcanic rock mass; black symbols).

rock on the sample lengthscale. The Young's modulus of a typically fractured volcanic rock mass varies from a couple of GPa (for the most porous host rocks) to ~15 GPa (for the least porous host rocks) (Fig. 15). The range of Young's modulus values has therefore been reduced from ~1 to ~50 GPa for intact rock to ~1 to ~15 GPa for a typically fractured rock mass (Fig. 15).

The ideal solution to determine the Young's modulus for volcano modelling would be to first determine the intact Young's modulus for the most representative material (or materials, if there is justification for mechanical layering, e.g., Manconi et al., 2007) for a given volcano and then upscale this value, or these values, using the Hoek-Diederichs equation (Eq. (7)) and estimates of the GSI determined from rock outcrops of the same volcano (using the GSI chart provided as Fig. 13). However, not only is this ideal solution not always feasible (the rock masses of interest may be entirely below the subsurface), but problems also exist when choosing a rock sample or rock samples that best represent a volcano composed of rocks of varying porosity, a factor that exerts a first-order influence on the Young's modulus (Fig. 5), and when choosing a rock mass structure or range of rock mass structures that best represent the structural state of a volcano. In other words, because volcanoes are extremely heterogeneous, it is often difficult to select representative intact rocks and representative GSI values. Nevertheless, we consider this approach will yield the most accurate model predictions. In the likely scenario that the authors of a particular study cannot measure the Young's modulus of a representative rock in the laboratory, or provide a representative GSI, we outline approaches below that can be used to determine upscaled Young's moduli estimates in the scenario when (1) the porosity of a representative rock(s) is known and the GSI value(s) is known (i.e. the ideal scenario), (2) the porosity of a representative rock(s) is known and the GSI value(s) is unknown, (3) the porosity of a representative rock(s) is unknown but the GSI value(s) is known, and (4) both porosity and GSI are unknown. This approach can be used to provide a single value of Young's modulus for an elastic half-space or, if there is geological or geophysical justification for splitting the half-space into domains characterised by different porosity and/or GSI values (such as, for example low-density/high-porosity zones identified by muon tomography; Lesparre et al., 2012; Rosas-Carbajal et al., 2017; Le Gonidec et al., 2019), then the approach can also be used to assign Young's modulus values to the different domains within the half-space. The data and equations required for estimating rock mass Young's modulus in the four scenarios described below can be found in the Microsoft Excel© spreadsheet available as Supplementary Material.

If the porosity of a rock considered representative of the volcano or volcano domain is known, or an average porosity is taken from a larger dataset (using, for example, the weighted abundance analysis presented in Bernard et al., 2015), and the GSI is known, empirical fits to our experimental data (Young's modulus as a function of porosity; Fig. 5) will offer reasonable estimates of the intact Young's modulus (Fig. 16a) for a given porosity. We present, respectively, both the power law and exponential fits to the experimental data (Fig. 16a):

$$E_i = 0.89 \times \phi^{-1.27} \quad (8)$$

$$E_i = 35.11\, e^{-6.47\phi} \quad (9)$$

These empirical fits were determined using Microsoft Excel© (see the spreadsheet that accompanies this contribution as Supplementary Material). We chose to use empirical fits to our data, rather than adopting theoretical approaches (e.g., Hashin and Shtrikman, 1963; Kemeny and Cook, 1986; Mavko et al., 2009; Torquato, 2013; Vasseur et al., 2016), because empirical fits do not assume

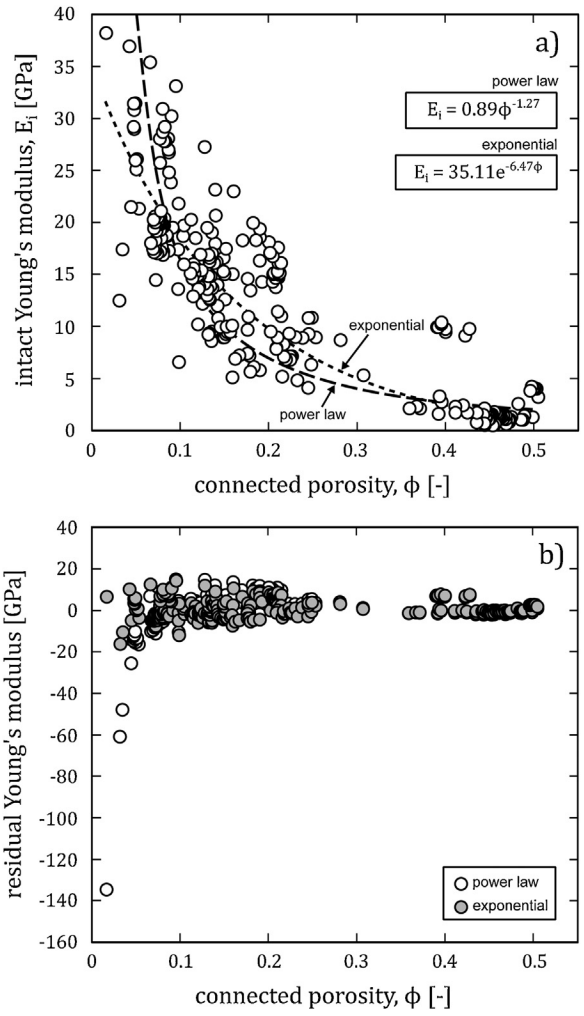

Fig. 16. (a) The intact Young's modulus for various volcanic rocks (see Table 2) as a function of porosity. The power law (long dashes) and exponential (short dashes) fits to the data are shown. (b) Residual Young's modulus (the difference between the model prediction and the data) for the power law (white symbols) and exponential (grey symbols) fits shown in panel (a).

a microstructure. For example, the approach of Kemeny and Cook (1986) assumes interacting microcracks and the cluster expansion method of Torquato (2013) assumes spherical cavities within a homogeneous medium. Volcanic rocks, however, often contain a combination of pores and microcracks (see Fig. 3). The residuals of these empirical fits show that (1) the fits to the data can vary by up to 15 GPa from the intact Young's modulus measured in the laboratory and (2) the power law fit considerably overestimates (on one occasion by more than 100 GPa) the Young's modulus when the porosity is below 0.05 (Fig. 16b). Even when the low-porosity (≤0.05) data are excluded, the exponential fit to the data still outperforms the power law fit (the residual average is 0.6 for the exponential fit and, excluding the low-porosity data (≤0.05), the residual average for the power law fit is 1.4). We therefore recommend that Eq. (9) is used ahead of Eq. (8) when estimating the intact Young's modulus. However, we also note that the exponential fit underestimates the Young's modulus when porosity is zero, or very close to zero (several of the rocks measured have a higher Young's modulus than the ~35 GPa estimated by the exponential fit when porosity equals zero; Fig. 16a; Table 2). Based on the data provided in Fig. 10, we consider it likely that, when porosity is at or very close to zero, the intact Young's modulus of a volcanic rock will be in the range 40–60 GPa (similar to the ranges presented in González de Vallejo and Ferrer, 2011). The data are available as Supplementary Material in case a theoretical approach is preferred (i.e. if there is justification to assume a specific microstructure).

It is often easier to measure the bulk density of a rock than to measure its porosity. For example, in the laboratory and in the field, the dry bulk density of a rock, ρ_b, can be simply determined using Archimedes principle, such that:

$$\rho_b = \frac{W}{W - W_1} \tag{10}$$

where W is the weight of the dry rock and W_1 is the weight of the rock submersed in water (see Kueppers et al., 2005; Farquharson et al., 2015). Furthermore, geophysical methods such as muon or gravity surveying provide estimates of the density, not porosity, of a volcano or volcanic rock mass (e.g., Tanaka et al., 2007; Lesparre et al., 2012; Nishiyama et al., 2014; Rosas-Carbajal et al., 2017; Le Gonidec et al., 2019). We therefore provide here a means to estimate porosity, for use in Eq. (9), when only the density of the rock, or rock mass, is known (Fig. 17). We first measured the density of powders of volcanic rocks chosen to span the common volcanic rock types: tuff (the Neapolitan Yellow Tuff, Italy), basalt (from Mt. Etna), andesite (from Volcán de Colima), dacite (from Mt. St. Helens), and obsidian (from Hrafntinnuhryggur, Iceland). Powdered aliquots of these samples were prepared, weighed, and their volumes measured using a helium pycnometer. These measurements permit the calculation of the solid (skeletal) density, i.e. the density of the rock when the porosity equals zero. The solid densities, ρ_s, for the tuff, basalt, andesite, dacite, and obsidian were measured to be 2307, 2909, 2669, 2614, and 2393 kg.m^{-3}, respectively. Total porosity, ϕ_T, can then be plotted as a function of bulk sample density, ρ_b, using the following relation (Fig. 17a):

$$\phi_T = 1 - \frac{\rho_b}{\rho_s} \tag{11}$$

To estimate total porosity using geophysical data, for which the saturation state of the rocks cannot be considered as dry, we also provide total porosity as a function of bulk density for completely water saturated rock (assuming a water density, ρ_w, of 1000 kg.m^{-3}; Fig. 17b). We note that these data can also be used to provide total porosity estimates for rock masses characterised by different degrees of saturation:

$$\rho_{psat} = \rho_b + c\phi_T\rho_w \tag{12}$$

where ρ_{psat} is the density of a partially saturated rock and c is the degree of saturation. Therefore, if ρ_{psat} is measured using muon tomography, for example, then the total porosity can be estimated using the bulk density of the rock type (see data provided above) and an estimate of the degree of saturation. Using the GSI determined for the volcano (or domain, if the volcano is to be split into different domains characterised by different values of GSI) under investigation and the intact Young's modulus estimated using the porosity or density, as described above, the rock mass Young's modulus can be determined using Eq. (7). It is important to note that volcanic rocks, depending on their genesis, can contain variably quantities of isolated porosity (see, for example, Colombier et al., 2017), where total porosity is the sum of the connected and isolated porosity. Because Eqs. (8) and (9) are fits to intact Young's modulus as a function of connected porosity, using total porosities in these empirical equations may underestimate the intact Young's modulus if the rock contains significant isolated porosity.

If the porosity (or density) of a rock considered representative of the volcano or volcano domain is known, but the GSI is unknown, then we first recommend that the intact Young's modulus be estimated as described above. In the absence of site investigations to determine a representative GSI value, we propose herein that a GSI of 55 likely best represents the structure of a volcanic rock mass

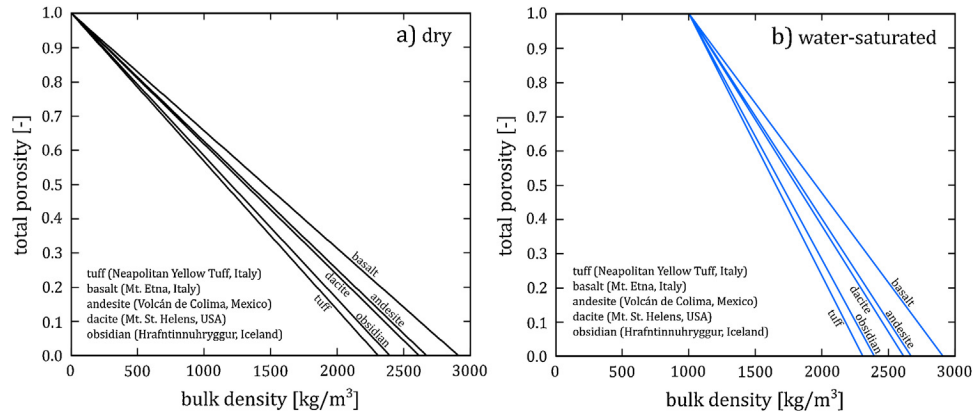

Fig. 17. Total porosity as a function of bulk density for tuff (Neapolitan Yellow Tuff, Italy), basalt (Mt. Etna, Italy), andesite (Volcán de Colima, Mexico), dacite (Mt. St. Helens, USA), and obsidian (Hrafntinnuhryggur, Iceland). Panel (a) shows modelled curves for the dry case (pores filled with air) and panel (b) shows modelled curves for water-saturated case (pores filled with water). See text for details. (For interpretation of the references to colour in this figure legend, the reader is referred to the web version of this article).

(Fig. 15), which are typically highly fractured (e.g., Moon et al., 2005; Apuani et al., 2005a, 2005b; del Potro and Hürlimann, 2008; Justo et al., 2010; Schaefer et al., 2013; Miranda et al., 2018). A GSI of 55 is typical of a "very blocky" rock mass with a "good" to "fair" structure quality, as defined by our volcanic GSI chart (Fig. 13). Although this GSI estimate may appear low, we highlight that volcano modelling often considers very large rock masses (on the scale of a couple of hundred to a couple of thousand metres) and GSI estimates are often reduced as the scale of interest increases (e.g., Fig. 14). Using the intact Young's modulus estimated using the porosity or density, as described above, and a GSI of 55, the rock mass Young's modulus can be determined using Eq. (7).

If the porosity (or density) is unknown but the GSI is known, we recommend that the average porosity derived from large datasets be used. Field studies have provided the average porosity of rocks sampled in block-and-ash flow deposits for Volcán de Colima and Mt. Unzen (Kueppers et al., 2005; Mueller et al., 2011; Farquharson et al., 2015; Lavallée et al., 2019). These studies have shown the average porosity and the predominant porosity class of dome rocks from Volcán de Colima to be 0.2 (Lavallée et al., 2019) and between 0.1 and 0.25 (Heap et al., 2015a), respectively. The porosity of dome rocks from Unzen volcano was found to be bimodal, with peaks at porosity values of 0.08 and 0.2 (Kueppers et al., 2005). Based on these studies, we propose herein that a porosity of 0.15 is a reasonable estimate for the average porosity of the rocks that typically form a volcanic edifice. A porosity of 0.15 is also the median value for the porosity of the samples listed in Table 2. This estimate is in general agreement with geophysical data collected at active volcanoes, although porosity is rarely reported. Setiawan (2002) determined porosity of 0.1–0.2 within the shallow subsurface of Gunung Merapi, in line with an average edifice porosity value of 0.21 reported by Tiede et al. (2005) for the same volcano, based on gravimetric inversion. Using a similar two-phase effective medium estimation, Arnulf et al. (2013) calculated porosities of 0.1–0.2 for the upper parts of the edifice of Lucky Strike volcano (located on the Mid-Atlantic ridge). Finally, neutron porosity logs collected at Mt. Unzen during the Unzen Volcano Scientific Drilling Project revealed average *in situ* porosities of lava flows and dykes of 0.15–0.20 (Nakada et al., 2005; Sakuma et al., 2008). Therefore, if values of GSI are known, but porosity or density values are not, we suggest that a porosity value of 0.15 is used, which corresponds to an intact Young's modulus, E_i, of 13.3 GPa using the empirical exponential fit to our experimental data (Eq. (9)). Using the GSI determined for the volcano or volcano domain and an E_i of 13.3 GPa, the rock mass Young's modulus can be determined using Eq. (7).

In the scenario in which both GSI and porosity are unknowns, a scenario to be avoided if possible, we consider it reasonable to assume a GSI of 55 and a porosity of 0.15 (i.e. an E_i value of 13.3 GPa). Using Eq. (7), this yields a rock mass Young's modulus estimate of 5.4 GPa. We highlight that our estimate of 5.4 GPa for the Young's modulus of a volcano is generally low compared to the values typically used in volcano modelling (Table 1).

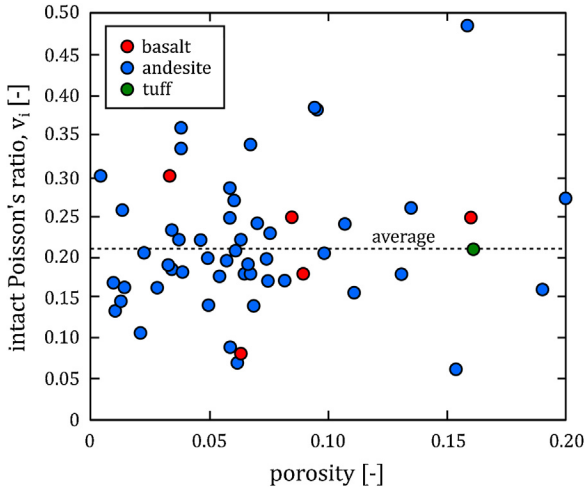

Fig. 18. The intact Poisson's ratio for various volcanic rocks (see Table 4) as a function of porosity. The data are separated by rock type: basalt (red symbols), andesite (blue symbols), and tuff (green symbols). Dotted line shows the average Poisson's ratio of the presented data (0.21). (For interpretation of the references to colour in this figure legend, the reader is referred to the web version of this article).

3.3. Estimating the Poisson's ratio and Young's, shear, and bulk modulus of a fractured volcanic rock mass

Although this review has focused on the Young's modulus, the most important elastic constant for volcano modelling (Eq. (1); Fig. 2), we can also discuss the upscaling of Poisson's ratio, shear modulus, and bulk modulus. In collating the rare published values of Poisson's ratio for volcanic rocks determined from laboratory stress-strain data (data from Nordyke and Wray, 1964; Saito and Kawamura, 1986; Ito and Hayashi, 1991; Özsan and Akın, 2002; Siratovich et al., 2014; Mordensky et al., 2018), we found that Poisson's ratio does not appear to depend on porosity or rock type (Fig. 18; Table 4). This may be considered surprising, since the Poisson's ratio of common crustal minerals and rock types are known to differ (e.g., Gercek, 2007), and Poisson's ratio should also depend on microstructural parameters such as the microcrack density (e.g., Walsh, 1965b). The absence of a discernable trend in Fig. 18 is there-

Table 4
Collated experimental data (porosity and Poisson's ratio) used in this study (see Fig. 18).

Rock type	Volcano/rock source region	Experimental condition	Porosity (-)	Poisson's ratio (-)	Reference
andesite	Rotokawa geothermal field (New Zealand)	dry	0.11	0.24	Siratovich et al. (2012)
andesite	Rotokawa geothermal field (New Zealand)	dry	0.13	0.26	Siratovich et al. (2012)
andesite	Rotokawa geothermal field (New Zealand)	dry	0.07	0.19	Siratovich et al. (2012)
andesite	Rotokawa geothermal field (New Zealand)	dry	0.06	0.25	Siratovich et al. (2012)
andesite	Rotokawa geothermal field (New Zealand)	dry	0.13	0.18	Siratovich et al. (2012)
andesite	Rotokawa geothermal field (New Zealand)	dry	0.06	0.09	Siratovich et al. (2012)
andesite	Rotokawa geothermal field (New Zealand)	dry	0.06	0.27	Siratovich et al. (2012)
andesite	Rotokawa geothermal field (New Zealand)	dry	0.07	0.34	Siratovich et al. (2012)
andesite	Rotokawa geothermal field (New Zealand)	dry	0.07	0.20	Siratovich et al. (2012)
andesite	Rotokawa geothermal field (New Zealand)	dry	0.07	0.24	Siratovich et al. (2012)
andesite	Rotokawa geothermal field (New Zealand)	dry	0.07	0.14	Siratovich et al. (2012)
andesite	Rotokawa geothermal field (New Zealand)	dry	0.07	0.17	Siratovich et al. (2012)
andesite	Rotokawa geothermal field (New Zealand)	dry	0.06	0.22	Siratovich et al. (2012)
andesite	Rotokawa geothermal field (New Zealand)	dry	0.08	0.23	Siratovich et al. (2012)
andesite	Rotokawa geothermal field (New Zealand)	dry	0.06	0.18	Siratovich et al. (2012)
andesite	Ruapehu (New Zealand)	dry	0.06	0.29	Mordensky et al. (2018)
andesite	Ruapehu (New Zealand)	dry	0.08	0.17	Mordensky et al. (2018)
andesite	Ruapehu (New Zealand)	dry	0.03	0.18	Mordensky et al. (2018)
andesite	Ruapehu (New Zealand)	dry	0.04	0.18	Mordensky et al. (2018)
andesite	Ruapehu (New Zealand)	dry	0.01	0.26	Mordensky et al. (2018)
andesite	Ruapehu (New Zealand)	dry	0.03	0.19	Mordensky et al. (2018)
andesite	Ruapehu (New Zealand)	dry	0.09	0.38	Mordensky et al. (2018)
andesite	Ruapehu (New Zealand)	dry	0.06	0.20	Mordensky et al. (2018)
andesite	Ruapehu (New Zealand)	dry	0.19	0.16	Mordensky et al. (2018)
andesite	Ruapehu (New Zealand)	dry	0.20	0.27	Mordensky et al. (2018)
andesite	Ruapehu (New Zealand)	dry	0.15	0.06	Mordensky et al. (2018)
andesite	Ruapehu (New Zealand)	dry	0.16	0.49	Mordensky et al. (2018)
andesite	Ruapehu (New Zealand)	dry	0.03	0.16	Mordensky et al. (2018)
andesite	Ruapehu (New Zealand)	dry	0.10	0.38	Mordensky et al. (2018)
andesite	Ruapehu (New Zealand)	dry	0.11	0.16	Mordensky et al. (2018)
andesite	Ruapehu (New Zealand)	dry	0.04	0.36	Mordensky et al. (2018)
andesite	Ruapehu (New Zealand)	dry	0.01	0.16	Mordensky et al. (2018)
andesite	Ruapehu (New Zealand)	dry	0.01	0.17	Mordensky et al. (2018)
andesite	Ruapehu (New Zealand)	dry	0.02	0.21	Mordensky et al. (2018)
andesite	Ruapehu (New Zealand)	dry	0.01	0.14	Mordensky et al. (2018)
andesite	Ruapehu (New Zealand)	dry	0.02	0.11	Mordensky et al. (2018)
andesite	Ruapehu (New Zealand)	dry	0.04	0.33	Mordensky et al. (2018)
andesite	Ruapehu (New Zealand)	dry	0.01	0.13	Mordensky et al. (2018)
andesite	Ruapehu (New Zealand)	dry	0.07	0.18	Mordensky et al. (2018)
andesite	Ruapehu (New Zealand)	dry	0.05	0.20	Mordensky et al. (2018)
andesite	Ruapehu (New Zealand)	dry	0.10	0.20	Mordensky et al. (2018)
andesite	Ruapehu (New Zealand)	dry	0.06	0.07	Mordensky et al. (2018)
andesite	Ruapehu (New Zealand)	dry	0.06	0.21	Mordensky et al. (2018)
andesite	Ruapehu (New Zealand)	dry	0.03	0.23	Mordensky et al. (2018)
andesite	Uruş Dam (Turkey)	dry	0.04	0.22	Özsan and Akın (2002)
andesite	Not mentioned	dry	0.00	0.30	Saito and Kawamura (1986)
andesite	Not mentioned	dry	0.05	0.14	Saito and Kawamura (1986)
andesite	Kofu andesite (Japan)	dry	0.05	0.22	Ito and Hayashi (1991)
andesite	Honkomatsu andesite (Japan)	dry	0.05	0.18	Ito and Hayashi (1991)
basalt	Uruş Dam (Turkey)	dry	0.03	0.30	Özsan and Akın (2002)
basalt	Nevada Test Site (USA)	dry	0.16	0.25	Nordyke and Wray (1964)
basalt	Nevada Test Site (USA)	dry	0.09	0.18	Nordyke and Wray (1964)
basalt	Nevada Test Site (USA)	dry	0.06	0.08	Nordyke and Wray (1964)
basalt	Nevada Test Site (USA)	dry	0.09	0.25	Nordyke and Wray (1964)
tuff	Uruş Dam (Turkey)	dry	0.16	0.21	Özsan and Akın (2002)

fore likely the result of a combination of the paucity of currently available data and the variability and complexity of volcanic materials. In the absence of a larger dataset, we consider it reasonable to assume that a sensible value for the Poisson's ratio of volcanic rock is 0.21, the average value of the collated values (Fig. 18; Table 4; note that the median and mode are 0.2 and 0.18, respectively). A Poisson's ratio of 0.21 is also within the range for volcanic rocks provided in Gudmundsson (2011). We again highlight that the Poisson's ratio of the elastic medium only plays a small role in determining, for example, source/magma overpressure (Fig. 2). An empirical equation to upscale the Poisson's ratio measured on the sample lengthscale, ν_i, to the rock mass scale, ν_{rm}, was proposed by Vásárhelyi (2009):

$$\nu_{rm} = -0.002GSI + \nu_i + 0.2 \quad (13)$$

The shear modulus, G, and the bulk modulus, K, can then be determined using the relationships between the elastic properties:

$$G = \frac{E}{2(1+\nu)} \quad (14)$$

$$K = \frac{E}{3(1-2\nu)} \quad (15)$$

Therefore, if we take values of E_i and ν_i for volcanic rocks containing a porosity of 0.15 (a reasonable estimate for the average porosity of volcanic rock; E_i = 13.3 GPa; ν_i = 0.21), we can determine upscaled estimates for the four elastic moduli (i.e. E_{rm}, ν_{rm},G_{rm}, and K_{rm}) as a function of GSI (Fig. 19). We find that Poisson's ratio increases and the Young's, shear, and bulk modulus decrease as GSI decreases (Fig. 19). An increase in Poisson's ratio with increasing damage was also observed during stress-cycling experiments

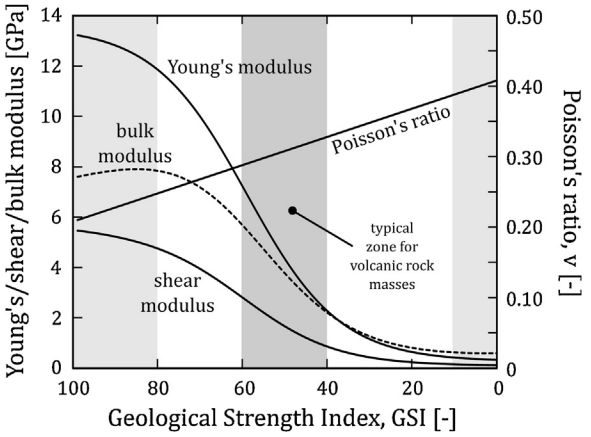

Fig. 19. Young's modulus, shear modulus, bulk modulus, and Poisson's ratio as a function of the Geological Strength Index (GSI). The intact (GSI = 100) elastic modulus was taken as 13.3 GPa (the intact elastic modulus for a rock with 0.15 porosity) and the intact (GSI = 100) Poisson's ratio was taken as 0.21 (the average of the data presented in Fig. 18). The intact (GSI = 100) shear and bulk modulus were calculated using Eqs. (14) and (15). The change in Young's modulus and Poisson's ratio as a function of GSI were calculated using Eqs. (7) and (13), respectively. The rock mass shear and bulk modulus were then calculated using Eqs. (14) and (15). The dark grey zone (GSI = 40–60) highlights the elastic properties for what we consider as typically fractured volcanic rock masses. These estimates will change for different rock masses characterised by different porosities. The light grey zones (high and low values of GSI) do not meet the criteria for the generalised Hoek-Brown failure criterion (see also Fig. 13).

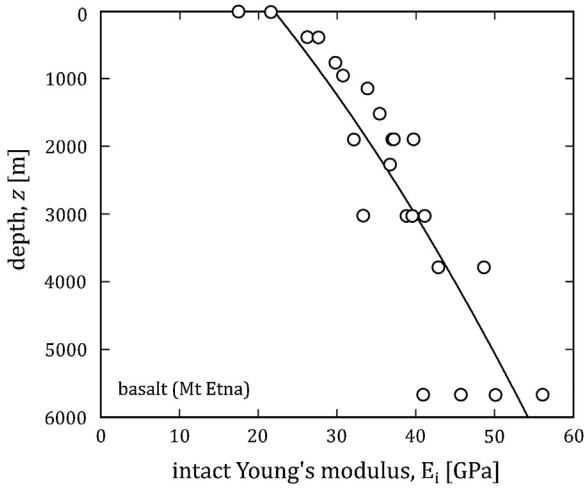

Fig. 20. Intact Young's modulus as a function of depth for basalts from Mt. Etna (Italy) (the same data shown in Fig. 10b). Line is an empirical second-order polynomial fit to the data. See text for details.

performed on volcanic rocks (e.g., Heap et al., 2009, 2010; Kendrick et al., 2013). For intact rock (i.e., on the lengthscale of a laboratory sample), the values of E_{rm}, ν_{rm}, G_{rm}, and K_{rm} are 13.3 GPa, 0.21, 5.5 GPa, and 7.6 GPa, respectively. At the other end of the scale, where GSI = 10, the ν_{rm} increases to about 0.4 and E_{rm}, G_{rm}, and K_{rm} all decrease to below 1 GPa. The 75% reduction in the shear modulus of the elastic medium in the model of Got et al. (2017), as a result of progressive damage (i.e. the progressive generation of new fractures) over a seven-year period (at Grimsvötn volcano), is therefore consistent with the decrease in rock mass shear modulus as a function of GSI predicted herein (Fig. 19). At typical values of GSI for volcanic rock masses, a GSI of 55, the values of E_{rm}, ν_{rm}, G_{rm}, and K_{rm} for a rock mass with an intact rock porosity of 0.15 are 5.4 GPa, 0.3, 2.1 GPa, and 4.5 GPa, respectively (Fig. 19). The equations for calculating rock mass Young's modulus, Poisson's ratio, bulk modulus, and shear modulus are available in accompanying Microsoft Excel© spreadsheet (see Supplementary Materials).

4. Rock mass Young's modulus as a function of depth

The depth of interest for volcano modelling typically ranges from the surface down to several kilometres (see the papers listed in Table 1). However, our suggested approach to upscale Young's moduli—the Hoek-Diederichs equation—relies on empirical relationships between the rock mass Young's modulus measured *in situ* in tunnels within the subsurface (depths of a few hundred metres) and the intact Young's modulus measured under room pressure conditions (Hoek and Diederichs, 2006). Here we present two methods that could be used to provide values of Young's moduli that may better represent rock at depth. Both methods rely on modifying the intact Young's modulus, E_i, to be used in the Hoek-Diederichs equation (Eq. (7)).

First, since it is generally accepted that porosity decreases as a function of depth in the Earth's crust, decreasing the porosity used to determine E_i (Eqs. (8) and (9)) could provide a means to estimate the rock mass Young's modulus, E_{rm}, at depth. The bulk density, and therefore porosity, at depth can be estimated using the following relation (Wilson and Head, 1994):

$$\rho_{b(z)} = \frac{\rho_s}{\left[1 + \left\{\phi_s - (1-\phi_s)\right\}\right] \exp(-\lambda \rho_s g z)} \quad (16)$$

where $\rho_{b(z)}$ is the bulk rock density at a given depth, ϕ_s is the porosity at the surface, g is the acceleration due to gravity (taken as 9.81 m.s^{-2}), z is the depth, and λ is a constant assumed to be 1.18×10^{-8} Pa^{-1} (Head and Wilson, 1992). As an example, if we assume that ρ_s is 2909 kg.m^{-3} (the solid density of basalt, see above) and ϕ_s is 0.15 (considered herein as a reasonable estimate for the average porosity of a volcanic rock, see above), the bulk rock density at a depth of 2000 m using Eq. (16) is 2669 kg.m^{-3}. Using Eq. (11), the porosity of the basalt at a depth of 2000 m is 0.08. Using the exponential fit to our data (Eq. (9)), the intact Young's modulus is increased from 13.3 GPa at the surface to 20.9 GPa at a depth of 2000 m. The rock mass Young's modulus (Eq. (7)) is therefore increased from 5.4 to 8.4 GPa at depths of 0 and 2000 m, respectively.

Another method to provide estimates of the rock mass Young's modulus of volcanic rocks at depth is to interrogate the data shown in Fig. 10. The experimental data presented in Fig. 10 show that the intact Young's modulus of volcanic rocks, which are often microcracked (e.g., Fig. 3), increases as a function of effective pressure or depth. An increase in Young's modulus as a function of increasing confining pressure has been observed previously for basalt (e.g., Adam and Otheim, 2013), granite (e.g., Blake et al., 2019), and variety of metamorphic and sedimentary rocks (Wu et al., 2019 and references therein). If effective pressure, *Peff*, is converted to depth using $Peff = \rho_b \times g \times z$, where g and ρ_b are taken as 9.81 m.s^{-2} and 2700 kg.m^{-3} (i.e. the bulk density of the basalts in Fig. 10b), respectively, we can plot the Young's modulus as a function of depth for the basalts from Mt. Etna (Fig. 20). We chose to perform this analysis on the basalt data due to the large range of effective pressure (from 0 to 150 MPa; Fig. 10b). An estimation of intact Young's modulus for a given depth, $E_{i(z)}$, can therefore be provided by the empirical second-order polynomial fit to these data (Fig. 20):

$$E_{i(z)} = -6.07 \times 10^{-7} z^2 + 7.90 \times 10^{-3} z + E_i \quad (17)$$

For example, using the intact Young's modulus determined for a porosity of 0.15 (considered herein as a reasonable estimate for the average porosity of a volcanic rock, see above) of 13.3 GPa (using Eq. (9)), Eq. (17) predicts an intact Young's modulus of 26.7 GPa for rock at a depth of 2000 m. Using a GSI of 55 (considered herein

as a reasonable estimate for the average GSI of a volcanic rock mass, see above), this provides rock mass Young's moduli of 5.4 and 10.9 GPa at depths of 0 and 2000, respectively (using Eq. (7)). We highlight that the estimate of rock mass Young's modulus for a depth of 2000 m is slightly higher using this latter technique (10.9 versus 8.4 GPa). The equations for estimating rock mass Young's modulus at depth are available in accompanying Microsoft Excel© spreadsheet (see Supplementary Materials).

However, it is unclear to what extent the Hoek-Diederichs equation is suitable for predicting rock mass Young's moduli at depths greater than a few hundred metres. For example, the rock mass Young's modulus for rock at a depth of several kilometres may be higher than that measured in subsurface tunnels, because macroscopic fractures at several kilometres depth will more likely be closed or "locked". As such, estimations of rock mass Young's modulus that use either of the methods described above to provide values of intact Young's modulus for the Hoek-Diederichs equation (Eq. (7)), or those that simply use an intact Young's modulus of a rock measured in the laboratory at an elevated confining pressure, may underestimate the rock mass Young's modulus at depth and should be treated with caution.

Several studies provide empirical relationships to estimate rock mass Young's modulus at depth. Verman et al. (1997), for example, provide an empirical depth correction factor to be used in conjunction with assessments of rock mass structure. The approach of Verman et al. (1997) shows that rock mass Young's modulus increases with depth and that the pressure dependence is related to the competence of the rock. However, a robust relationship between rock mass structure and the correction factor proposed would be required in order to apply the correction factor to sites other than the two investigated by Verman et al. (1997). Further, the maximum depth of the *in situ* data provided in Verman et al. (1997) is less than 500 m. Other approaches, such as that of Asef and Reddish (2002), compare the Young's modulus of intact and jointed samples (containing one to four joints) deformed in laboratory deformation experiments. This approach estimates the Young's modulus of a "jointed rock mass" under a given confining pressure (up to 30 MPa), but does not, however, provide estimates for rock masses characterised by a range of rock mass structures (i.e. rock masses characterised by different GSI values). Further, although the maximum confining pressure used by Asef and Reddish (2002) (30 MPa, equivalent to a depth of about 1.2 km) is applicable to the modelling of volcanic systems, their experiments were performed on sandstone. Nevertheless, Asef and Reddish (2002), as well as Arora (1987), show that jointed rock Young's modulus can increase by a factor of up to 5, 20, or even 200 at high confining pressure, much higher than the increases in intact Young's modulus shown in Figs. 10 and 20. More work is needed to assess the effect of confinement on fractured rock masses comprising interlocking blocks of volcanic rock in order to determine the magnitude of the increase and to confidently include this in our proposed method.

To conclude, although the above-described methods could be used to provide depth-dependent rock mass Young's moduli for volcanic rock, caution is required due to the uncertain applicability of the Hoek-Diederichs equation to rock masses at depths greater than a few hundred metres. Resolving this issue is certainly non-trivial and would require numerous measurements of rock mass Young's modulus (using *in situ* jacking tests, for example) in tunnels or boreholes at depths of several kilometres within a volcano or volcanic terrain. We additionally note that it may not be possible to infer the Young's modulus required for volcano modelling at depths of a few kilometres using seismic velocities: experiments on fine-grained granite have shown that Young's modulus determined using stress-strain data (dry and water-saturated) and elastic wave velocities still differ (by about 20%) at effective pressures as high as 130 MPa (Blake et al., 2019).

5. Case studies: Kīlauea volcano (Hawai'i, USA) and Mt. Unzen (Japan)

We provide analysis of two case study volcanoes—Kīlauea volcano and Mt. Unzen—to demonstrate how our proposed method can be used to provide intact and upscaled Young's modulus estimates. To do so, we use density data from an experimental drill hole at the summit of Kīlauea volcano (from Keller et al., 1979) and porosity data from the USDP-4 borehole drilled within Mt. Unzen (from Sakuma et al., 2008).

The borehole at Kīlauea volcano was drilled to a depth of 1262 m approximately 1 km from the south edge of Halema'uma'u Crater between April 6 and July 9, 1973 (Keller et al., 1974, 1979). The vast majority of the rocks penetrated by the borehole are olivine basalt, with minor amounts of olivine-poor basalt, olivine diabase, and picrite diabase (Keller et al., 1979; Fig. 21). Geophysical logging provided bulk density as a function of depth (Fig. 21a; data from Keller et al., 1979). First, we converted these data to porosity using Eq. (11), assuming a ρ_r of 3000 kg.m^{-3} (Fig. 21b). A solid density slightly higher than the 2909 kg.m^{-3} measured for the sample of basalt of Mt. Etna (Fig. 17) was used to avoid negative porosities: some of the measured bulk densities were as high as 3000 kg.m^{-3} (Keller et al., 1979). We assumed that the rock was dry (pores filled with air) and wet (pores filled with water with a density of 1000 kg.m^{-3}) above and below the water table (at a depth of 491 m; Keller et al., 1979), respectively. Intact Young's modulus was then estimated using Eq. (9) (black line in Fig. 21c). In the absence of GSI assessments, we upscale our values of intact Young's moduli using Eq. (7) and GSI = 55 (the GSI proposed for an average volcanic rock mass, see above) (blue line in Fig. 21c). We provide in Fig. 21d, as a function of depth, "depth-corrected" values of intact Young's moduli, estimated using Eq. (17), and values of "depth-corrected" rock mass Young's moduli (calculated using Eq. (7) and a GSI of 55). We highlight that we do not favour the approach of Eq. (17) over that of Eq. (16): we simply use one of these proposed methods to provide an example of how such data can be "corrected" for depth. We note that the Young's moduli calculated for the very low porosity zone between a depth of 460 and 480 m are likely underestimated as a result of using the exponential fit to the experimental data (Eq. (9); see Fig. 16 and above discussion).

The borehole at Mt. Unzen was drilled to a depth of 1995 m between 2003 and 2004 (Nakada et al., 2005; Sakuma et al., 2008). The rock types intersected are lava flows, lava dykes, pyroclastic rocks, and volcanic breccias (Sakuma et al., 2008; Fig. 22). Geophysical logging provided porosity as a function of depth between a depth of ~800 and ~1780 m (Fig. 22a; data from Sakuma et al., 2008). Intact Young's modulus was then estimated using Eq. (9) (black line in Fig. 22b) and we upscaled these values using Eq. (7) and GSI = 55 (blue line in Fig. 22b). "Depth-corrected" values of intact Young's moduli, estimated using Eq. (17), and values of "depth-corrected" rock mass Young's moduli (calculated using Eq. (7) and a GSI of 55) are provided in Fig. 22c as a function of depth.

The data of Fig. 21c and Fig. 22b reveal that the average intact and rock mass Young's modulus for the basalts of Kīlauea volcano and the volcanic rocks of Mt. Unzen are 10.8 and 8.0 GPa, respectively, and 4.4 and 3.3 GPa, respectively. Interestingly, there is no systematic reduction of porosity, and therefore increase in Young's modulus, with depth (Figs. 21b and 22 a). The presence of porosity in volcanic rocks at depth is consistent with experiments that have shown that lithostatic pressures of 200–400 MPa (depths between 7500 and 15,000 m) are required for the cataclastic collapse of pores (i.e. porosity reduction) in basalts (Zhu et al., 2016 and references therein). For Kīlauea volcano, the units that contain ash layers (units I and II; Fig. 21) are characterised by low values of Young's modulus and high values of Young's modulus characterise the thick, dense lavas (units IV, V, and VI; Fig. 21). For

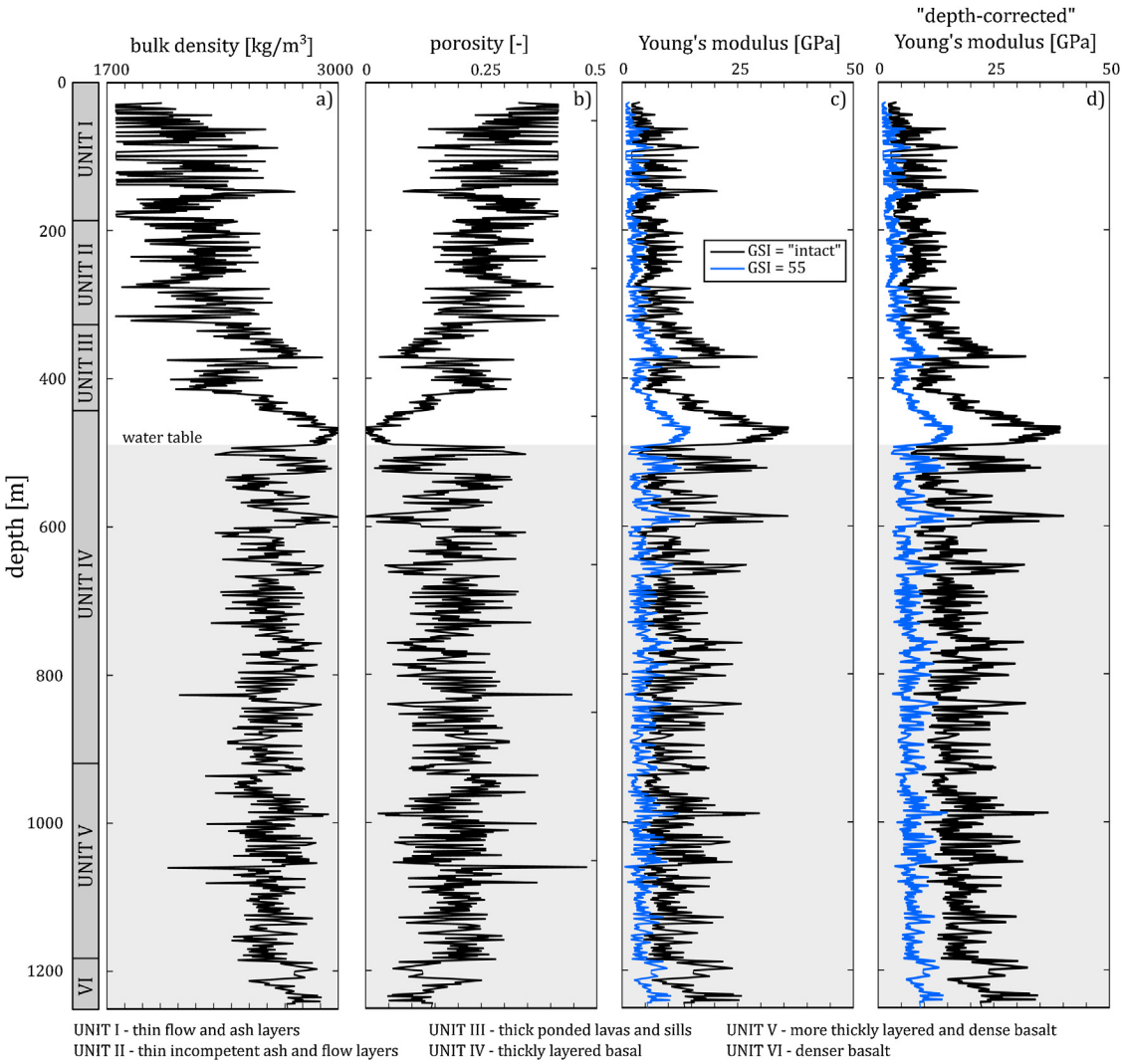

Fig. 21. (a) Bulk density, (b) porosity, (c) Young's modulus, and (d) "depth-corrected" Young's modulus (using Eq. (12)) as a function of depth for Kīlauea volcano (USA). Bulk density data are from geophysical logging within a deep borehole drilled into the summit of Kīlauea volcano in 1973 (data from Keller et al., 1979). Geological interpretation from Keller et al. (1979). Porosity is calculated from the density data using Eq. (8). Intact Young's modulus is estimated using Eq. (9), and rock mass Young's modulus is estimated using a GSI of 55 and Eq. (7). See text for details.

Mt. Unzen, high values of Young's modulus are observed for the lavas and dykes (Fig. 22). The lower average Young's modulus for Mt. Unzen is a consequence of the higher porosities of the rocks encountered by the borehole (Figs. 21b and 22 a). If these values are "corrected" for depth using Eq. (17), the predictions of the values of intact and rock mass Young's modulus increase (Figs. 21d and 22 c). For example, the average "depth-corrected" intact and rock mass Young's modulus for the basalts of Kīlauea volcano and the volcanic rocks of Mt. Unzen are 15.2 and 15.7 GPa, respectively, and 6.2 and 6.4 GPa, respectively. Therefore, although the rocks encountered by the borehole are of higher porosity at Mt. Unzen, when the data are "corrected" for depth using Eq. (17), the estimates of Young's modulus for Mt. Unzen are higher than those for Kīlauea volcano. This is the result of the relative depths of the datasets: the maximum depths of the Mt. Unzen and Kīlauea volcano boreholes are ~1780 and 1262 m, respectively. We highlight that the estimated values of rock mass Young's moduli are low compared to the values typically used in volcano modelling (Table 1). However, we note that the rock mass Young's moduli below a few hundred metres are likely underestimated due to the "locking" of fractures at depth, as mentioned above and discussed in the "Method limitations" section below. Further, the depth "corrections" assume that the increase in intact Young's modulus with depth can be described by Eq. (17), an empirical relationship that describes data from triaxial experiments performed on basalts from Mt. Etna (Fig. 20). Volcanic rocks with different microstructural characteristics (e.g., microcrack densities) than the basalts from Mt. Etna used in these experiments will likely be described by different empirical relationships. However, we consider that the estimates of rock mass Young's modulus presented in Figs. 21 and 22 as the most robust estimates possible with the data and tools currently available.

6. Method limitations

Although we have presented a useful and practical tool to estimate the Young's moduli of a volcanic rock mass, the method suffers from several limitations. First, the Hoek-Diederichs equation (Hoek and Diederichs, 2006) is an empirical relation that was built using data collected in tunnels through mainly sedimentary rocks (260 tests in sedimentary rock, 179 in igneous rock, and 55 in metamorphic rock; Hoek and Diederichs, 2006). Of the 179 igneous rocks, only 46 were basalt, 11 were andesite, and 5 were "andesite-tuff" (Hoek and Diederichs, 2006). There is therefore a possibility that Eq. (7) would differ if the data used in its formulation were volcanic rocks only. Volcanic rock masses may be generally more fractured and therefore less stiff than metamorphic rock masses, for example.

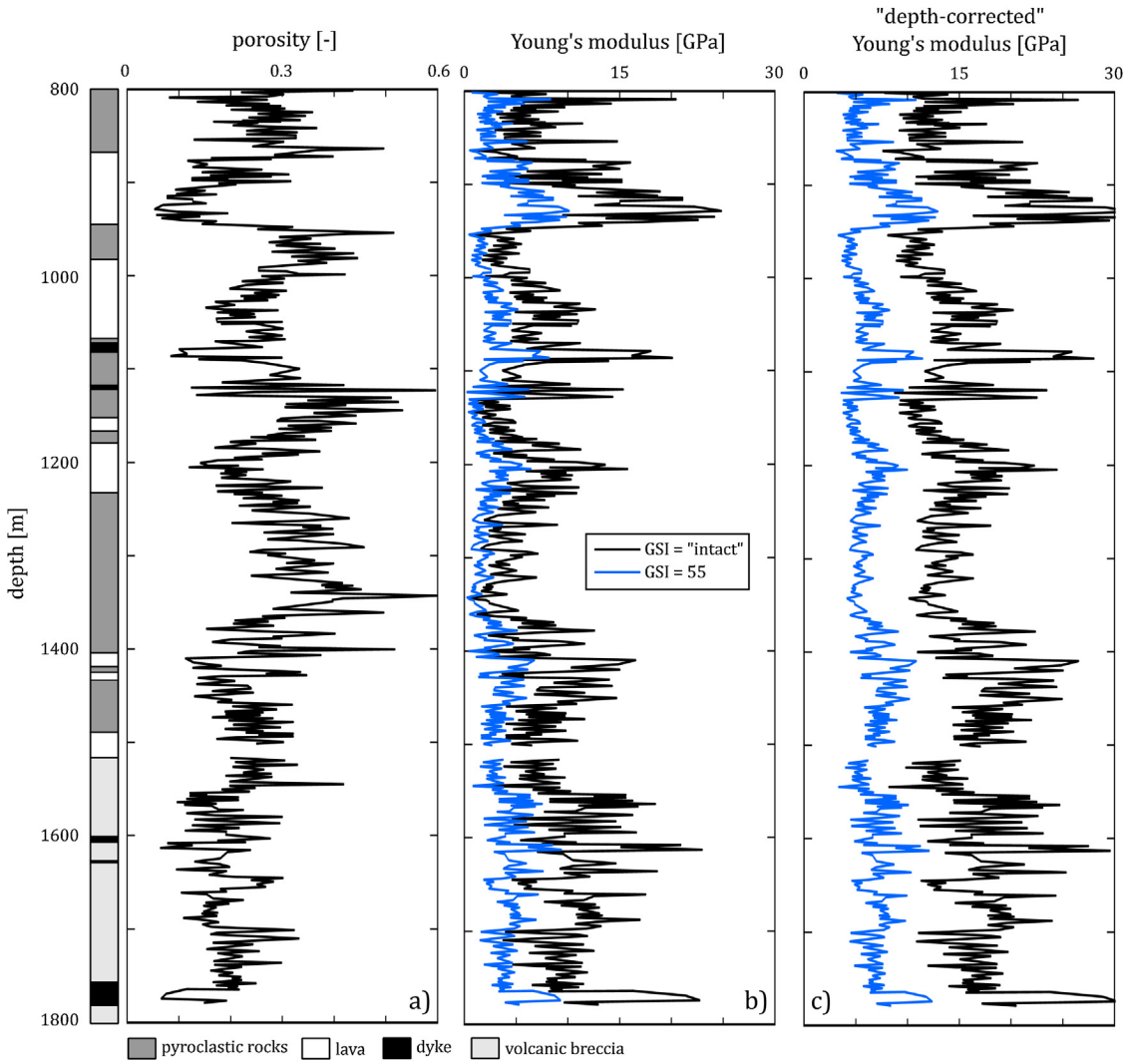

Fig. 22. (a) Porosity, (b) Young's modulus, and (c) "depth-corrected" Young's modulus (using Eq. (17)) as a function of depth for Mt. Unzen (Japan). Porosity data are from geophysical logging within a borehole drilled into Mt. Unzen in 2003–2004 (data from Sakuma et al., 2008). Geological interpretation from Sakuma et al. (2008). Intact Young's modulus is estimated using Eq. (9), and rock mass Young's modulus is estimated using a GSI of 55 and Eq. (7). See text for details.

The Hoek-Diederichs equation (Hoek and Diederichs, 2006) also relies on an accurate assessment of the structure (fracture density and fracture quality; Fig. 13) of a rock mass, which can lead to some subjectivity (see also Marinos et al., 2005). A key strength of the GSI scheme is its descriptive aspect; however, continued discussion within the engineering community has prompted the development of quantified GSI methods to remove subjectivity or to aid inexperienced users. The most commonly used are: Sonmez and Ulusay (1999), Cai et al. (2004), Russo (2009), and Hoek and Diederichs (2013). Bertuzzi et al. (2016) compared the descriptive and quantified schemes and the greatest weakness they found was the disassociation of the vertical axis—the rock structure—from the scale of the problem. This arises because the quantified schemes all use scale-independent measures of joint spacing, joint volume, or RQD, whereas the GSI should be assessed according to the scale of the problem investigated. If possible, and especially for inexperienced users to aid user calibration, one of the quantitative methods referenced above could be used alongside, but not in place of, the descriptive method. Bertuzzi et al. (2016) have shown that differences in GSI of up to 10 points should be expected between the quantitative and descriptive results.

Eqs. (8) and (9), which estimate the intact Young's elastic modulus, are based on connected porosity and Young's modulus data for 276 rock samples. Although we consider the porosity as the most useful metric to estimate the Young's modulus, this is clearly a simplification. Indeed, we have shown here that Young's modulus depends on rock microstructure (the microcrack density (Fig. 7) and pore geometry, for example), explaining the high degree of scatter seen in Fig. 5. Additionally, the Young's modulus predicted by the empirical power law (Eq. (8)) and exponential (Eq. (9)) fits to the data and the Young's modulus measured in the laboratory can differ by up to 15 GPa (Fig. 16b). Although more data may help fine-tune the presented empirical relations (and can be implemented using our accompanying Microsoft Excel© spreadsheet), we highlight that such simplifications are a necessary evil in developing an easy-to-use tool that well describes volcanic rocks, which are invariably microstructurally and texturally complex and heterogeneous (see, for example, Fig. 3). We outline above a multitude of avenues for future laboratory experiments, which may also help improve the predictions provided by the presented technique. With regard to the suitability of our dataset (Table 2), we also highlight that the majority of the data are for andesite and that data for several volcanic rock types, such as pumice and obsidian, are absent. More data, on more rock types, will further improve the predictions provided by Eqs. (8) and (9).

Our data and analysis focuses on providing upscaled Young's moduli for volcanic rock masses. However, for some volcanoes or volcanic terrains, volcanic rocks may only occupy the top few kilo-

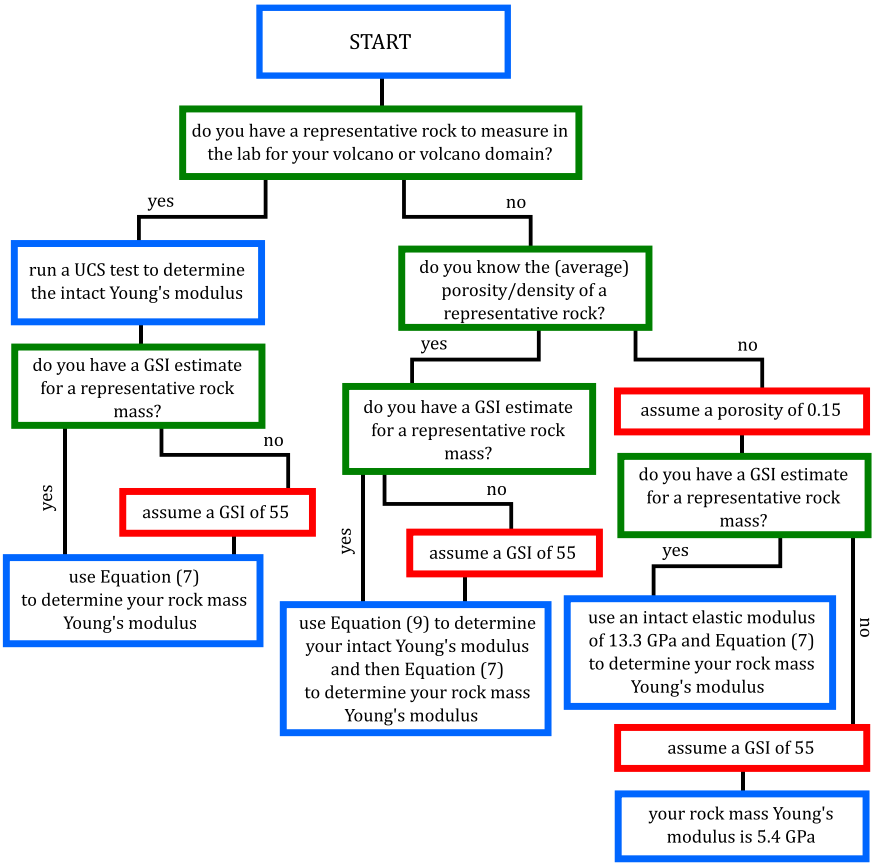

Fig. 23. Flow chart outlining the method to estimate the Young's modulus of a volcanic rock mass presented herein. Estimates can be fine-tuned using additional information about the studied volcano or volcanic terrain, but we also provide average values for the porosity and Geological Strength Index (GSI) for scenarios for which these parameters are unknowns. We highlight that, if of interest, values of intact Young's modulus, E_i, can be first "depth-corrected" using one of the two methods described in Section 4. See text for details.

metres. Mt. Etna, for instance, is underlain by thick successions of sedimentary rocks (the sandstones and clays of the Apenninic-Maghrebian Chain and the carbonate rocks of the Hyblean Plateau; Branca et al., 2011; Heap et al., 2013; Wiesmaier et al., 2015). Therefore, it is likely that, for very deep elastic half-space models, the elastic moduli of the rock types beneath the lava pile should also be considered.

Finally, as highlighted above, the depth of interest for volcano modelling typically ranges from the surface down to several kilometres (see the papers listed in Table 1). However, it is unclear at present as to whether it is appropriate to use values of intact Young's modulus measured at elevated confining pressures (or intact Young's modulus at depth using the methods described above) in the Hoek-Diederichs equation (Eq. (7)). The refinement of the Hoek-Diederichs equation to provide upscaled Young's modulus for deep volcanic rock masses would not only require numerous measurements of rock mass Young's modulus in tunnels or boreholes at depths of several kilometres within a volcano or volcanic terrain (if possible), but also many more studies that investigate the pressure-dependence of the elastic moduli of volcanic rock in the laboratory (i.e. triaxial deformation experiments on suites of common volcanic rock types). We consider estimating rock mass elastic moduli for deep volcanic rock masses as the main outstanding challenge in providing more realistic elastic moduli for volcano modelling.

7. Concluding remarks

We propose herein an easy-to-use tool to determine the Young's modulus for volcanic rock masses for use in elastic analytical solutions and numerical models that are widely used in volcanology to interpret ground deformation signals detected at the surface. To date, modellers have used a variety of techniques, reviewed here (Table 1), to obtain a value or values of Young's modulus to represent their elastic medium. Unfortunately, and due to the paucity of laboratory studies that provide Young's moduli for volcanic rocks and studies that tackle the topic of upscaling these values to the relevant lengthscale, these methods are often non-ideal. Our proposed method relies on a new suite of experimental data for volcanic rocks and a widely used tool in geotechnics, the Hoek-Diederichs equation (Hoek and Diederichs, 2006). The Hoek-Diederichs equation requires two input variables: the intact Young's modulus of the rock (i.e. the Young's modulus of a rock on the lengthscale of a laboratory sample) and the Geological Strength Index of the rock mass (an assessment of the structure of a rock mass based on the fracture density and fracture quality). Importantly, the proposed method can be improved with laboratory measurements of Young's modulus for representative materials and/or structural assessments of the studied area, but do not rely on them. In the absence of this information, we suggest what we consider as reasonable values for the intact Young's modulus and the Geological Strength Index for a typically porous volcanic rock and a typically macrofractured volcanic rock mass, respectively. The former is determined using empirical relationships, developed herein using 276 experiments on volcanic rocks, between porosity and the intact Young's modulus. An instructive flow chart for our proposed method is provided as Fig. 23. Based on the limitations outlined above, there may be some justification for using values of rock mass Young's modulus slightly higher than those estimated using the method outlined herein (for the modelling of deep pressure sources, for example). However, although we have proposed two methods to account for the depth-dependence of intact Young's modulus, the inclusion of

"depth-corrected" values into the Hoek-Diederichs equation may not be entirely appropriate (see discussion above). Those interested in using our approach to provide values of Young's modulus for their model are, of course, welcome to increase or decrease the estimations the method provides, within reason and with accompanying justification, to suit their volcano case study. However, unless there is a clear justification, such as a rock mass characterised by a very low porosity and a very low fracture density, we advise against using values of Young's modulus in excess of 20–30 GPa. Using another empirical relationship to estimate the Poisson's ratio of a rock mass (from Vásárhelyi, 2009), we also provide a means to estimate upscaled values of Poisson's ratio, shear modulus, and bulk modulus for a volcanic rock mass (Eqs. (13), (14), and (15); Fig. 19). Whichever value is adopted for a particular study, we encourage the authors not only to provide their values (in a table, for example), but also to outline their justification for choosing these parameters. We provide a Microsoft Excel© spreadsheet (as Supplementary Materials) containing the data and necessary equations to calculate rock mass elastic moduli that can be updated when new data become available.

The goal of this contribution is to provide data and analysis to assist the selection of elastic moduli for volcano modelling. The selection of the most appropriate elastic moduli will, in turn, provide the most accurate model predictions and therefore the most reliable information regarding the unrest of a particular volcano or volcanic terrain. Although our contribution has focussed on Mogi source modelling, we highlight that the data and analysis provided in this review can be used to provide elastic moduli for a wide variety of geological, geophysical, and engineering applications. Finally, we stress that the approach presented herein is by no means complete. More laboratory data and a more satisfactory method to account for the pressure-dependence of elastic moduli at volcanoes and volcanic terrains are now required (which can be included in our accompanying Microsoft Excel© spreadsheet). We hope this review will inspire new research in this direction and new interdisciplinary collaboration.

Declaration of Competing Interest

We decalre no conflicts of interest.

Acknowledgements

This review has benefitted from the many engaging conversations the first and second authors have had at conferences and meetings in the last years. The first and second authors also acknowledge an Erskine Fellowship at the University of Canterbury awarded to the first author, which kick-started the idea for this paper. The first author additionally thanks Thierry Reuschlé and Bertrand Renaudié. The second author acknowledges New Zealand Ministry of Business, Innovation and Employment Catalyst grant UOCX1508 "Energy Straight from Magma". The experimental data presented in this study are, for the most part, unpublished data that were collected during mechanical studies performed in collaboration with many scientists. Although non-exhaustive, we thank Nick Varley, Yan Lavallée, Frédéric Dondin, Ben Kennedy, Yoshitaka Nara, Alexandra Kushnir, Sergio Vinciguerra, Kelly Russell, Salvatore Martino, and Gian Marco Marmoni. The basalt from Krafla was exported with permission from the Icelandic Institute of Natural History (and we thank Holly Unwin for organising permission). Kelly Russell, Martin Harris, Stephan Kolzenberg, and particularly Amy Ryan are thanked for their help in furnishing the laboratory with the samples from Chaos Crags. The constructive comments of Agust Gudmundsson and an anonymous reviewer helped improve this manuscript.

Appendix A. Supplementary data

Supplementary material related to this article can be found, in the online version, at doi:https://doi.org/10.1016/j.jvolgeores.2019.106684.

References

Adam, L., Otheim, T., 2013. Elastic laboratory measurements and modeling of saturated basalts. J. Geophys. Res. Solid Earth 118 (3), 840–851.
Adelinet, M., Fortin, J., Guéguen, Y., Schubnel, A., Geoffroy, L., 2010. Frequency and fluid effects on elastic properties of basalt: experimental investigations. Geophys. Res. Lett. 37 (2).
Ahmed, A.S., Revil, A., Byrdina, S., Coperey, A., Gailler, L., Grobbe, N., et al., 2018. 3D electrical conductivity tomography of volcanoes. J. Volcanol. Geotherm. Res. 356, 243–263.
Albino, F., Pinel, V., Sigmundsson, F., 2010. Influence of surface load variations on eruption likelihood: application to two Icelandic subglacial volcanoes, Grímsvötn and Katla. Geophys. J. Int. 181 (3), 1510–1524.
Albino, F., Amelung, F., Gregg, P., 2018. The role of pore fluid pressure on the failure of magma reservoirs: insights from Indonesian and Aleutian arc volcanoes. J. Geophys. Res. Solid Earth 123 (2), 1328–1349.
Amelung, F., Jónsson, S., Zebker, H., Segall, P., 2000. Widespread uplift and 'trapdoor'faulting on Galapagos volcanoes observed with radar interferometry. Nature 407 (6807), 993.
Amelung, F., Yun, S.H., Walter, T.R., Segall, P., Kim, S.W., 2007. Stress control of deep rift intrusion at Mauna Loa volcano, Hawai'i. Science 316, 1026–1030, http://dx.doi.org/10.1126/science.1140035.
Anderson, K., Lisowski, M., Segall, P., 2010. Cyclic ground tilt associated with the 2004–2008 eruption of Mount St. Helens. J. Geophys. Res. 115, B11201, http://dx.doi.org/10.1029/2009JB007102.
Anderson, O.L., Schreiber, E., Liebermann, R.C., Soga, N., 1968. Some elastic constant data on minerals relevant to geophysics. Rev. Geophys. 6 (4), 491–524.
Apuani, T., Corazzato, C., Cancelli, A., Tibaldi, A., 2005a. Physical and mechanical properties of rock masses at Stromboli: a dataset for volcano instability evaluation. Bull. Eng. Geol. Environ. 64 (4), 419.
Apuani, T., Corazzato, C., Cancelli, A., Tibaldi, A., 2005b. Stability of a collapsing volcano (Stromboli, italy): limit equilibrium analysis and numerical modelling. J. Volcanol. Geotherm. Res. 144 (1-4), 191–210.
Arora, V.K., 1987. Strength and Deformational Behaviour of Jointed Rocks, Doctoral Dissertation. IIT Delhi, India.
Arnulf, A.F., Harding, A.J., Singh, S.C., Kent, G.M., Crawford, W.C., 2013. Nature of upper crust beneath the Lucky Strike volcano using elastic full waveform inversion of streamer data. Geophys. J. Int. 196 (3), 1471–1491.
Asef, M.R., Reddish, D.J., 2002. The impact of confining stress on the rock mass deformation modulus. Geotechnique 52 (4), 235–241.
Bagnardi, M., Amelung, F., 2012. Space-geodetic evidence for multiple magma reservoirs and subvolcanic lateral intrusions at Fernandina Volcano, Galápagos Islands. J. Geophys. Res. B Solid Earth 117, 1–19, http://dx.doi.org/10.1029/2012JB009465.
Bagnardi, M., Amelung, F., Poland, M.P., 2013. A new model for the growth of basaltic shields based on deformation of Fernandina volcano, Galápagos Islands. Earth Planet. Sci. Lett. 377–378, 358–366, http://dx.doi.org/10.1016/j.epsl.2013.07.016.
Bagnardi, M., Poland, M.P., Carbone, D., Baker, S., Battaglia, M., Amelung, F., 2014. Gravity changes and deformation at Kīlauea Volcano, Hawai'i, associated with summit eruptive activity, 2009-2012. J. Geophys. Res. Solid Earth 119, 7288–7305, http://dx.doi.org/10.1002/2014JB011506.
Baker, S., Amelung, F., 2012. Top-down inflation and deflation at the summit of Klauea Volcano, Hawai'i observed with InSAR. J. Geophys. Res. B Solid Earth 117, http://dx.doi.org/10.1029/2011JB009123.
Bakker, R.R., Frehner, M., Lupi, M., 2016. How temperature-dependent elasticity alters host rock/magmatic reservoir models: a case study on the effects of ice-cap unloading on shallow volcanic systems. Earth Planet. Sci. Lett. 456, 16–25.
Barton, N., 2006. Rock Quality, Seismic Velocity, Attenuation and Anisotropy. Taylor and Francis, London.
Bass, J.D., 1995. Elasticity of minerals, glasses, and melts. Mineral Physics & Crystallography: a Handbook of Physical Constants, 2., pp. 45–63.
Baud, P., Schubnel, A., Wong, T.F., 2000a. Dilatancy, compaction, and failure mode in Solnhofen limestone. J. Geophys. Res. Solid Earth 105 (B8), 19289–19303.
Baud, P., Zhu, W., Wong, T.F., 2000b. Failure mode and weakening effect of water on sandstone. J. Geophys. Res. Solid Earth 105 (B7), 16371–16389.
Baud, P., Exner, U., Lommatzsch, M., Reuschlé, T., Wong, T.F., 2017. Mechanical behavior, failure mode, and transport properties in a porous carbonate. J. Geophys. Res. Solid Earth 122 (9), 7363–7387.
Bazargan, M., Gudmundsson, A., 2019. Dike-induced stresses and displacements in layered volcanic zones. J. Volcanol. Geotherm. Res. 384, 189–205.
Beauducel, F., Cornet, F.-H., Suhanto, E., Duquesnoy, T., Kasser, M., 2000. Constraints on magma flux from displacements data at Merapi volcano, Java, Indonesia. J. Geophys. Res. Solid Earth 105, 8193–8203, http://dx.doi.org/10.1029/1999JB900368.
Berckhemer, H., Baier, B., Gebrande, H., Makris, J., Menzel, H., Miller, H., Vees, R., 1975. Deep seismic soundings in the Afar region and on the highland of Ethiopia. In: Pilger, A., Rösler, A. (Eds.), Proceedings of an International Symposium on the

Afar Region and RiftRelated Problems, Bad Bergzabren, Germany. Schweizerbart, Stuttgart, Germany, pp. 89–107.
Bernard, B., Kueppers, U., Ortiz, H., 2015. Revisiting the statistical analysis of pyroclast density and porosity data. Solid Earth 6 (3), 869–879.
Bertuzzi, R., Douglas, K., Mostyn, G., 2016. Comparison of quantified and chart GSI for four rock masses. Eng. Geol. 202, 24–35.
Bieniawski, Z.T., 1978. Determining rock mass deformability: experience from case histories. Int. J. Rock Mech. Min. Sci. 15 (5), 237–247.
Bieniawski, Z.T., 1984. Rock Mechanic Design in Mining and Tunnelling. Balkema.
Bieniawski, Z.T., 1989. Engineering Rock Mass Classification. Wiley Interscience, New York.
Birch, F., 1966. Compressibility; elastic constants, Handbook of physical constants. Mera. Geol. Soc. Am. 97, 97–174.
Blake, O.O., Faulkner, D.R., Tatham, D.J., 2019. The role of fractures, effective pressure and loading on the difference between the static and dynamic Poisson's ratio and Young's modulus of Westerly granite. Int. J. Rock Mech. Min. Sci. 116, 87–98.
Bonaccorso, A., 1996. Dynamic inversion of ground deformation data for modeling volcanic sources (Etna 1991-93). Geophys. Res. Lett. 23 (5), 451–454.
Bonaccorso, A., Davis, P.M., 1999. Models of ground deformation from vertical volcanic conduits with application to eruptions of Mount St. Helens and Mount Etna. J. Geophys. Res. Solid Earth 104, 10531–10542, http://dx.doi.org/10.1029/1999JB900054.
Bonafede, M., Dragoni, M., Quareni, F., 1986. Displacement and stress fields produced by a centre of dilation and by a pressure source in a viscoelastic halfspace: application to the study of ground deformation and seismic activity at Campi Flegrei, Italy. Geophys. J. R. astr. Soc. 87, 455–485, http://dx.doi.org/10.1111/j.1365-246X.1986.tb06632.x.
Bonafede, M., Ferrari, C., 2009. Analytical models of deformation and residual gravity changes due to a Mogi source in a viscoelastic medium. Tectonophysics 471 (1-2), 4–13.
Branca, S., Coltelli, M., Groppelli, G., Lentini, F., 2011. Geological map of Etna volcano, 1: 50,000 scale. Ital. J. Geosci. 130 (3), 265–291.
Bubeck, A., Walker, R.J., Healy, D., Dobbs, M., Holwell, D.A., 2017. Pore geometry as a control on rock strength. Earth Planet. Sci. Lett. 457, 38–48.
Budiansky, B., O'connell, R.J., 1976. Elastic moduli of a cracked solid. Int. J. Solids Struct. 12 (2), 81–97.
Byrdina, S., Friedel, S., Vandemeulebrouck, J., Budi-Santoso, A., Suryanto, W., Rizal, M.H., Winata, E., 2017. Geophysical image of the hydrothermal system of Merapi volcano. J. Volcanol. Geotherm. Res. 329, 30–40.
Cai, M., Kaiser, P.K., Uno, H., Tasaka, Y., Minami, M., 2004. Estimation of rock mass deformation modulus and strength of jointed hard rock masses using the GSI system. Int. J. Rock Mech. Min. Sci. 41 (1), 3–19.
Carrier, A., Got, J.L., Peltier, A., Ferrazzini, V., Staudacher, T., Kowalski, P., Boissier, P., 2015. A damage model for volcanic edifices: implications for edifice strength, magma pressure, and eruptive processes. J. Geophys. Res. Solid Earth 120 (1), 567–583.
Castagna, A., Ougier-Simonin, A., Benson, P.M., Browning, J., Walker, R.J., Fazio, M., Vinciguerra, S., 2018. Thermal damage and pore pressure effects of the brittle-ductile transition in Comiso Limestone. J. Geophys. Res. Solid Earth 123 (9), 7644–7660.
Cayol, V., Cornet, F.H., 1998a. Effects of topography on the interpretation of the deformation field of prominent volcanoes-Application to Etna. Geophys. Res. Lett. 25, 1979–1982, http://dx.doi.org/10.1029/98GL51512.
Cayol, V., Cornet, F.H., 1998b. Three-dimensional modeling of the 1983–1984 eruption at Piton de la Fournaise Volcano, Réunion Island. J. Geophys. Res. 103, 18025, http://dx.doi.org/10.1029/98JB00201.
Cayol, V., Cornet, F.H., 1997. 3D mixed boundary elements for elastostatic deformation field analysis. Int. J. Rock Mech. Min. Sci. (1997) 32, 275–287.
Cerfontaine, B., Collin, F., 2018. Cyclic and fatigue behaviour of rock materials: review, interpretation and research perspectives. Rock Mech. Rock Eng. 51 (2), 391–414.
Chadwick, W.W., Archuleta, R.J., Swanson, D.A., 1988. The mechanics of ground deformation precursory to dome-building extrusions at Mount St. Helens 1981-1982. J. Geophys. Res. Solid Earth 93, 4351–4366, http://dx.doi.org/10.1029/JB093iB05p04351.
Chang, C., Zoback, M.D., Khaksar, A., 2006. Empirical relations between rock strength and physical properties in sedimentary rocks. J. Pet. Sci. Eng. 51 (3-4), 223–237.
Cheng, C., Johnston, D.H., 1981. Dynamic and static moduli. Geophys. Res. Lett. 8 (1), 39–42.
Christensen, N.I., 1996. Poisson's ratio and crustal seismology. J. Geophys. Res. Solid Earth 101 (B2), 3139–3156.
Christensen, N.I., Mooney, W.D., 1995. Seismic velocity structure and composition of the continental crust: a global view. J. Geophys. Res. Solid Earth 100 (B6), 9761–9788.
Ciccotti, M., Mulargia, F., 2004. Differences between static and dynamic elastic moduli of a typical seismogenic rock. Geophys. J. Int. 157 (1), 474–477.
Coats, R., Kendrick, J.E., Wallace, P.A., Miwa, T., Hornby, A.J., Ashworth, J.D., et al., 2018. Failure criteria for porous dome rocks and lavas: a study of Mt. Unzen, Japan. Solid Earth 9 (6), 1299–1328.
Colombier, M., Wadsworth, F.B., Gurioli, L., Scheu, B., Kueppers, U., Di Muro, A., Dingwell, D.B., 2017. The evolution of pore connectivity in volcanic rocks. Earth Planet. Sci. Lett. 462, 99–109.
Crescentini, L., Amoruso, A., 2007. Effects of crustal layering on the inversion of deformation and gravity data in volcanic areas: An application to the Campi Flegrei caldera, Italy. Geophys. Res. Lett. 34 (9).
Davis, P.M., Hastie, L.M., Stacey, F.D., 1974. Stresses within an active volcano—with particular reference to Kīlauea. Tectonophysics 22 (3-4), 355–362.
Davis, P.M., 1986. Surface deformation due to inflation of an arbitrarily oriented triaxial ellipsoidal cavity in an elastic half-space, with reference to Kīlauea volcano, Hawai'i. J. Geophys. Res. Solid Earth 91, 7429–7438, http://dx.doi.org/10.1029/JB091iB07p07429.
Delcamp, A., Roberti, G., de Vries, B.V.W., 2016. Water in volcanoes: evolution, storage and rapid release during landslides. Bull. Volcanol. 78 (12), 87.
Deere, D.U., 1968. Geological considerations. In: Stagg, K.G., Zienkiewicz, O.C. (Eds.), Rock Mechanics in Engineering Practice. John Wiley & Sons, London, pp. 1–20, 1968.
Deere, D.U., Deere, D.W., 1988. The rock quality designation (RQD) index in practice. In: Kirkaldie, L. (Ed.), Rock Classification Systems for Engineering Purposes. ASTM International, pp. 91–101.
Delgado, F., Pritchard, M., Lohman, R., Naranjo, J.A., 2014. The 2011 Hudson volcano eruption (Southern Andes, Chile): pre-eruptive inflation and hotspots observed with InSAR and thermal imagery. Bull. Volcanol. 76, 815, http://dx.doi.org/10.1007/s00445-014-0815-9.
del Potro, R., Hürlimann, M., 2008. Geotechnical classification and characterisation of materials for stability analyses of large volcanic slopes. Eng. Geol. 98 (1-2), 1–17.
del Potro, R., Hürlimann, M., 2009. The decrease in the shear strength of volcanic materials with argillic hydrothermal alteration, insights from the summit region of Teide stratovolcano, Tenerife. Eng. Geol. 104 (1-2), 135–143.
de Zeeuw-van Dalfsen, E., Pedersen, R., Hooper, A., Sigmundsson, F., 2012. Subsidence of Askja caldera 2000–2009: modelling of deformation processes at an extensional plate boundary, constrained by time series InSAR analysis. J. Volcanol. Geotherm. Res. 213, 72–82.
Dingwell, D.B., 1996. Volcanic Dilemma—Flow or Blow? Science 273 (5278), 1054–1055.
Dondin, F.J., Heap, M.J., Robertson, R.E.A., Dorville, J.M., Carey, S., 2017. Flank instability assessment at Kick-'em-Jenny submarine volcano (Grenada, Lesser Antilles): a multidisciplinary approach using experiments and modeling. Bull. Volcanol. 79 (1), 5.
Durán, E.L., Adam, L., Wallis, I.C., Barnhoorn, A., 2019. Mineral alteration and fracture influence on the elastic properties of volcaniclastic rocks. J. Geophys. Res. Solid Earth 124 (5), 4576–4600.
Eissa, E.A., Kazi, A., 1988. Relation between static and dynamic Young's moduli of rocks. Int. J. Rock Mech. Min. Geomech. Abstr. 25 (6).
Ellis, S.M., Wilson, C.J.N., Bannister, S., Bibby, H.M., Heise, W., Wallace, L., Patterson, N., 2007. A future magma inflation event under the rhyolitic Taupo volcano, New Zealand: numerical models based on constraints from geochemical, geological, and geophysical data. J. Volcanol. Geotherm. Res. 168 (1-4), 1–27.
Elsworth, D., Mattioli, G., Taron, J., Voight, B., Herd, R., 2008. Implications of magma transfer between multiple reservoirs on eruption cycling. Science 322, 246–248, http://dx.doi.org/10.1126/science.1161297.
Evans, B., Fredrich, J.T., Wong, T.F., 1990. The brittle-ductile transition in rocks: recent experimental and theoretical progress. The Brittle-Ductile Transition in Rocks. Geophys. Monogr. Ser. 56, 1–20.
Farquharson, J., Heap, M.J., Varley, N.R., Baud, P., Reuschlé, T., 2015. Permeability and porosity relationships of edifice-forming andesites: a combined field and laboratory study. J. Volcanol. Geotherm. Res. 297, 52–68.
Farquharson, J.I., Wild, B., Kushnir, A.R., Heap, M.J., Baud, P., Kennedy, B., 2019. Acid-induced dissolution of andesite: evolution of permeability and strength. J. Geophys. Res. Solid Earth.
Folch, A., Martí, J., 2004. Geometrical and mechanical constraints on the formation of ring-fault calderas. Earth Planet. Sci. Lett. 221, 215–225, http://dx.doi.org/10.1016/S0012-821X(04)00101-3.
Fortin, J., Stanchits, S., Vinciguerra, S., Guéguen, Y., 2011. Influence of thermal and mechanical cracks on permeability and elastic wave velocities in a basalt from Mt. Etna volcano subjected to elevated pressure. Tectonophysics 503 (1-2), 60–74.
Frolova, J., Ladygin, V., Rychagov, S., Zukhubaya, D., 2014. Effects of hydrothermal alterations on physical and mechanical properties of rocks in the Kuril–Kamchatka island arc. Eng. Geol. 183, 80–95.
Fukushima, Y., Cayol, V., Durand, P., 2005. Finding realistic dike models from interferometric synthetic aperture radar data: the February 2000 eruption at Piton de la Fournaise. J. Geophys. Res. Solid Earth 110, 1–15, http://dx.doi.org/10.1029/2004JB003268.
Galera, J.M., Alvarez, M., Bieniawski, Z.T., 2007. Evaluation of the deformation modulus of rock masses using RMR, comparison with dilatometer tests. In: Underground Works Under Special Conditions: Proceedings of the ISRM Workshop W1, Madrid, Spain, 6-7 July 2007.
Galgana, G.A., Newman, A.V., Hamburger, M.W., Solidum, R.U., 2014. Geodetic observations and modeling of time-varying deformation at Taal Volcano, Philippines. J. Volcanol. Geotherm. Res. 271, 11–23, http://dx.doi.org/10.1016/J.JVOLGEORES.2013.11.005.
Gercek, H., 2007. Poisson's ratio values for rocks. Int. J. Rock Mech. Min. Sci. 44 (1), 1–13.
Geyer, A., Gottsmann, J., 2010. The influence of mechanical stiffness on caldera deformation and implications for the 1971–1984 Rabaul uplift (Papua New Guinea). Tectonophysics 483 (3-4), 399–412.
Ghorbani, A., Revil, A., Coperey, A., Ahmed, A.S., Roque, S., Heap, M.J., et al., 2018. Complex conductivity of volcanic rocks and the geophysical mapping of alteration in volcanoes. J. Volcanol. Geotherm. Res. 357, 106–127.

González de Vallejo, L.I., Ferrer, M., 2011. Geological Engineering. CRC Press/Balkema, Leiden, The Netherlands, pp. 153.
Got, J.L., Carrier, A., Marsan, D., Jouanne, F., Vogfjörd, K., Villemin, T., 2017. An analysis of the nonlinear magma-edifice coupling at Grimsvötn volcano (Iceland). J. Geophys. Res. Solid Earth 122 (2), 826–843.
Grandin, R., Socquet, A., Jacques, E., Mazzoni, N., de Chabalier, J.B., King, G.C.P., 2010. Sequence of rifting in Afar, Manda-Hararo rift, Ethiopia, 2005–2009: time-space evolution and interactions between dikes from interferometric synthetic aperture radar and static stress change modeling. J. Geophys. Res. Solid Earth 115 (B10).
Grapenthin, R., Sigmundsson, F., Geirsson, H., Arnadóttir, T., Pinel, V., 2006. Icelandic rhythmics: annual modulation of land elevation and plate spreading by snow load. Geophys. Res. Lett. 33 (24).
Grapenthin, R., Ófeigsson, B.G., Sigmundsson, F., Sturkell, E., Hooper, A., 2010. Pressure sources versus surface loads: analyzing volcano deformation signal composition with an application to Hekla volcano, Iceland. Geophys. Res. Lett. 37, http://dx.doi.org/10.1029/2010GL044590, n/a-n/a.
Griffiths, L., Heap, M.J., Xu, T., Chen, C.F., Baud, P., 2017. The influence of pore geometry and orientation on the strength and stiffness of porous rock. J. Struct. Geol. 96, 149–160.
Grosfils, E.B., 2007. Magma reservoir failure on the terrestrial planets: assessing the importance of gravitational loading in simple elastic models. J. Volcanol. Geotherm. Res. 166 (2), 47–75.
Gudmundsson, A., 1988. Effect of tensile stress concentration around magma chambers on intrusion and extrusion frequencies. J. Volcanol. Geotherm. Res. 35 (3), 179–194.
Gudmundsson, A., 1990. Emplacement of dikes, sills and crustal magma chambers at divergent plate boundaries. Tectonophysics 176 (3-4), 257–275.
Gudmundsson, A., 2002. Emplacement and arrest of sheets and dykes in central volcanoes. J. Volcanol. Geotherm. Res. 116 (3-4), 279–298.
Gudmundsson, A., Brenner, S.L., 2004. How mechanical layering affects local stresses, unrests, and eruptions of volcanoes. Geophys. Res. Lett. 31 (16).
Gudmundsson, A., 2006. How local stresses control magma-chamber ruptures, dyke injections, and eruptions in composite volcanoes. Earth. Rev. 79 (1-2), 1–31.
Gudmundsson, A., 2011. Rock Fractures in Geological Processes. Cambridge University Press.
Gudmundsson, A., 2012. Magma chambers: formation, local stresses, excess pressures, and compartments. J. Volcanol. Geotherm. Res. 237, 19–41.
Guéguen, Y., Palciauskas, V., 1994. Introduction to the Physics of Rocks. Princeton University Press.
Hamling, I.J., Ayele, A., Bennati, L., Calais, E., Ebinger, C.J., Keir, D., Lewi, E., Wright, T.J., Yirgu, G., 2009. Geodetic observations of the ongoing Dabbahu rifting episode: new dyke intrusions in 2006 and 2007. Geophys. J. Int. 178, 989–1003, http://dx.doi.org/10.1111/j.1365-246X.2009.04163.x.
Harnett, C.E., Kendrick, J.E., Lamur, A., Thomas, M.E., Stinton, A., Wallace, P.A., et al., 2019. Evolution of Mechanical Properties of Lava Dome Rocks Across the 1995–2010 Eruption of Soufrière Hills Volcano, Montserrat. Front. Earth Sci. 7.
Hashin, Z., Shtrikman, S., 1963. A variational approach to the theory of the elastic behaviour of multiphase materials. J. Mech. Phys. Solids 11 (2), 127–140.
Hautmann, S., Gottsmann, J., Sparks, R.S.J., Mattioli, G.S., Sacks, I.S., Strutt, M.H., 2010. Effect of mechanical heterogeneity in arc crust on volcano deformation with application to Soufrière Hills Volcano, Montserrat, West Indies. J. Geophys. Res. Solid Earth 115 (B9).
Hautmann, S., Hidayat, D., Fournier, N., Linde, A.T., Sacks, I.S., Williams, C.P., 2013. Pressure changes in the magmatic system during the December 2008/January 2009 extrusion event at Soufrière Hills Volcano, Montserrat (W.I.), derived from strain data analysis. J. Volcanol. Geotherm. Res. 250, 34–41, http://dx.doi.org/10.1016/J.JVOLGEORES.2012.10.006.
Head, J.W., Wilson, L., 1992. Magma reservoirs and neutral buoyancy zones on Venus: implications for the formation and evolution of volcanic landforms. J. Geophys. Res. Planets 97 (E3), 3877–3903.
Healy, D., Rizzo, R.E., Cornwell, D.G., Farrell, N.J., Watkins, H., Timms, N.E., et al., 2017. FracPaQ: a MATLAB™ toolbox for the quantification of fracture patterns. J. Struct. Geol. 95, 1–16.
Heap, M.J., Baud, P., Meredith, P.G., Vinciguerra, S., Bell, A.F., Main, I.G., 2011. Brittle creep in basalt and its application to time-dependent volcano deformation. Earth Planet. Sci. Lett. 307 (1-2), 71–82.
Heap, M.J., Baud, P., Meredith, P.G., Vinciguerra, S., Reuschlé, T., 2014b. The permeability and elastic moduli of tuff from Campi Flegrei, Italy: implications for ground deformation modelling. Solid Earth 5 (1), 25–44.
Heap, M.J., Farquharson, J.I., Baud, P., Lavallée, Y., Reuschlé, T., 2015a. Fracture and compaction of andesite in a volcanic edifice. Bull. Volcanol. 77 (6), 55.
Heap, M.J., Farquharson, J.I., Wadsworth, F.B., Kolzenburg, S., Russell, J.K., 2015c. Timescales for permeability reduction and strength recovery in densifying magma. Earth Planet. Sci. Lett. 429, 223–233.
Heap, M.J., Faulkner, D.R., Meredith, P.G., Vinciguerra, S., 2010. Elastic moduli evolution and accompanying stress changes with increasing crack damage: implications for stress changes around fault zones and volcanoes during deformation. Geophys. J. Int. 183 (1), 225–236.
Heap, M.J., Gravley, D.M., Kennedy, B.M., Gilg, H.A., Bertolett, E., Barker, S.L., 2019c. Quantifying the role of hydrothermal alteration in creating geothermal and epithermal mineral resources: the Ohakuri ignimbrite (Taupō Volcanic Zone, New Zealand). J. Volcanol. Geotherm. Res., 106703, http://dx.doi.org/10.1016/j.jvolgeores.2019.106703.
Heap, M.J., Kennedy, B.M., Pernin, N., Jacquemard, L., Baud, P., Farquharson, J.I., et al., 2015b. Mechanical behaviour and failure modes in the Whakaari (White Island volcano) hydrothermal system, New Zealand. J. Volcanol. Geotherm. Res. 295, 26–42.
Heap, M.J., Lavallée, Y., Laumann, A., Hess, K.U., Meredith, P.G., Dingwell, D.B., 2012. How tough is tuff in the event of fire? Geology 40 (4), 311–314.
Heap, M.J., Lavallée, Y., Petrakova, L., Baud, P., Reuschlé, T., Varley, N.R., Dingwell, D.B., 2014a. Microstructural controls on the physical and mechanical properties of edifice-forming andesites at Volcán de Colima, Mexico. J. Geophys. Res. Solid Earth 119 (4), 2925–2963.
Heap, M.J., Mollo, S., Vinciguerra, S., Lavallée, Y., Hess, K.U., Dingwell, D.B., et al., 2013. Thermal weakening of the carbonate basement under Mt. Etna volcano (Italy): implications for volcano instability. J. Volcanol. Geotherm. Res. 250, 42–60.
Heap, M.J., Russell, J.K., Kennedy, L.A., 2016. Mechanical behaviour of dacite from Mount St. Helens (USA): A link between porosity and lava dome extrusion mechanism (dome or spine)? J. Volcanol. Geotherm. Res. 328, 159–177.
Heap, M.J., Vinciguerra, S., Meredith, P.G., 2009. The evolution of elastic moduli with increasing crack damage during cyclic stressing of a basalt from Mt. Etna volcano. Tectonophysics 471 (1-2), 153–160.
Heap, M.J., Wadsworth, F.B., 2016. Closing an open system: pore pressure changes in permeable edifice rock at high strain rates. J. Volcanol. Geotherm. Res. 315, 40–50.
Heap, M.J., Coats, R., Chen, C.F., Varley, N., Lavallée, Y., Kendrick, J., et al., 2018a. Thermal resilience of microcracked andesitic dome rocks. J. Volcanol. Geotherm. Res. 367, 20–30.
Heap, M.J., Farquharson, J.I., Kushnir, A.R., Lavallée, Y., Baud, P., Gilg, H.A., Reuschlé, T., 2018b. The influence of water on the strength of Neapolitan Yellow Tuff, the most widely used building stone in Naples (Italy). Bull. Volcanol. 80 (6), 51.
Heap, M., Kushnir, A., Griffiths, L., Wadsworth, F., Marmoni, G.M., Fiorucci, M., et al., 2018c. Fire resistance of the Mt. Epomeo Green Tuff, a widely-used building stone on Ischia Island (Italy). Volcanica 1 (1), 33–48.
Heap, M.J., Troll, V.R., Kushnir, A.R., Gilg, H.A., Collinson, A.S., Deegan, F.M., Darmawan, H., Seraphine, N., Neuberg, J., Walter, T.R., 2019b. Hydrothermal alteration of andesitic lava domes can lead to explosive volcanic behaviour. Nat. Commun. 10 (1), 5063, http://dx.doi.org/10.1038/s41467-019-13102-8.
Heap, M.J., Villeneuve, M., Kushnir, A.R., Farquharson, J.I., Baud, P., Reuschlé, T., 2019a. Rock mass strength and elastic modulus of the Buntsandstein: an important lithostratigraphic unit for geothermal exploitation in the Upper Rhine Graben. Geothermics 77, 236–256.
Hoek, E., Diederichs, M.S., 2006. Empirical estimation of rock mass modulus. Int. J. Rock Mech. Min. Sci. 43 (2), 203–215.
Hoek, E., Carter, T.G., Diederichs, M.S., 2013. Quantification of the Geological Strength Index Chart. In 47th US Rock mechanics/geomechanics Symposium. American Rock Mechanics Association.
Hoek, E., Brown, E.T., 1997. Practical estimates of rock mass strength. Int. J. Rock Mech. Min. Sci. 34 (8), 1165–1186.
Hoek, E., Brown, E.T., 2019. The Hoek–Brown failure criterion and GSI–2018 edition. J. Rock Mech. Geotech. Eng. 11 (3), 445–463.
Holohan, E.P., Schöpfer, M.P.J., Walsh, J.J., 2011. Mechanical and geometric controls on the structural evolution of pit crater and caldera subsidence. J. Geophys. Res. Solid Earth 116 (B7).
Ito, T., Hayashi, K., 1991. Physical background to the breakdown pressure in hydraulic fracturing tectonic stress measurements. Int. J. Rock Mech. Min. Sci. 28 (4), 285–293.
Jónsson, S., 2009. Stress interaction between magma accumulation and trapdoor faulting on Sierra Negra volcano, Galápagos. Tectonophysics 471, 36–44, http://dx.doi.org/10.1016/j.tecto.2008.08.005.
Jónsson, S., Zebker, H., Amelung, F., 2005. On trapdoor faulting at Sierra Negra volcano, Galápagos. J. Volcanol. Geotherm. Res. 144, 59–71, http://dx.doi.org/10.1016/j.jvolgeores.2004.11.029.
Jousset, P., Mori, H., Okada, H., 2003. Elastic models for the magma intrusion associated with the 2000 eruption of Usu Volcano, Hokkaido, Japan. J. Volcanol. Geotherm. Res. 125, 81–106, http://dx.doi.org/10.1016/S0377-0273(03)00090-8.
Justo, J.L., Justo, E., Azañón, J.M., Durand, P., Morales, A., 2010. The use of rock mass classification systems to estimate the modulus and strength of jointed rock. Rock Mech. Rock Eng. 43 (3), 287–304.
Kavanagh, J.L., Menand, T., Sparks, R.S.J., 2006. An experimental investigation of sill formation and propagation in layered elastic media. Earth Planet. Sci. Lett. 245 (3-4), 799–813.
Kavanagh, J.L., Menand, T., Daniels, K.A., 2013. Gelatine as a crustal analogue: determining elastic properties for modelling magmatic intrusions. Tectonophysics 582, 101–111.
Kavanagh, J.L., Burns, A.J., Hazim, S.H., Wood, E.P., Martin, S.A., Hignett, S., Dennis, D.J., 2018. Challenging dyke ascent models using novel laboratory experiments: implications for reinterpreting evidence of magma ascent and volcanism. J. Volcanol. Geotherm. Res. 354, 87–101.
Kayabasi, A., Gokceoglu, C., 2018. Deformation modulus of rock masses: an assessment of the existing empirical equations. Geotech. Geol. Eng. 36 (4), 2683–2699.
Keir, D., Pagli, C., Bastow, I.D., Ayele, A., 2011. The magma-assisted removal of Arabia in Afar: evidence from dike injection in the Ethiopian rift captured using InSAR and seismicity. Tectonics 30, http://dx.doi.org/10.1029/2010TC002785, n/a-n/a.
Keller, G.V., Murray, J.C., Skokan, J.J., Skokan, C.K., 1974. CSM research drill hole at summit of Kilauea Volcano. Mines Mag 64 (5), 14–18.
Keller, G.V., Grose, L.T., Murray, J.C., Skokan, C.K., 1979. Results of an experimental drill hole at the summit of Kilauea Volcano, Hawaii. J. Volcanol. Geotherm. Res. 5 (3-4), 345–385.

Kemeny, J., Cook, N.G.W., 1986. Effective moduli, non-linear deformation and strength of a cracked elastic solid. Int. J. Rock Mech. Min. Sci. 23 (2), 107–118.
Kendrick, J.E., Smith, R., Sammonds, P., Meredith, P.G., Dainty, M., Pallister, J.S., 2013. The influence of thermal and cyclic stressing on the strength of rocks from Mount St. Helens, Washington. Bull. Volcanol. 75 (7), 728.
Kueppers, U., Scheu, B., Spieler, O., Dingwell, D.B., 2005. Field-based density measurements as tool to identify preeruption dome structure: set-up and first results from Unzen volcano, Japan. J. Volcanol. Geotherm. Res. 141 (1-2), 65–75.
Kulhawy, F.H., Goodman, R.E., 1980. Design of foundations on discontinuous rock. In: International Conference on Structural Foundations on Rock, 1980, Sydney, Australia, pp. 209–220, Vol. 1.
Kushnir, A.R., Martel, C., Bourdier, J.L., Heap, M.J., Reuschlé, T., Erdmann, S., et al., 2016. Probing permeability and microstructure: unravelling the role of a low-permeability dome on the explosivity of Merapi (Indonesia). J. Volcanol. Geotherm. Res. 316, 56–71.
Lamur, A., Lavallée, Y., Iddon, F.E., Hornby, A.J., Kendrick, J.E., von Aulock, F.W., Wadsworth, F.B., 2018. Disclosing the temperature of columnar jointing in lavas. Nat. Commun. 9 (1), 1432.
Lavallée, Y., Benson, P.M., Heap, M.J., Hess, K.U., Flaws, A., Schillinger, B., et al., 2013. Reconstructing magma failure and the degassing network of dome-building eruptions. Geology 41 (4), 515–518.
Lavallée, Y., Heap, M.J., Kendrick, J.E., Kueppers, U., Dingwell, D.B., 2019. The fragility of volcán de colima—a material constraint. In: Volcán De Colima. Springer, Berlin, Heidelberg, pp. 241–266.
Le Gonidec, Y., Rosas-Carbajal, M., de Bremond d'Ars, J., Carlus, B., Ianigro, J.C., Kergosien, B., et al., 2019. Abrupt changes of hydrothermal activity in a lava dome detected by combined seismic and muon monitoring. Sci. Rep. 9 (1), 3079.
Lesparre, N., Gibert, D., Marteau, J., Komorowski, J.C., Nicollin, F., Coutant, O., 2012. Density muon radiography of La Soufriere of Guadeloupe volcano: comparison with geological, electrical resistivity and gravity data. Geophys. J. Int. 190 (2), 1008–1019.
Liu, E., Hudson, J.A., Pointer, T., 2000. Equivalent medium representation of fractured rock. J. Geophys. Res. Solid Earth 105 (B2), 2981–3000.
Lu, Z., Wicks, C., Dzurisin, D., Thatcher, W., Freymueller, J.T., McNutt, S.R., Mann, D., 2000. Aseismic inflation of Westdahl volcano, Alaska, revealed by satellite radar interferometry. Geophys. Res. Lett. 27, 1567–1570, http://dx.doi.org/10.1029/1999GL011283.
Lundgren, P., Berardino, P., Coltelli, M., Fornaro, G., Lanari, R., Puglisi, G., Sansosti, E., Tesauro, M., 2003. Coupled magma chamber inflation and sector collapse slip observed with synthetic aperture radar interferometry on Mt. Etna volcano. J. Geophys. Res. Solid Earth 108, http://dx.doi.org/10.1029/2001JB000657.
Maccaferri, F., Bonafede, M., Rivalta, E., 2010. A numerical model of dyke propagation in layered elastic media. Geophys. J. Int. 180 (3), 1107–1123.
Manconi, A., Walter, T.R., Amelung, F., 2007. Effects of mechanical layering on volcano deformation. Geophys. J. Int. 170 (2), 952–958.
Manconi, A., Walter, T.R., Manzo, M., Zeni, G., Tizzani, P., Sansosti, E., Lanari, R., 2010. On the effects of 3-D mechanical heterogeneities at Campi Flegrei caldera, southern Italy. J. Geophys. Res. Solid Earth 115 (B8).
Marinos, V.I.I.I., Marinos, P., Hoek, E., 2005. The geological strength index: applications and limitations. Bull. Eng. Geol. Environ. 64 (1), 55–65.
Marmoni, G.M., Martino, S., Heap, M.J., Reuschlé, T., 2017. Gravitational slope-deformation of a resurgent caldera: New insights from the mechanical behaviour of Mt. Nuovo tuffs (Ischia Island, Italy). J. Volcanol. Geotherm. Res. 345, 1–20.
Martínez-Martínez, J., Benavente, D., García-del-Cura, M.A., 2012. Comparison of the static and dynamic elastic modulus in carbonate rocks. Bull. Eng. Geol. Environ. 71 (2), 263–268.
Marsden, L.H., Neuberg, J., Thomas, M., Mothes, P., Ruiz, M., 2019. Combining magma flow and deformation modelling to explain observed changes in tilt. Front. Earth Sci. 7, 219.
Masterlark, T., Haney, M., Dickinson, H., Fournier, T., Searcy, C., 2010. Rheologic and structural controls on the deformation of Okmok volcano, Alaska: FEMS, InSAR and ambient noise tomography. J. Geophys. Res. 115, B02409, http://dx.doi.org/10.1029/2009JB006324.
Masterlark, T., Feigl, K.L., Haney, M., Stone, J., Thurber, C., Ronchin, E., 2012. Nonlinear estimation of geometric parameters in FEMs of volcano deformation: Integrating tomography models and geodetic data for Okmok volcano, Alaska. J. Geophys. Res. Solid Earth 117 (B2).
Masters, T.G., Shearer, P.M., 1995. Seismic models of the earth: elastic and anelastic. Global Earth Physics: a Handbook of Physical Constants, 1., pp. 88–103.
Mavko, G., Mukerji, T., Dvorkin, J., 2009. The Rock Physics Handbook: Tools for Seismic Analysis of Porous Media. Cambridge University Press.
Mayer, K., Scheu, B., Montanaro, C., Yilmaz, T.I., Isaia, R., Aßbichler, D., Dingwell, D.B., 2016. Hydrothermal alteration of surficial rocks at Solfatara (Campi Flegrei): petrophysical properties and implications for phreatic eruption processes. J. Volcanol. Geotherm. Res. 320, 128–143.
Mavonga, T.G., 2010. Crustal structure beneath two seismic broadband stations revealed from teleseismic P wave receiver function analysis in the Virunga volcanic area, Western Rift. J. Afr. Earth Sci. 58, 820–828, http://dx.doi.org/10.1016/j.jafrearsci.2009.11.003.
McTigue, D.F., 1987. Elastic stress and deformation near a finite spherical magma body: resolution of the point source paradox. J. Geophys. Res. Solid Earth 92 (B12), 12931–12940.
Miranda, T., Sousa, L.R., Gomes, A.T., Tinoco, J., Ferreira, C., 2018. Geomechanical characterization of volcanic rocks using empirical systems and data mining techniques. Joumal Rock Mech. Geotech. Eng. 10 (1), 138–150.
Mitchell, T.M., Faulkner, D.R., 2012. Towards quantifying the matrix permeability of fault damage zones in low porosity rocks. Earth Planet. Sci. Lett. 339, 24–31.
Mogi, K., 1958. Relations between the eruptions of various volcanoes and the deformations of the ground surfaces around them. Earthq Res Inst 36, 99–134.
Moon, V., Bradshaw, J., Smith, R., de Lange, W., 2005. Geotechnical characterisation of stratocone crater wall sequences, White Island Volcano, New Zealand. Eng. Geol. 81 (2), 146–178.
Mordensky, S.P., Villeneuve, M.C., Kennedy, B.M., Heap, M.J., Gravley, D.M., Farquharson, J.I., Reuschlé, T., 2018. Physical and mechanical property relationships of a shallow intrusion and volcanic host rock, Pinnacle Ridge, Mt. Ruapehu, New Zealand. J. Volcanol. Geotherm. Res. 359, 1–20.
Mordensky, S.P., Heap, M.J., Kennedy, B.M., Gilg, H.A., Villeneuve, M.C., Farquharson, J.I., Gravley, D.M., 2019. Influence of alteration on the mechanical behaviour and failure mode of andesite: implications for shallow seismicity and volcano monitoring. Bull. Volcanol. 81 (8), 44.
Mueller, S., Scheu, B., Kueppers, U., Spieler, O., Richard, D., Dingwell, D.B., 2011. The porosity of pyroclasts as an indicator of volcanic explosivity. J. Volcanol. Geotherm. Res. 203 (3-4), 168–174.
Nakao, S., Morita, Y., Yakiwara, H., Oikawa, J., Ueda, H., Takahashi, H., Ohta, Y., Matsushima, T., Iguchi, M., 2013. Volume change of the magma reservoir relating to the 2011 Kirishima Shinmoe-dake eruption-Charging, discharging and recharging process inferred from GPS measurements. Earth Planets Space 65, 505–515, http://dx.doi.org/10.5047/eps.2013.05.017.
Nara, Y., Meredith, P.G., Yoneda, T., Kaneko, K., 2011. Influence of macro-fractures and micro-fractures on permeability and elastic wave velocities in basalt at elevated pressure. Tectonophysics 503 (1-2), 52–59.
Nakada, S., Uto, K., Sakuma, S., Eichelberger, J.C., Shimizu, H., 2005. Scientific results of conduit drilling in the Unzen Scientific Drilling Project (USDP). Sci. Drill. 1, 18–22.
Neuberg, J.W., Collinson, A.S., Mothes, P.A., Ruiz, M.C., Aguaiza, S., 2018. Understanding cyclic seismicity and ground deformation patterns at volcanoes: intriguing lessons from Tungurahua volcano, Ecuador. Earth Planet Sci. Lett. 482, 193–200.
Newman, A.V., Dixon, T.H., Ofoegbu, G.I., Dixon, J.E., 2001. Geodetic and seismic constraints on recent activity at Long Valley Caldera, California; evidence for viscoelastic rheology. J. Volcanol. Geotherm. Res. 105 (3), 183–206.
Newman, A.V., Dixon, T.H., Gourmelen, N., 2006. A four-dimensional viscoelastic deformation model for Long Valley Caldera, California, between 1995 and 2000. J. Volcanol. Geotherm. Res. 150, 244–269.
Newman, A.V., Stiros, S., Feng, L., Psimoulis, P., Moschas, F., Saltogianni, V., Jiang, Y., Papazachos, C., Panagiotopoulos, D., Karagianni, E., Vamvakaris, D., 2012. Recent geodetic unrest at Santorini Caldera, Greece. Geophys. Res. Lett. 39, 1–5, http://dx.doi.org/10.1029/2012GL051286.
Nicolas, A., Fortin, J., Regnet, J.B., Dimanov, A., Guéguen, Y., 2016. Brittle and semi-brittle behaviours of a carbonate rock: influence of water and temperature. Geophys. J. Int. 206 (1), 438–456.
Nishiyama, R., Tanaka, Y., Okubo, S., Oshima, H., Tanaka, H.K.M., Maekawa, T., 2014. Integrated processing of muon radiography and gravity anomaly data toward the realization of high-resolution 3-D density structural analysis of volcanoes: case study of Showa-Shinzan lava dome, Usu, Japan. J. Geophys. Res.: Solid Earth 119 (1), 699–710.
Nishimura, T., Ozawa, S., Murakami, M., Sagiya, T., Tada, T., Kaidzu, M., Ukawa, M., 2001. Crustal deformation caused by magma migration in the northern Izu Islands, Japan. Geophys. Res. Lett. 28, 3745–3748, http://dx.doi.org/10.1029/2001GL013051.
Nordyke, M.D., Wray, W., 1964. Cratering and radioactivity results from a nuclear cratering detonation in basalt. J. Geophys. Res. 69 (4), 675–689.
Obrizzo, F., Pingue, F., Troise, C., De Natale, G., 2004. Bayesian inversion of 1994-1998 vertical displacements at Mt Etna: evidence for magma intrusion. Geophys. J. Int. 157, 935–946, http://dx.doi.org/10.1111/j.1365-246X.2004.02160.x.
Oddsson, B., 1981. Engineering properties of some weak Icelandic volcanic rocks. In: Akai, K., Hayashi, M., Nishimatsu, Y. (Eds.), Weak Rock: Soft, Fractured, and Weathered Rock, vol. 1. A. A. Ballcema, Rotterdam, pp. 197–204.
Okubo, C.H., 2004. Rock mass strength and slope stability of the Hilina slump, Kīlauea volcano, Hawai'i. J. Volcanol. Geotherm. Res. 138 (1-2), 43–76.
Özsan, A., Akın, M., 2002. Engineering geological assessment of the proposed Uruş dam, Turkey. Eng. Geol. 66 (3-4), 271–281.
Pagli, C., Sigmundsson, F., Árnadóttir, T., Einarsson, P., Sturkell, E., 2006. Deflation of the Askja volcanic system: constraints on the deformation source from combined inversion of satellite radar interferograms and GPS measurements. J. Volcanol. Geotherm. Res. 152, 97–108, http://dx.doi.org/10.1016/j.jvolgeores.2005.09.014.
Palano, M., Puglisi, G., Gresta, S., 2008. Ground deformation patterns at Mt. Etna from 1993 to 2000 from joint use of InSAR and GPS techniques. J. Volcanol. Geotherm. Res. 169, 99–120, http://dx.doi.org/10.1016/j.jvolgeores.2007.08.014.
Palmström, A., Singh, R., 2001. The deformation modulus of rock masses—comparisons between in situ tests and indirect estimates. Tunn. Undergr. Space Technol. 16 (2), 115–131.
Paulatto, M., Minshull, T.A., Baptie, B., Dean, S., Hammond, J.O., Henstock, T., et al., 2010. Upper crustal structure of an active volcano from refraction/reflection tomography, Montserrat, Lesser Antilles. Geophys. J. Int. 180 (2), 685–696.
Pells, P.J., Bieniawski, Z.T., Hencher, S.R., Pells, S.E., 2017. Rock quality designation (RQD): time to rest in peace. Can. Geotech. J. 54 (6), 825–834.
Peltier, A., Scott, B., Hurst, T., 2009. Ground deformation patterns at White Island volcano (New Zealand) between 1967 and 2008 deduced from levelling data. J. Volcanol. Geotherm. Res. 181, 207–218, http://dx.doi.org/10.1016/j.jvolgeores.2009.01.020.

Pinel, V., Sigmundsson, F., Sturkell, E., Geirsson, H., Einarsson, P., Gudmundsson, M.T., Högnadóttir, T., 2007. Discriminating volcano deformation due to magma movements and variable surface loads: application to Katla subglacial volcano, Iceland. Geophys. J. Int. 169 (1), 325–338.
Pinel, V., Jaupart, C., 2000. The effect of edifice load on magma ascent beneath a volcano. Philos. Trans. R. Soc. Lond. Ser. A: Math. Phys. Eng. Sci. 358 (1770), 1515–1532.
Rivalta, E., Taisne, B., Bunger, A.P., Katz, R.F., 2015. A review of mechanical models of dike propagation: schools of thought, results and future directions. Tectonophysics 638, 1–42.
Pola, A., Crosta, G., Fusi, N., Barberini, V., Norini, G., 2012. Influence of alteration on physical properties of volcanic rocks. Tectonophysics 566, 67–86.
Puglisi, G., Bonforte, A., 2004. Dynamics of Mount Etna Volcano inferred from static and kinematic GPS measurements. J. Geophys. Res. Solid Earth 109, 1–15, http://dx.doi.org/10.1029/2003JB002878.
Rosas-Carbajal, M., Komorowski, J.C., Nicollin, F., Gibert, D., 2016. Volcano electrical tomography unveils edifice collapse hazard linked to hydrothermal system structure and dynamics. Sci. Rep. 6, 29899.
Rosas-Carbajal, M., Jourde, K., Marteau, J., Deroussi, S., Komorowski, J.C., Gibert, D., 2017. Three-dimensional density structure of La Soufrière de Guadeloupe lava dome from simultaneous muon radiographies and gravity data. Geophys. Res. Lett. 44 (13), 6743–6751.
Rubin, A.M., Pollard, D.D., 1987. Origins of blade-like dikes in volcanic rift zones. In: Decker, R.W., Wright, T. (Eds.), Volcanism in Hawai'i. U.S. Geological Survey Prof, pp. 1449–1470, Paper, 1350.
Rubin, A.M., Pollard, D.D., 1988. Dike-induced faulting in rift zones of Iceland and Afar. Geology 16, 413–417.
Russo, G., 2009. A new rational method for calculating the GSI. Tunn. Undergr. Space Technol. 24 (1), 103–111.
Saito, M., Kawamura, M., 1986. Resistance of the cement-aggregate interfacial zone to the propagation of cracks. Cem. Concr. Res. 16 (5), 653–661.
Sakuma, S., Kajiwara, T., Nakada, S., Uto, K., Shimizu, H., 2008. Drilling and logging results of USDP-4—penetration into the volcanic conduit of Unzen Volcano, Japan. J. Volcanol. Geotherm. Res. 175 (1-2), 1–12.
Sanderson, D.J., Nixon, C.W., 2015. The use of topology in fracture network characterization. J. Struct. Geol. 72, 55–66.
Schaefer, L.N., Oommen, T., Corazzato, C., Tibaldi, A., Escobar-Wolf, R., Rose, W.I., 2013. An integrated field-numerical approach to assess slope stability hazards at volcanoes: the example of Pacaya, Guatemala. Bull. Volcanol. 75 (6), 720.
Schaefer, L.N., Kendrick, J.E., Oommen, T., Lavallée, Y., Chigna, G., 2015. Geomechanical rock properties of a basaltic volcano. Front. Earth Sci. 3, 29.
Schlotfeldt, P., Carter, T.G., 2018. A new and unified approach to improved scalability and volumetric fracture intensity quantification for GSI and rockmass strength and deformability estimation. Int. J. Rock Mech. Min. Sci. 110, 48–67.
Schön, J.H., 2015. Physical Properties of Rocks: Fundamentals and Principles of Petrophysics, Vol. 65. Elsevier.
Schultz, R.A., 1996. Relative scale and the strength and deformability of rock masses. J. Struct. Geol. 18 (9), 1139–1149.
Segall, P., 2010. Earthquake and Volcano Deformation. Princeton University Press.
Setiawan, A., 2002. Modelling of Gravity Changes on Merapi Volcano Observed Between 1997–2000, Ph.D. Thesis. Darmstadt Univ. of Technol., Darmstadt, Germany.
Shea, T., Houghton, B.F., Gurioli, L., Cashman, K.V., Hammer, J.E., Hobden, B.J., 2010. Textural studies of vesicles in volcanic rocks: an integrated methodology. J. Volcanol. Geotherm. Res. 190 (3-4), 271–289.
Siratovich, P.A., Heap, M.J., Villeneuve, M.C., Cole, J.W., Reuschlé, T., 2014. Physical property relationships of the Rotokawa Andesite, a significant geothermal reservoir rock in the Taupo Volcanic Zone, New Zealand. Geotherm. Energy 2 (1), 10.
Smith, R., Sammonds, P.R., Kilburn, C.R., 2009. Fracturing of volcanic systems: experimental insights into pre-eruptive conditions. Earth Planet. Sci. Lett. 280 (1-4), 211–219.
Sonmez, H., Ulusay, R., 1999. Modifications to the geological strength index (GSI) and their applicability to stability of slopes. Int. J. Rock Mech. Min. Sci. 36 (6), 743–760.
Stein, R.S., Briole, P., Ruegg, J.-C., Tapponnier, P., Gasse, F., 1991. Contemporary, holocene, and quaternary deformation of the Asal rift, Djibouti: Implications for the mechanics of slow spreading ridges. J. Geophys. Res. 96 (21), 806, http://dx.doi.org/10.1029/91JB02118, 789–21.
Taisne, B., Jaupart, C., 2009. Dike propagation through layered rocks. J. Geophys. Res. Solid Earth 114 (B9).
Taisne, B., Tait, S., Jaupart, C., 2011. Conditions for the arrest of a vertical propagating dyke. Bull. Volcanol. 73 (2), 191–204.
Tait, S., Jaupart, C., Vergniolle, S., 1989. Pressure, gas content and eruption periodicity of a shallow, crystallising magma chamber. Earth Planet. Sci. Lett. 92 (1), 107–123.
Tanaka, H.K., Nakano, T., Takahashi, S., Yoshida, J., Takeo, M., Oikawa, J., et al., 2007. High resolution imaging in the inhomogeneous crust with cosmic-ray muon radiography: The density structure below the volcanic crater floor of Mt. Asama, Japan. Earth Planet. Sci. Lett. 263 (1-2), 104–113.
Tiede, C., Camacho, A.G., Gerstenecker, C., Fernández, J., Suyanto, I., 2005. Modeling the density at Merapi volcano area, Indonesia, via the inverse gravimetric problem. Geochem. Geophys. Geosystems 6 (9).
Thomas, M.E., Petford, N., Bromhead, E.N., 2004. Volcanic rock-mass properties from Snowdonia and Tenerife: implications for volcano edifice strength. J. Geol. Soc. 161 (6), 939–946.
Todesco, M., Rutqvist, J., Chiodini, G., Pruess, K., Oldenburg, C.M., 2004. Modeling of recent volcanic episodes at Phlegrean Fields (Italy): geochemical variations and ground deformation. Geothermics 33, 531–547, http://dx.doi.org/10.1016/j.geothermics.2003.08.014.
Torquato, S., 2013. Random Heterogeneous Materials: Microstructure and Macroscopic Properties. Springer Science and Business Media, New York, http://dx.doi.org/10.1007/978-1-4757-6355-3.
Touloukian, Y.S., 1981. Physical Properties of Rocks and Minerals. McGraw-Hill, New York.
Ukawa, M., Fujita, E., Ueda, H., Kumagai, T., Nakajima, H., Morita, H., 2006. Long-term geodetic measurements of large scale deformation at Iwo-jima caldera, Japan. J. Volcanol. Geotherm. Res. 150, 98–118.
Vajdova, V., Baud, P., Wong, T.F., 2004. Compaction, dilatancy, and failure in porous carbonate rocks. J. Geophys. Res. Solid Earth 109 (B5).
van Heerden, W.L., 1987. General relations between static and dynamic moduli of rocks. Int. J. Rock Mech. Min. Sci. 24 (6), 381–385.
Vásárhelyi, B., 2009. A possible method for estimating the Poisson's rate values of the rock masses. Acta Geod. Geophys. Hung. 44 (3), 313–322.
Verman, M., Singh, B., Viladkar, M.N., Jethwa, J.L., 1997. Effect of tunnel depth on modulus of deformation of rock mass. Rock Mech. Rock Eng. 30 (3), 121–127.
Vasseur, J., Wadsworth, F.B., Lavallée, Y., Dingwell, D.B., 2016. Dynamic elastic moduli during isotropic densification of initially granular media. Geophys. J. Int. 204 (3), 1721–1728.
Vinciguerra, S., Trovato, C., Meredith, P.G., Benson, P.M., 2005. Relating seismic velocities, thermal cracking and permeability in Mt. Etna and Iceland basalts. Int. J. Rock Mech. Min. Sci. 42 (7-8), 900–910.
Vyalov, S.S., 1986. Rheolottical Fundamentals of Soil Mechanics. Elsevier, New York, pp. 564.
Walsh, J.B., 1965a. The effect of cracks on the uniaxial elastic compression of rocks. J. Geophys. Res. 70 (2), 399–411.
Walsh, J.B., 1965b. The effect of cracks in rocks on Poisson's ratio. J. Geophys. Res. 70 (20), 5249–5257.
Wang, H.F., 2000. Theory of Linear Poroelasticity: With Applications to Geomechanics. Princeton Univ. Press, Princeton, N. J, pp. 287.
Watters, R.J., Zimbelman, D.R., Bowman, S.D., Crowley, J.K., 2000. Rock mass strength assessment and significance to edifice stability, Mount Rainier and Mount Hood, Cascade Range volcanoes. Pure Appl. Geophys. 157 (6-8), 957–976.
Wauthier, C., Cayol, V., Kervyn, F., D'Oreye, N., 2012. Magma sources involved in the 2002 Nyiragongo eruption, as inferred from an InSAR analysis. J. Geophys. Res. Solid Earth 117, 1–20, http://dx.doi.org/10.1029/2011JB008257.
Wauthier, C., Cayol, V., Poland, M., Kervyn, F., d'Oreye, N., Hooper, A., Samsonov, S., Tiampo, K., Smets, B., 2013. Nyamulagira's magma plumbing system inferred from 15 years of InSAR. Geol. Soc. Lond. Spec. Publ. 380, 39–65, http://dx.doi.org/10.1144/SP380.9.
Wauthier, C., Cayol, V., Smets, B., D'Oreye, N., Kervyn, F., 2015. Magma pathways and their interactions inferred from InSAR and stress modeling at Nyamulagira Volcano, D.R. Congo. Remote Sens. (Basel) 7, 15179–15202, http://dx.doi.org/10.3390/rs71115179.
Wiesmaier, S., Heap, M.J., Branca, S., Gilg, H.A., Kueppers, U., Hess, K.U., et al., 2015. Variability in composition and physical properties of the sedimentary basement of Mt Etna, Italy. J. Volcanol. Geotherm. Res. 302, 102–116.
Wilson, L., Head III, J.W., 1994. Mars: review and analysis of volcanic eruption theory and relationships to observed landforms. Rev. Geophys. 32 (3), 221–263.
Wong, T.F., David, C., Zhu, W., 1997. The transition from brittle faulting to cataclastic flow in porous sandstones: mechanical deformation. J. Geophys. Res. Solid Earth 102 (B2), 3009–3025.
Wright, H.M., Cashman, K.V., Gottesfeld, E.H., Roberts, J.J., 2009. Pore structure of volcanic clasts: measurements of permeability and electrical conductivity. Earth Planet. Sci. Lett. 280 (1-4), 93–104.
Wu, X., Jiang, Y., Guan, Z., Gong, B., 2019. Influence of confining pressure-dependent Young's modulus on the convergence of underground excavation. Tunn. Undergr. Space Technol. 83, 135–144.
Wyering, L.D., Villeneuve, M.C., Wallis, I.C., Siratovich, P.A., Kennedy, B.M., Gravley, D.M., Cant, J.L., 2014. Mechanical and physical properties of hydrothermally altered rocks, Taupo Volcanic Zone, New Zealand. J. Volcanol. Geotherm. Res. 288, 76–93.
Yoshioka, N., Scholz, C.H., 1989. Elastic properties of contacting surfaces under normal and shear loads: 2. Comparison of theory with experiment. J. Geophys. Res. Solid Earth 94 (B12), 17691–17700.
Yun, S., Segall, P., Zebker, H., 2006. Constraints on magma chamber geometry at Sierra Negra Volcano, Galápagos Islands, based on InSAR observations. J. Volcanol. Geotherm. Res. 150, 232–243, http://dx.doi.org/10.1016/j.jvolgeores.2005.07.009.
Zhang, L., Einstein, H.H., 2004. Using RQD to estimate the deformation modulus of rock masses. Int. J. Rock Mech. Min. Sci. 41 (2), 337–341.
Zhang, L., 2017. Evaluation of rock mass deformability using empirical methods–A review. Undergr. Space 2 (1), 1–15.
Zhu, W., Baud, P., Vinciguerra, S., Wong, T.F., 2011. Micromechanics of brittle faulting and cataclastic flow in Alban Hills tuff. J. Geophys. Res. Solid Earth 116 (B6).
Zhu, W., Baud, P., Vinciguerra, S., Wong, T.F., 2016. Micromechanics of brittle faulting and cataclastic flow in Mount Etna basalt. J. Geophys. Res. Solid Earth 121 (6), 4268–4289.